TUHH

Technische Universität Hamburg-Harburg

Master Thesis

WEINMANN

medical technology

Institut für Regelungstechnik

TECHNISCHE UNIVERSITÄT HAMBURG-HARBURG

INSTITUT FÜR REGELUNGSTECHNIK

Prof. Dr. Herbert Werner

Prof. Dr. Uwe Weltin

Design and Control of a Novel Portable Mechanical Ventilator

Author

cand. M. Sc. Christian Hoffmann

Supervisor

Dr. Ing. Florian Dietz

March, 21st 2011

cand. M. Sc. Christian Hoffmann
Student ID: 20522587

Task description for a Master Thesis

Design and Control of a Novel Portable Mechanical Ventilator

The company Weinmann Geräte für Medizin GmbH + Co. KG is developing mechanical ventilator technology for both homecare and emergency applications. In the framework of the pre-development department related to emergency medicine R&D, it is the aim of this thesis to investigate possible solutions for the design and control of a novel mechanical ventilator. This new device is to overcome certain drawbacks imposed by the design of the most current product — the MEDUMAT Transport — , which directly affect application scenarios.

After the derivation of concepts, one of them is to be chosen and realised in hardware as a functional model. Due to strongly varying environmental conditions, which cannot be reproduced by the facilities available at Weinmann, a physical simulation model is to be designed as well. The controller design is to prove the feasibility of the concept and/or shall lead to reevaluations. The simulation model is to be obtained by white box modelling and experimental validation of the single components' parameters. Further non measureable parameter dependencies are to be introduced by physical insight. In some modes of operation, the plant will be overactuated. Resulting possible advantages with regard to energy efficiency and increased quality of control are to be investigated and exploited. Robust controller design techniques and/or proof of robustness are mandatory, since patients' airways' parameters are generally unknown and only range within known bounds.

A concise list of tasks is as follows:

Task 1 Literature research on artificial ventilation, pulmonary mechanics, pneumatics, control theory and competitor's state of the art solutions.

Task 2 Establishing a detailed requirement profile based on two main factors: Economical use of resources (namely electric energy and oxygen supply) and control of the inspired fraction of oxygen within the full physically possible extent (21 vol. % to 100 vol. %) while maintaining support for all common modes of ventilation.

Task 3 Methodical derivation of concepts for the realisation of the ventilator's principles of operation subject to the requirement profile.

Task 4 Assessment of significantly different, yet comparable concepts, which promise the best performance in terms of the requirement profile. Selection of a primary concept, subject to further investigation.

Task 5 Construction of a functional model for the chosen concept.

Task 6 Modelling of the functional model for controller design.

Task 7 Controller design and optimisation under the constraints imposed by the available hardware.

Task 8 Discussion of the results.

Dr. Ing. Florian Dietz
Hamburg, November, 12th 2010

Statutory Declaration / *Erklärung an Eides Statt*

I hereby affirm the sole authorship of this thesis, that it has been completed under the supervision common to the institute and that no sources or auxiliary means have been used other than specified.

Ich versichere, diese Arbeit im Rahmen der am Arbeitsbereich üblichen Betreuung selbstständig angefertigt und keine anderen als die angegebenen Quellen und Hilfsmittel benutzt zu haben.

Christian Hoffmann
Hamburg, March, 21st 2011

Confidentiality Clause / *Sperrvermerk*

By request of the company WEINMANN Geräte für Medizin GmbH + Co. KG., the contents of this thesis — including any related data or drawings — are subject to confidentiality up to and including April 2016. No copies or transcripts may be created, digitally or manually. Exceptions to this clause require a written permission by the company WEINMANN Geräte für Medizin GmbH + Co. KG.

Auf Wunsch der Firma WEINMANN *Geräte für Medizin GmbH + Co. KG. ist die Weitergabe des Inhaltes dieser Arbeit und eventuell beiliegender Zeichnungen und Daten im Gesamten oder in Teilen bis einschließlich April 2016 grundsätzlich untersagt. Es dürfen keinerlei Kopien oder Abschriften auch in digitaler Form gefertigt werden. Ausnahmen bedürfen der schriftlichen Genehmigung der Firma Weinmann Geräte für Medizin GmbH + Co. KG.*

Acknowledgements / *Danksagung*

Diese Arbeit ist als externe Masterarbeit bei der Firma Weinmann Geräte für Medizin GmbH + Co. KG entstanden. Aus diesem Grunde möchte ich mich gleichermaßen bei Herrn Prof. Herbert Werner, Herrn Prof. Uwe Weltin als auch bei Herrn Dr. Florian Dietz bedanken, die mir diese lehrreiche und wertvolle Erfahrung ermöglicht haben.

Für die teils intensive, teils den notwendigen kreativen Freiraum lassende Betreuung während der Anfertigung der Arbeit möchte ich mich zusätzlich zu Herrn Dr. Dietz auch bei Herrn Dr. Frank Herrmann bedanken. Das Zurückholen auf den Boden "regelungstechnischer Tatsachen", sowie zahlreiche pragmatische Anregungen haben mir gut getan.

Besonders möchte ich mich auch bei Herrn Dipl.-Ing. Christian Neuhaus für sein schier unerschöpfliches elektrotechnisches Wissen, Herrn Dipl.-Ing. Marcus Diehl für seine interessante Vorarbeit und bei den Herren Dr.-Ing. Nikolaus Voss und M.Sc. Jörn Matthies für ihre Unterstützung seitens der Informatik bedanken. Herrn Dipl.-Ing. Heye Heegardt danke ich für seine ruhige Art, die mir ermöglicht hat, aus einem scheinbar weit tragenden Defekt ausschließlich Verbesserungen herauszuarbeiten. Darüberhinaus gilt mein Dank den Herren Dipl.-Ing. John Alberts und Dipl.-Ing. Benjamin Adametz für einen entscheidenden gedanklichen Funken.

Meinem Mit-Diplomanden Erik-Jörn Witt möchte ich für seine witzige, sympathische Art danken und ich wünsche Ihm mit seiner Arbeit viel Erfolg.

Den größten Dank schulde und erbringe ich jedoch gern meiner Familie: meinen Eltern, sowie meinem Bruder, die mich während der Anfertigung durchgängig unterstützt haben und zu jeder beliebigen Zeit für mich da waren.

Christian Hoffmann
Hamburg, March, 21st 2011

Abstract / *Zusammenfassung*

The subject of this thesis is the design and control of a novel mechanical ventilator. It is motivated by an increase in applicability in the field, in case of lacking supply of pre-pressurised oxygen. The design is derived from morphological analysis with regard to its primary required functionality: volume flow, pressure and positive–end–expiratory pressure control, as well as the control of the inspired fraction of oxygen in the full spectrum, ranging from 21 vol. % to 100 vol. %. The pneumatic system is nonlinearly modelled and a functional model is constructed for verification and integration. Particular emphasis is laid on designing discrete time $\mathcal{H}_\infty$ norm based sensitivity shaping controllers, which guarantee robust stability and performance against uncertain patient and ambient parameters. The proposed controller scheme also gives rise to the exploitation of available degrees of freedom for energy efficient ventilation. An extension of an existing theorem to ensure robustness for static l_2 gain optimal anti–windup compensation for discrete time controllers is proposed and successfully applied to the plant. Simulation and experimental results are presented and — where applicable — compared to previous works.

Thema dieser Arbeit ist der Entwurf und die Regelung eines neuartigen Beatmungsgeräts. Dies ist motiviert durch eine Steigerung der Einsatzfähigkeit im Falle nicht verfügbarer Drucksauerstoffreserven. Die Erarbeitung eines Konzeptes erfolgt mit Hilfe einer morphologischen Analyse auf Basis der Primärfunktionen volumenkontrollierter und druckkontrollierter Regelung, sowie der Regelung des positiven end-exspiratorischen Drucks und der Sauerstoffkonzentration des Inspirationsgases zwischen 21 vol. % *und* 100 vol. %. *Das pneumatische System wird nicht–linear modelliert und ein entsprechendes Funktionsmuster zur Verifikation und Integration konstruiert. Ein besonderer Schwerpunkt liegt in der Synthese zeitdiskreter Regler basierend auf dem* $\mathcal{H}_\infty$ *Sensitivity Shaping Verfahren zur Gewährleistung robuster Stabilität und Regelqualität gegenüber Unsicherheiten bezüglich der Atemwegsparameter des Patienten und Umgebungsbedingungen. Der Vorschlag eines besonderen Regelungsschemas ermöglicht die Ausnutzung verbleibender Freiheitsgrade zur Optimierung der Energieeffizienz während der Beatmung. Eine Erweiterung eines bestehenden Theorems mit dem Ziel, Robustheit für statische,* l_2 *optimale Anti–Windup Kompensation für zeitdiskrete Regler zu garantieren, wird entwickelt und erfolgreich auf die Regelstrecke angewandt. Simulationen, sowie experimentelle Ergebnisse werden präsentiert und — wenn möglich — mit vorangegangenen Arbeiten verglichen.*

Nomenclature

Control Theory and General Mathematics

$\mathbf{0}$	Zero Matrix	
$\mathbf{A}$	State Space System Gain Matrix	
$\mathbf{a}$	Some Vector $\mathbf{a}$ in Bold Notation	
a	Some Scalar a in Regular Notation	
$\mathbf{B}$	State Space Input Gain Matrix	
$\mathbf{C}$	State Space Output Gain Matrix	
$\mathbf{D}$	State Space Direct Feedthrough Gain Matrix	
$G_{y,u}(s)$	Continuous Time Transfer Function from $U(s)$ to $Y(s)$	
$\mathbf{I}$	Identity Matrix	
$(\cdot)^*$	Normalised Value	
$\mathcal{P}(s), \mathcal{P}(z)$	Continuous or Discrete Time Generalised Plant in Caligraphic Script	
s	Complex Frequency Variable in Continuous Time LaPlace Domain	
$\sigma(G(j\omega))$	Singular Values of System G at Frequency ω	
$\bar{\sigma}(\cdot)$, $\underline{\sigma}(\cdot)$	Maximum or Minimum Singular Value	
$*$	Symmetric Completion inside Matrix	
τ	Time Constant	s
T_s	Sampling Time	s
ω	Frequency	$\frac{\mathrm{rad}}{\mathrm{s}}$
$\mathbf{x}(k)$	Discrete Time State (or any other) Vector at Time $t = k \cdot T_s$	
$\mathbf{X}(z)$	Discrete Time State (or any other) Vector at Frequency z	

$X(s)$	Continuous Time State (or any other) Vector at Frequency s	
$x(t)$	Continuous Time State (or any other) Vector at Time t	
z	Complex Frequency Variable in Discrete Time Domain	

Electrics

C	Capacitance	$\frac{\mathrm{A\,s}}{\mathrm{V}}$
i	Current	A
R	Resistance	$\frac{\mathrm{V}}{\mathrm{A}}$
v	Voltage	V

Pneumatics

C	Compliance	$\frac{\mathrm{m^2\,s^2}}{\mathrm{kg}}$
$\mu = \nu\rho$	Dynamic Viscosity	$\frac{\mathrm{N\,s}}{\mathrm{m^2}}$
$\nu = \frac{\mu}{\rho}$	Kinematic Viscosity	$\frac{\mathrm{m^2}}{\mathrm{s}}$
p_{dyn}	Dynamic Pressure	$\frac{\mathrm{kg}}{\mathrm{m\,s^2}}$
p_{stat}	Static Pressure	$\frac{\mathrm{kg}}{\mathrm{m\,s^2}}$
p_{total}	Total Pressure	$\frac{\mathrm{kg}}{\mathrm{m\,s^2}}$
R	Resistance	$\frac{\mathrm{kg}}{\mathrm{m^4\,s}}$
ϱ	Density	$\frac{\mathrm{kg}}{\mathrm{m^3}}$
$\dot{V}$	Volume Flow Rate	$\frac{\mathrm{m^3}}{\mathrm{s}}$
w	Flow Velocity	$\frac{\mathrm{m}}{\mathrm{s}}$

Pulmonary Mechanics / Human Physiology

C_{aw}	Compliance of the Human Airways	$\frac{\mathrm{L}}{\mathrm{mbar}}$
E_{aw}	Elastance of the Human Airways	$\frac{\mathrm{mbar}}{\mathrm{L}}$
f_V	Frequency of Ventilation	$\frac{1}{\mathrm{min}}$
$I : E$	Ratio of Durations of Inspiration versus Expiration: $I : E = \frac{T_{\mathrm{insp.}}}{T_{\mathrm{exp.}}}$	
$\mathrm{F_{iO_2}}$	Fraction of Inspired Oxygen	vol. %

p_{aw}	Pressure Applied to the Human Airways	mbar
R_{aw}	Resistance of the Human Airways	$\frac{\mathrm{mbar}}{\mathrm{L/\,min}}$
$T_{\mathrm{exp.}}$	Duration of Expiration	s
$T_{\mathrm{insp.}}$	Duration of Inspiration	s
T_{vc}	Total Duration of Ventilation Cycle: $T_V = T_{\mathrm{insp.}} + T_{\mathrm{exp.}}$	s
V_{T}	Tidal Volume	L

Subscripts and Superscripts

amb	Ambient
aw	Airways
blower	Related to the Blower
crit	Critical Value
cv	Check Valve
d	Delayed
dyn	Dynamic
exp	Expiration
i,j	From j to i
in	At the Inlet
insp	Inspiration
lam	Laminar
lbv	Large Bore Valve
leak	Leakage
max	Maximum
meas	Measured
min	Minimum
O_2	Oxygen

out	At the Outlet
ov	Oxygen Valve
pb	PEEP Blind
pcv	Pressure Control Valve
pilot	Pilot Pressure
pv	Patient Valve
stat	Static
thr	Throttle
turb	Turbulent
vh	Ventilation Hose

List of Selected Pneumatic Symbols (DIN ISO 1219) and Their Respective Electrical Counterparts

	Symbol	
	Pneumatics	Electrics
Potential Ground	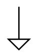 Atmosphere Pressure	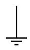 Ground
Potential Measurement (Absolute)	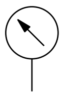 Pressure Measurement	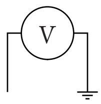 Voltage Measurement
Potential Measurement (Differential)	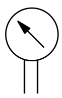 Differential Pressure Measurement	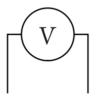 Differential Voltage Measurement
Flux Measurement	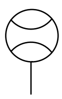 Flow Measurement	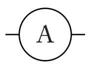 Current Measurement

	Symbol	
	Pneumatics	Electrics
Resistance	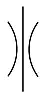 Throttle $R = \frac{p}{Q}$	 Resistor $R = \frac{v}{i}$
Controllable Resistance	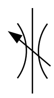 Controllable Throttle 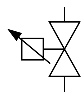 Proportional Valve (High Press. Inlet) $R = R(\alpha)$	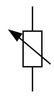 Controllable Resistor $R = R(\alpha)$
Capacitive Energy Storage	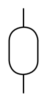 Compliance $C = \frac{\mathrm{d}V}{\mathrm{d}p}$	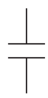 Capacitance $C = \frac{\mathrm{d}Q}{\mathrm{d}v}$

	Symbol	
	Pneumatics	Electrics
Potential Source	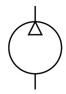 Blower  Gas Bottle	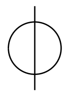 Voltage Source
Flux Source	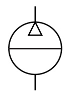 Pump 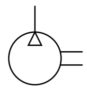 Compressor 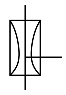 Venturi Injector (non-consistent to DIN ISO 1219)	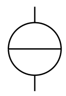 Current Source
Potential Controller	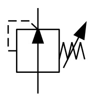 Pressure Control Valve $p = \text{const.}$	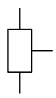 Voltage Controller $V = \text{const.}$
Rectification	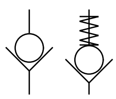 (Spring Loaded) Check Valve	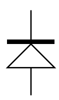 Diode

Symbols without Correspondency

	Symbol
	Pneumatics
Fluid Composition Alteration	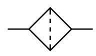 Filter
Fluid Composition Measurement	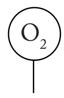 (O_2) Concentration Measurement
Temperature	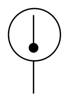 Temperature Measurement
Special Check Valves	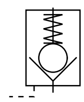 Pilot-to-Open Check Valve 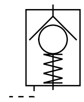 Pilot-to-Close Check Valve

Abbreviations

ARDS	Acute Respiratory Distress Syndrome
ASL	Active Servo Lung
BLDC	Brushless Direct Current (Motor)
BMI	Bilinear Matrix Inequality
COPD	Chronic Obstructive Pulmonary Disease
CMV	Continuous Mandatory Ventilation
CPAP	Continuous Positive Airway Pressure
CPR	Cardio-Pulmonary Reanimation
CSV	Continuous Spontaneous Ventilation
EC	Electronically Commutated (Motor)
EMF	Electro–Magnetic Force
EPAP	Expiratory Positive Airways Pressure
F_{iO_2}	Fraction of Inspired Oxygen
LMI	Linear Matrix Inequality
LPV	Linear–Parameter–Varying
MIMO	Multiple Input Multiple Output
NIV	Non–Invasive Ventilation
PCV	Pressure Controlled Ventilation
PEEP	Positive End-Expiratory Pressure
PSV	Pressure Supported Ventilation
PRVC	Pressure Regulated Volume Controlled
VCV	Volume Controlled Ventilation
ICU	Intensive Care Unit
IPAP	Inspiratory Positive Airways Pressure
IPPV	Intermittent Positive Pressure Ventilation
IMV	Intermittent Mandatory Ventilation
IV	Invasive Ventilation
SIMV	Synchronised Intermittent Mandatory Ventilation
SISO	Single Input Single Output

Contents

1 Introduction

1.1 Motivation

Modern–day emergency and transport ventilation devices, like the Dräger Oxylog 3000 or the Weinmann MEDUMAT Transport rely on prepressurised oxygen supplies, in order to operate. If said supplies are depleted, the devices are inoperable, despite them still having access to electrical energy. Taking into consideration, that a typical bottle[1] of prepressurised oxygen lasts for about 2.5 h, given a patient breathing 12 times a minute while consuming half a liter per breath of pure oxygen, long–range transports require additional supplies. Delivering oxygen to the patient, however, is not even always a necessity and less developed countries, e.g. The Gambia in western Africa, often lack clinical, as well as mobile oxygen supplies [25], [39]. Consequently, it is suggested, that appropriate technology includes ventilators not dependent on compressed gas [45].

It is also well known, that an abundance of oxygen in the inspired gas will result in reactive oxygen intermediates, which can cause lung injury [38]. Oxygen is generally considered potentially toxic for concentrations exceeding 40 vol. % and the afore–mentioned devices can only provide concentrations just as low. While both access to oxygen in some parts of the world and during transport is limited and oxygen can — in some circumstances — do more harm than good, the main motivation in developing a novel mechanical ventilator resides in the need for devices, which can operate without oxygen and administer concentrations ranging between 21 vol. % and 100 vol. % as desired.

Whereas prepressurised gas is the main pneumatic power source of current devices, an electro–mechanical power source frequently used in ventilation devices for homecare purposes is the blower, a near ideal pressure source. However, defined volume flow rates are often administered to the patient in emergency medicine, which is best done by near ideal flow sources. This thesis will therefore also focus on deriving concepts that suit the requirements on emergency transport ventilators and cover the problem of robust feedback control extensively.

[1] A typical bottle is assumed to carry 2 L at 200 bar, which accounts for 400 L at ambient pressure.

1.2 Framework of the Thesis

This thesis' came into existence as a cooperation between the WEINMANN Department of Pre-Development and the Institute of Control Systems of the HAMBURG UNIVERSITY OF TECHNOLOGY. The institute kindly supported the author's research at WEINMANN and agreed in confidentiality, while providing useful scientific input with respect to modern control theory. The people at WEINMANN, on the other hand, continue to take their part in supporting education by enabling students to graduate on topics, which are both scientific and immediately practical. The result is thus a work of applied control theory, as well as of product related research.

1.3 Aims of the Thesis

This thesis' aim is to derive and evaluate concepts for a novel mechanical ventilation device. The concepts' common objectives mainly reside in rendering dependency on prepressurised gas obsolete and enabling to apply oxygen concentrations of 21 vol. % to 100 vol. % to the patient. A single concept is to be chosen for further investigation, as it will be both simulated as a physical model and constructed as a functional model for verification and integration purposes. Benefits and drawbacks with regard to previously existing designs are to be analysed, in order to enhance knowledge about a possible future optimal design. Integration is subject to an extensive controller design phase, in which it is not only the aim to provide basic functionality to the functional model, but also to investigate possible new solutions for issues, that are related to similar, existing designs.

1.4 Outline of the Thesis

The thesis is structured as follows: Chapter 1 has established a basic understanding about this thesis' motivation, the framework in which it has been written and its aims.

Chapter 2 continues by recalling fundamentals with regard to fluidics, pneumatics and their application to mechanical ventilation in a comprehensive and concise way. The chapter's final section additionally covers relevant control theoretical aspects.

A requirement profile is formulated at the beginning of chapter 3 and concepts for novel designs of mechanical ventilators adhereing to the notions expressed therein are derived by morphological analysis. Their assessment leads to the selection of a concept, which is subject to nonlinear modelling in chapter 4.

To verify the simulations, the concept is constructed as a functional model. The components used for this purpose and the overall hardware layout are briefly described in chapter 5.

Chapter 6 documents controller synthesis under the special consideration of robustness against parametric uncertainties. A scheme is developed to enable energy efficient feed-forward control in addition to reference tracking based closed–loop control. Suitable controllers are applied to both simulation and the functional model. The results are presented in chapter 7, leading into the final chapter 8, where a conclusion is drawn and a brief outlook to possible future work is given.

2 Fundamentals

This chapter's aim is to cover all aspects necessary to provide a fundamental understanding of the physical processes, physiology, engineering and control involved with mechanical ventilation.

The first two sections are devoted to fluidics in general. Section 2.1 deals with the properties and mixture of fluids relevant in mechanical ventilation. Section 2.2 continues with basic definitions and constitutive equations, required for the modelling of dynamic pneumatic systems. In section 2.3 on pulmonary mechanics, this is applied to the human airways in terms of the so–called *single compartment model*. The following section 2.4 sheds light on more general aspects with regard to mechanical ventilation, covering its aims, types of control, modes, associated parameters and terminology. The chapter closes with an overview of the control theory applied in this thesis. Basic notions of continuous and discrete time systems are given. Signal and system norms are defined and their use to express design objectives is briefly explored. Methods and tools for the synthesis of robustly stable $\mathcal{H}_\infty$ controllers are explained, that also guarantee robust performance. Eventually, a theorem is reproduced from [41], which allows the augmentation of general discrete time controllers with anti–windup compensation.

2.1 Fluid Properties

Ventilation gas for application in emergency medicine is comprised of three different kinds of fluids: Pure oxygen, ambient air and water. Though ambient air is a mixture itself, it will be regarded as a basic fluid with known characteristic constants. Furthermore, the fluids will be considered ideal throughout the thesis.

2.1.1 Ideal Gases and Fluid Mixture

The ideal gas law can be applied for gas phases of non associating substances for pressures up to 5 bar [1]:

$$p \cdot v = R_\mathrm{x} \cdot T \tag{2.1}$$

$$\text{with } v = \frac{1}{\varrho} \text{ as the gas' specfic volume,}$$

$$R_\mathrm{x} \text{ as the substance's gas constant in } \frac{\mathrm{J}}{\mathrm{kg\,K}}.$$

In mixture, ideal gases are assumed to not react or interact with each other. In a confined space, they homogeneously fill up the complete volume.

Definition 2.1 (Dalton's Law)**.** *In a mixture of ideal gases the partial pressures p_i of all substances $i = 1, \dots, k$ are added:*

$$p_{\text{total}} = \sum_{i=1}^{k} p_i. \tag{2.2}$$

Likewise, their volumes V_i and amount of particles n_i are summed up:

$$V_{\text{total}} = \sum_{i=1}^{k} V_i, \qquad n_{\text{total}} = \sum_{i=1}^{k} n_i.$$

For non-ideal gases volumes are also known to contract or expand upon mixture.

Volume fractions Φ_j can be computed for each substance j as ratios with respect to the total volume of the mixture:

$$\Phi_j = \frac{V_j}{\sum_{i=1}^{k} V_i},$$

The above formula is also valid, if the volumes V_i are replaced volume flows $\dot{V}_i$. Thus, the fraction becomes a volume flow fraction $\dot{\Phi}_j$, which can be used to obtain the molar mass of a mixture of fluids.

$$\tilde{M}_{\text{mix}} = \sum_{i=1}^{k} \dot{\Phi}_i \cdot \tilde{M}_i. \tag{2.3}$$

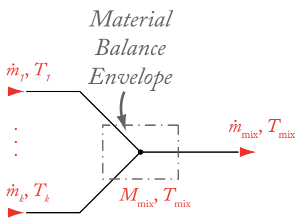

Figure 2.1: Model of Dynamic Behaviour of the Mixing Temperature of Multiple Fluid Flows

A mixture's temperature T_{mix} is given by the static equilibrium of enthalpies, in which the temperature of every component T_i equals that of the mixture, i.e.

$$T_{\text{mix}} = T_i \quad \text{for } i = 1, \dots, k$$

holds.

	Thermophysical Properties				
	Invariant		Standard Conditions		
Substance	$R/\frac{\mathrm{J}}{\mathrm{kg\,K}}$	$M/\frac{\mathrm{g}}{\mathrm{mol}}$	$c_p/\frac{\mathrm{J}}{\mathrm{kg\,K}}$	$\varrho/\frac{\mathrm{kg}}{\mathrm{m}^3}$	$\eta/10^{-6}\,\frac{\mathrm{kg}}{\mathrm{m}^3}$
Dry Air	287.12	28.9583	1006.6	1.1885	18.447
Oxygen	259.8329	31.9988	919.6	1.292	20.65
Water Vapour	461.5	18.0153	1840.0	0.7475	13.000

Table 2.1: Thermophysical Properties of the Relevant Substances Water, Ambient Air and Oxygen under Standard Conditions ($\vartheta = 25\,°\mathrm{C}, p = 1013,25\,\mathrm{mbar}$) [1]

A model of isobaric instationary fluid-mixture is given in figure 2.1. The outlet temperature T_{mix} shall be the temperature of — and constant all over — the control mass. In equilibrium $\frac{\mathrm{d}T_{\mathrm{mix}}}{\mathrm{d}t}$ vanishes and

$$\sum_{i=1}^{k} \dot{m}_i c_{p,\mathrm{mix}} T_{\mathrm{mix}} = \sum_{i=1}^{k} \dot{m}_i c_{p,i} T_i$$

with $c_{p,\mathrm{mix}}$ as the mixture's heat capacity.

holds. Under the assumption of equal densities and heat capacities, the mixture's equilibrium temperature remains only a function of fluid volume flows:

$$T_{\mathrm{mix}} = \frac{\sum_{i=1}^{k} \dot{V}_i T_i}{\sum_{i=1}^{k} \dot{V}_i} = \sum_{i=1}^{k} \dot{\Phi}_i T_i. \tag{2.4}$$

Table 2.1 displays thermophysical properties of the substances relevant for mechanical ventilation purposes. Though heat capacity and density are functions of temperature and/or pressure and would have to be compared on a wider basis than just standard conditions, for the purpose of this thesis, the values are deemed sufficiently close to each other for the purposes of this thesis, which justifies the above–mentioned simplifications.

2.1.2 Humid Air

Humid air is a mixture of dry air and water vapour. According to the assumptions with regard to mixtures of ideal gases, water vapour and air do not interact or influence each other.

Definition 2.2 (Absolute Humidity [24])**.** *The absolute humidity is defined as the ratio between the water vapour's mass m_{wv} and the volume V, in which it is contained:*

$$\varrho_{\mathrm{wv}} = \frac{m_{\mathrm{wv}}}{V} = \frac{p_{\mathrm{wv}}(T)}{R_{\mathrm{wv}} T}. \tag{2.5}$$

The absolute humidity is constrained by the water vapour's partial pressure in saturation $p_{\mathrm{wv,sat}}(T)$ according to the vapour pressure curve of water.

Definition 2.3 (MAGNUS formula: Vapour pressure curve of water [40])**.** *The* MAGNUS *formula is a reasonable approximation of the temperature dependent saturation pressure of water vapour valid for* $-45\,°C < \vartheta < 60\,°C$ *(cf. figure 2.2).*

$$p_{\mathrm{wv,sat}}(\vartheta) = 611.213\,\mathrm{Pa} \cdot \mathrm{e}^{\frac{17.5043\cdot\vartheta}{241.2+\vartheta}}, \tag{2.6}$$

with ϑ *as the temperature in* °C,

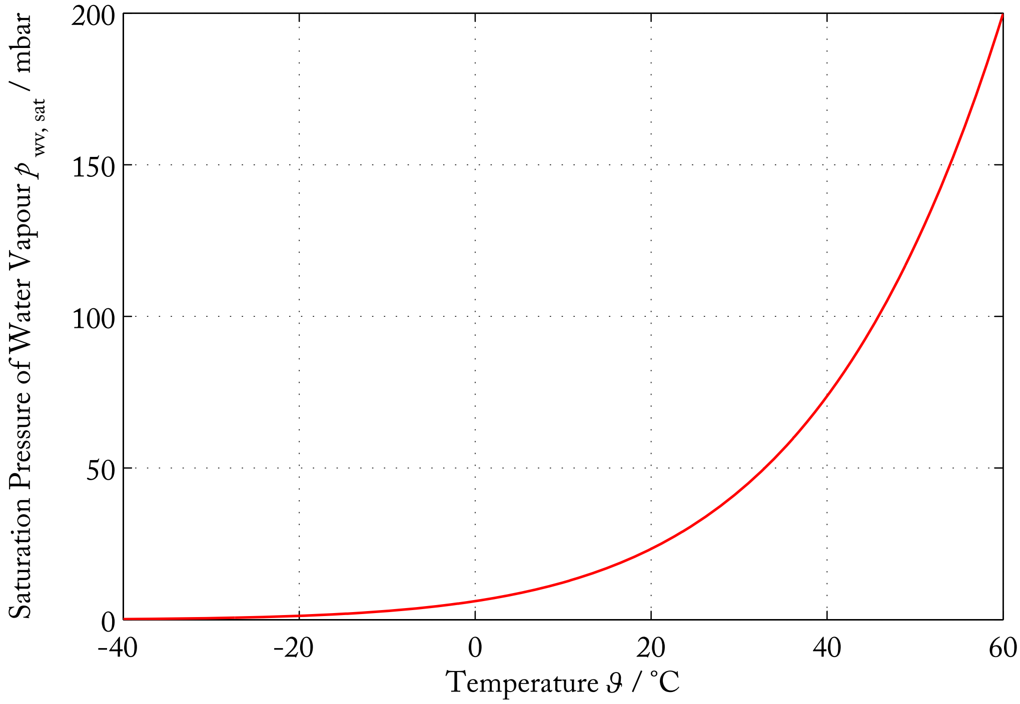

Figure 2.2: Vapour Pressure Curve of Water Calculated with the MAGNUS Formula

Definition 2.4 (Relative Humidity [24])**.** *The relative humidity is defined as the ratio between absolute humidity* ϱ_{w} *and its maximum value in saturation* $\varrho_{\mathrm{wv,sat}}$*:*

$$\varphi = \frac{\varrho_{\mathrm{wv}}}{\varrho_{\mathrm{wv,sat}}}. \tag{2.7}$$

Applying DALTON's law 2.2, the density ϱ_{ha} and the gas constant R_{ha} of humid air can be found:

$$\varrho_{\mathrm{ha}} = \frac{p_{\mathrm{da}}}{R_{\mathrm{da}}T} + \frac{p_{\mathrm{wv}}}{R_{\mathrm{wv}}T} \tag{2.8}$$

$$R_{\mathrm{ha}}(\vartheta, p, \varphi) = R_{\mathrm{da}} \cdot \frac{1}{1 - \varphi \cdot \frac{p_{\mathrm{wv,sat}}(\vartheta)}{p} \cdot \left(1 - \frac{R_{\mathrm{da}}}{R_{\mathrm{wv}}}\right)}, \tag{2.9}$$

with R_{da} as the gas constant of dry air,
R_{wv} as the gas constant of water vapour.

Reformulation of the density for dependence on the mixture's total pressure gives:

$$\varrho_{\mathrm{ha}}(\vartheta, p, \varphi) = \frac{p}{R_{\mathrm{ha}}(\vartheta, p, \varphi) \cdot (273.15\,\mathrm{K} + \vartheta)} \tag{2.10}$$

2.2 Fluid Mechanics and Pneumatics

In this section, fundamental equations and principles will be presented, which are the basic tools of the nonlinear modelling of the plant's dynamics described in chapter 4. They will enable the derivation of a pneumatic network analogon to the real world plant and the quantification of the pneumatic network's parameters.

2.2.1 Basic Definitions

Pneumatics can be described similar to electrical networks. Symbols based on the norm DIN ISO 1219 will be used throughout this thesis. For readers, who are more familiar with electrical networks, a correspondency table is given at the beginning of this document along with the general set of pneumatic symbols used in this thesis. The following definitions comprise a fundamental subset of pneumatic principles.

Definition 2.5 (Static Pressure, Dynamic Pressure, Total Pressure [6])**.** *The pressure p denotes the potential in pneumatics. Static pressure is defined as perpendicular force per area:*

$$p_{\mathrm{stat}} = \frac{F}{A}. \tag{2.11}$$

Dynamic pressure is the increase of pressure that would result from lossless and complete conversion of a fluid's kinetic energy into pressure:

$$p_{\mathrm{dyn}} = \frac{1}{2}\varrho w^2, \tag{2.12}$$

with w as the fluid's flow velocity in $\frac{\mathrm{m}}{\mathrm{s}}$.

Total pressure is the sum of dynamic and static pressure:

$$p_{\mathrm{total}} = p_{\mathrm{stat}} + p_{\mathrm{dyn}}. \tag{2.13}$$

Definition 2.6 (Volume Flow Rate [6])**.** *The volume flow rate — or flow, for short — is the volumentric quantity of a flowing fluid over time and denotes the* current *in pneumatics.*

$$\dot{V} = \frac{\mathrm{d}V}{\mathrm{d}t}. \tag{2.14}$$

Definition 2.7 (Resistance [32])**.** *The resistance establishes a relation between pressure and flow and quantifies the degree of impediment the flow encounters:*

$$R = \frac{\mathrm{d}p}{\mathrm{d}\dot{V}}. \tag{2.15}$$

Pneumatic Effect	
Visualisation	Formula
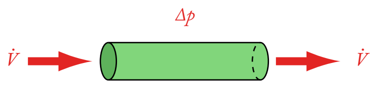	Resistance $\Delta p = R_{\mathrm{lam}}\dot{V}$ $\Delta p = R_{\mathrm{turb}}\dot{V}^2$
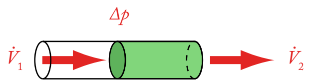	Compliance $\Delta p = \frac{1}{C}\int \dot{V}\mathrm{d}t$
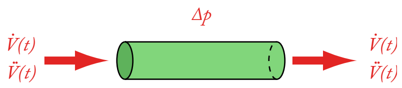	Inertance $\Delta p = L\ddot{V}$

Table 2.2: Overview about Pneumatic Effects and Constitutive Equations Relevant for Dynamic Modelling [47, slightly altered]

The mathematical law differs between the cases of laminar or turbulent flow:

$$\Delta p = R_{\mathrm{lam}}\dot{V}, \tag{2.16}$$

$$\Delta p = R_{\mathrm{turb}}\dot{V}^2. \tag{2.17}$$

Whether a flow can be considered laminar or turbulent is determined by the REYNOLDS number. Please refer to subsection 2.2.2 about fluid mechanics for details.

Definition 2.8 (Compliance [32])**.** *The compliance defines the relation between change in volume and change in pressure and models compressibility by storage of volume:*

$$C = \frac{\mathrm{d}V}{\mathrm{d}p}. \tag{2.18}$$

Definition 2.9 (Inertance / Inductivity [47])**.** *The inductivity defines the relation between change in pressure and change in flow and models the inertance of the mass, which is flowing:*

$$L = \frac{\mathrm{d}p}{\mathrm{d}\ddot{V}}. \tag{2.19}$$

Table 2.2 summarises the effects and constitutive equations relevant for dynamic modelling.

2.2.2 Fluid Mechanics

Fluid mechanics provide means of a mathematical formulation of the flow phenomena encountered in pneumatic systems. The following will give the theoretical tools.

Reynolds Number: Laminar and Turbulent Flow in Smooth Pipes

Definition 2.10 (Reynolds Number [47]). *A fluid's flow condition is characterised by the dimensionless* Reynolds *number:*

$$\mathrm{Re} = \frac{w \cdot d}{\nu}, \tag{2.20}$$

with d as the pipe's characteristic length in m,

ν *as the fluid's kinematic viscosity in* $\frac{\mathrm{m}^2}{\mathrm{s}}$

For $\mathrm{Re} < 2320 = \mathrm{Re}_{\mathrm{crit}}$ a flow is considered laminar, otherwise it is considered turbulent [6]. In reality, turbulent flow conditions can exist, despite $\mathrm{Re} < \mathrm{Re}_{\mathrm{crit}}$ and vice versa. Pipe or hose geometry can account for this, for instance.

For pipes with circular cross-section, the characteristic length becomes the diameter and flow velocity w can be expressed in terms of the volume flow $\dot{V}$:

$$\mathrm{Re} = \frac{4\dot{V}}{\nu \cdot d \cdot \pi}. \tag{2.21}$$

The kinematic viscosity is related to the dynamic viscosity by influence of the fluid's density:

$$\nu = \frac{\eta}{\varrho}, \tag{2.22}$$

with η as the fluid's dynamic viscosity in $\frac{\mathrm{m}^5}{\mathrm{kg\,s}}$.

Energy and Mass Conservation Energy conservation can be expressed by the sum of elementary forms of energy being constant:

$$\underbrace{pV}_{\text{Pressure Energy}} + \underbrace{\frac{1}{2}mw^2}_{\text{Kinetic Energy}} + \underbrace{mgz}_{\text{Potential Energy}} = \text{const.} \tag{2.23}$$

With hydraulic flows (incompressible), the change of intrinsic energy $W = h \cdot m$ is usually negligible [47]. Reformulation of the energy conservation equation 2.23 by division by m and multiplication by $\varrho = \text{const.}$ gives the Bernoulli equation.

Definition 2.11 (Bernoulli Equation [47]). *The* Bernoulli *equation is a special formulation of energy conservation in terms of pressures for incompressible fluids:*

$$\underbrace{\underbrace{p_1}_{p_{1,\mathrm{stat}}} + \underbrace{\frac{\varrho}{2}w_1^2}_{p_{1,\mathrm{dyn}}}}_{p_{1,\mathrm{total}}} + \varrho g z_1 = \underbrace{\underbrace{p_2}_{p_{2,\mathrm{stat}}} + \underbrace{\frac{\varrho}{2}w_2^2}_{p_{2,\mathrm{dyn}}}}_{p_{2,\mathrm{total}}} + \varrho g z_2 + \Delta p_{21,\mathrm{loss}} \tag{2.24}$$

$\Delta p_{21,\mathrm{loss}}$ *denotes the losses from* 1 *to* 2.

For compressible flows, energy conservation has to be formulated by means of the total enthalpy. Additionally, change in potential energy can usually be neglected in pneumatics.

$$\underbrace{\underbrace{h_1(p_1,T_1)}_{\text{1,Spec. Int. Energy}} + \underbrace{\frac{1}{2}w_1^2}_{\text{1,Spec. Kin. Energy}}}_{\text{1,Total Enthalpy}} = \underbrace{\underbrace{h_2(p_1,T_1)}_{\text{2,Spec. Int. Energy}} + \underbrace{\frac{1}{2}w_2^2}_{\text{2,Spec. Kin. Energy}}}_{\text{2,Total Enthalpy}} + \Delta h_{21,\text{loss}} \tag{2.25}$$

Definition 2.12 (Continuity Equation [47]). *The principle of mass conservation is formulated by the continuity equation:*

$$\begin{aligned} \dot{m}_1 &= \dot{m}_2, \\ A_1\varrho_1 w_1 &= A_2\varrho_2 w_2 \end{aligned} \tag{2.26}$$

These equations help to model pressure losses that occur for different flow phenomena.

Flow Through Smooth Pipes/Tubes Pressure loss occurs due to viscous friction of the fluid and is proportional to the square of the flow velocity w. Its reference value is therefore the dynamic pressure p_{dyn} at the entrance:

$$\Delta p = \zeta(w,...)\underbrace{\frac{\varrho}{2}w^2}_{p_{\text{dyn}}} \tag{2.27}$$

The resistance coefficient ζ depends on pipe geometry, surface properties and flow conditions. Strictly speaking this proportionality only holds true in case of turbulent flow conditions, where $\zeta(w,...) = \zeta$ is a true proportionality constant. In case of laminar flow conditions, the resistance coefficient is a function of the flow velocity w, which then leads to a linear equation in w.

For straight, circular pipe elements the resistance coefficient ζ is a function of the pipe's diameter d and its length l, as well as of the pipe resistance coefficient λ:

$$\zeta = \lambda \cdot \frac{l}{d} \tag{2.28}$$

The dependence of λ on the Reynolds number Re and the relative roughness of the pipe is indicated by figure 2.3.

A formula to equate pressure losses as a function of volume flow $\dot{V}$ goes as follows:

$$\Delta p = \zeta \cdot \frac{\varrho}{2}\left(\frac{\dot{V}}{A}\right)^2 = \underbrace{\left(\frac{\zeta\cdot\varrho}{2A^2}\right)}_{R} \cdot \dot{V}^2 = R\cdot\dot{V}^2 \tag{2.29}$$

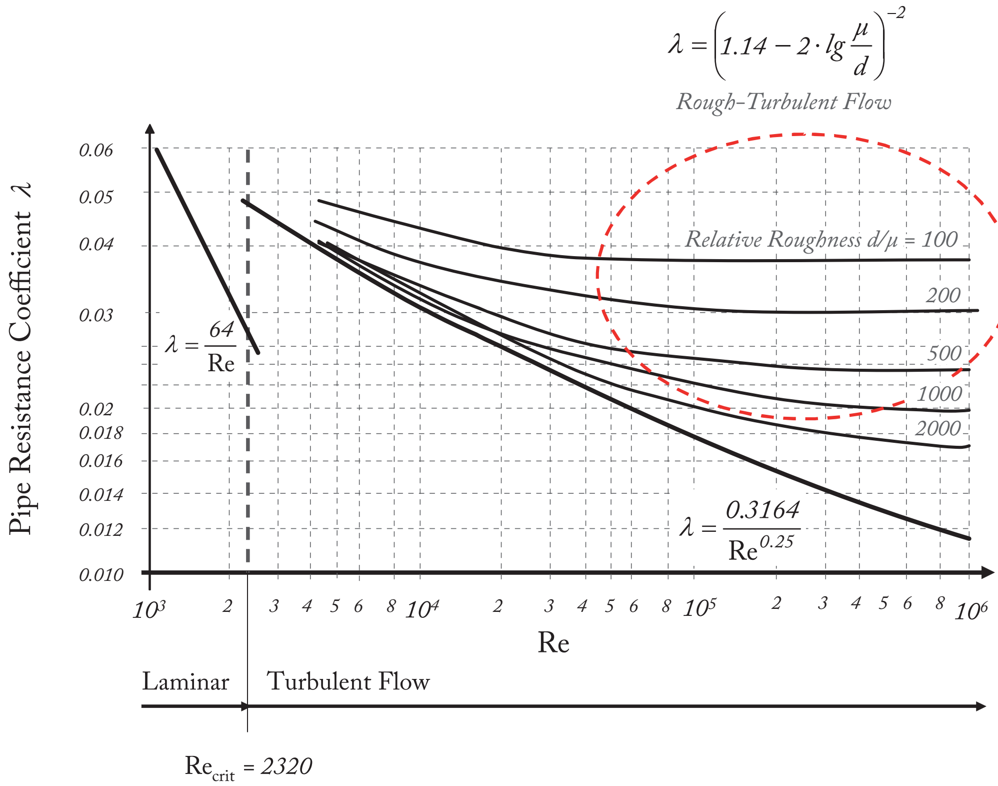

Figure 2.3: Pipe Resistance Coefficient vs. REYNOLDS Number [47]

This holds true for both the turbulent and laminar case. Inserting ζ for laminar flow conditions ($\mathrm{Re} < \mathrm{Re}_{\mathrm{crit}} = 2320$) eliminates the non-linearity [47]:

$$\Delta p = \left(\lambda_{lam} \cdot \frac{l}{d}\right) \cdot \frac{\varrho}{2} \cdot w^2 = 64 \frac{\nu}{w \cdot d} \cdot \frac{l}{d} \cdot \frac{\varrho}{2} \cdot w^2 = 64 \frac{\nu \cdot l \cdot \varrho}{2 \cdot d^2} \cdot w \underbrace{\left(\frac{128}{\pi} \frac{\nu \cdot l \cdot \varrho}{d^4}\right)}_{R_{\mathrm{lam}}} \cdot \dot{V}$$

In case of rough-turbulent flow (cf. figure 2.3), ζ is independent of the REYNOLDS number and

$$\Delta p = \underbrace{\left(\underbrace{\lambda \frac{l}{d}}_{\zeta} \frac{\varrho}{2} \frac{16}{\pi d^4}\right)}_{R_{\mathrm{turb}}} \dot{V}^2 \tag{2.30}$$

holds. Dependence on pipe or tube wall roughness also becomes apparent, when laminar and turbulent flow profiles are compared (cf. figure 2.4).

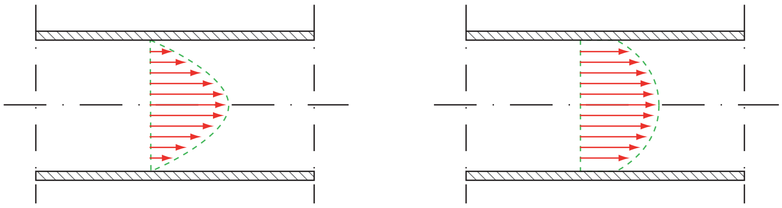

Figure 2.4: Laminar (l.) and Turbulent (r.) Flow [47]

Values for ζ for constructional elements, such as bends, can be drawn from tables (cf. [47]).

Although, in practical applications, resistance values of pipe or tube elements will probably be identified experimentally, these equations can provide first estimates. They also show, that pressure loss within pipes scales linearly with density and to the fourth power with the reciprocal of the diameter.

Flow Through Orifices Figure 2.5 depicts flow phenomena occurring at a sharp-edged orifice of area A_2. The pipe's and orifice's cross-sections are assumed to be circular in shape. Applying equation 2.25 gives:

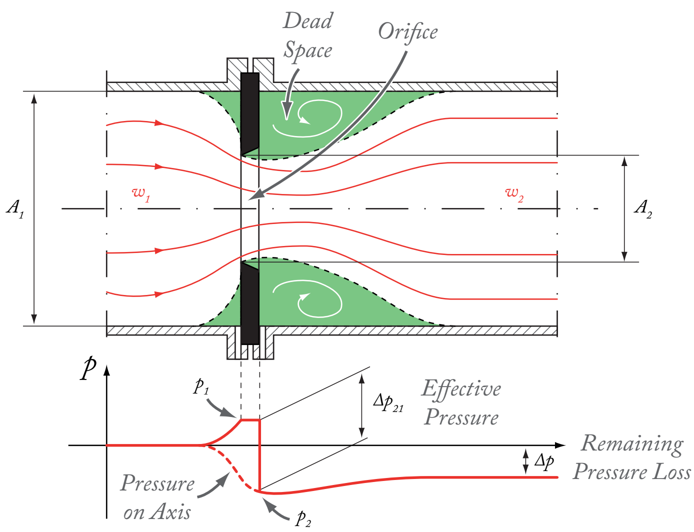

Figure 2.5: Phenomena Occurring at Flow Through Sharp-Edged Orifice [7]

$$p_1 + \frac{\varrho_1}{2} w_1^2 = p_2 + \frac{\varrho_2}{2} w_2^2 + \Delta h_{21,\text{loss}} \tag{2.31}$$

Together with the continuity equation 2.26, one can formulate an expression for the flow through the orifice [14]:

$$\begin{aligned} \dot{V} &= \alpha A_2 \sqrt{\frac{2(p_1 - p_2)}{\varrho_2}}, \\ \text{with } \alpha &= \frac{\kappa}{\sqrt{1 - \frac{\varrho_2}{\varrho_1}\beta^2\kappa^2}} \text{ as the flow coefficient,} \\ \text{and } \kappa &= \sqrt{1 - \frac{\Delta h_{21,\text{loss}}}{\frac{\varrho_2}{2} w_2^2}} \text{ as the loss coefficient.} \end{aligned} \tag{2.32}$$

The flow coefficient α corrects for flow contraction, friction losses and ratio of areas

$$\beta^2 = \frac{A_2^2}{A_1^2} = \frac{d_2^2}{d_1^2}. \tag{2.33}$$

For smooth pipes α approaches 1, whereas for sharp-edged orifices α ranges within $[0.59 \ldots 0.62]$. Ideally sharp-edged orifices can be calculated with $\alpha = 0.611$ under the assumption of potential flow (frictionless) [7].

Flow phenomena that happen due to the viscosity of the fluid, such as the formation of a dead space after the orifice (cf. figure 2.5) either decrease α (displacement effects) or enlarge α (rounding of the orifice) and depend on the REYNOLDS number [7].

More detailed formulae for the calculation of the flow coefficient $\alpha(\beta, \text{Re})$ by the READER-HARRIS/GALLAGHER–equation, and an empiricial formula for the loss coeff-cient κ (also known as the expansion factor ε) are given in [7] based on the Euronorm EN ISO 5167–2(2003) [17]. The assumption of $\alpha = 0.611$ is deemed sufficiently accurate for this thesis, though.

In order to quantify an orifice as a pneumatic resistance R_{orifice}, equation 2.32 can be reformulated in accordance with the general law for pressure drops over resistances in case of turbulent flow:

$$\begin{aligned} \Delta p &= R_{\text{orifice}} \cdot \dot{V}^2, \\ \text{where } R_{\text{orifice}} &= \frac{\varrho_2}{2\alpha^2 A_2^2}. \end{aligned} \tag{2.34}$$

Employing the conductance value, rather than the resistance can appear beneficial if $A_2 \to 0$, e.g. in case of variable throttles, that are capable of shutting off flow completely:

$$G_{\text{orifice}} = 2\frac{\alpha^2 A_2^2}{\varrho_2}. \tag{2.35}$$

Pneumatic Capacity/Compliance of a Pipe/Tube Segment [47] Compliance of a pipe/tube segment is a phenomenon induced by compressibility. The proportionality factor C can be calculated by

$$C = \beta \cdot V, \tag{2.36}$$

with β as the fluid's compressibility factor,
V as the fluid's volume inside the segment.

The compressibility factor of air for isothermal compression can be expressed by

$$C = \frac{\mathrm{d}V}{\mathrm{d}p} = \frac{V}{\varrho RT} \quad \Longrightarrow \quad \beta = \frac{1}{p} = \frac{1}{\varrho RT}, \tag{2.37}$$

with ϱ as the fluid's density,
T as the fluid's temperature in K.

For standard conditions[1] $\beta \approx 1 \cdot 10^{-5} \frac{1}{\mathrm{Pa}} = 1 \cdot 10^{-3} \frac{1}{\mathrm{mbar}}$ holds.

Inertance of a Pipe/Tube Segment [47] Inertance follows from NEWTON's law:

$$F = m \cdot a.$$

Formulated in terms of volume flow and pressure, a formula for the inertance of fluids inside pipe or tube segments can be derived:

$$\Delta p = \underbrace{\left(\varrho \frac{l}{A}\right)}_{L} \cdot \ddot{V}, \tag{2.38}$$

with ϱ as the fluid's density,
l as the pipe/tube segment's length,
A as the pipe/tube segment's cross-section area.

Equivalent Resistances for Laminar and Turbulent Flow Conditions [47] Resistances in series add up for both laminar and turbulent flow conditions, assuming that the volume flow remains constant (incompressibility):

$$R_{\text{series}} = \sum_i R_i. \tag{2.39}$$

For laminar flow conditions, resistances in parallel (cf. figure 2.6) are simplified to an equivalent resistance by taking the sum over the reciprocals:

$$\frac{1}{R_{\text{equiv,lam}}} = \sum_i \frac{1}{R_i}. \tag{2.40}$$

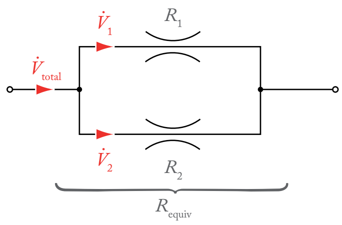

Figure 2.6: Flow Divider Circuitry

For turbulent flow conditions, the reciprocals' square roots are added:

$$\frac{1}{\sqrt{R_{\mathrm{equiv,turb}}}} = \sum_i \frac{1}{\sqrt{R_i}}. \tag{2.41}$$

During this thesis, density changes are assumed to be negligible, when calculating networks of resistances.

[1] $\vartheta = 25\,^\circ\mathrm{C}, p = 1013.25\,\mathrm{mbar}$

2.3 Pulmonary Mechanics

This section will provide a brief overview about pulmonary mechanics and put them in the context of the pneumatic modelling language. After that, the well-known single compartment model of the human lung is presented and its use is justified against different — generally more complex — models for the context of this thesis.

2.3.1 The Single Compartment Model of the Human Lung

The human airways can be modelled — with the pneumatic elements defined in section 2.2.1 — by what is widely-known as the single compartment model (see figure 2.7).

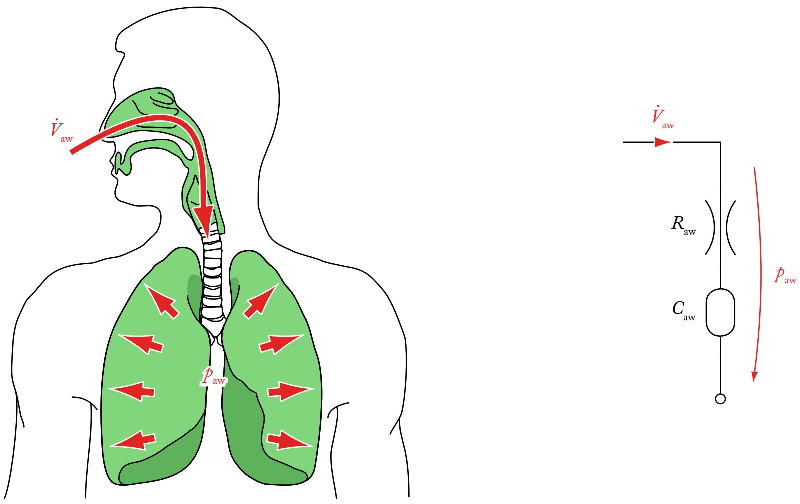

Figure 2.7: Simplified Drawing of the Human Respiratory Tract and its Pneumatic Model: The Single Compartment Model

It shall be noted at this point, that other more complex models exist, of which the DuBois model [27] is given as an example in figure 2.8. The DuBois model also takes into account tissue resistance and compliance, inertance regarding both the airways and the tissue, as well as a pressure source modelling spontaneous breathing. However, the single compartment model is often prefered in clinical practice, as the parameters of more complex approaches often pose difficulties in the identification of their respective values. Furthermore, in pneumatics the mass moved is generally small compared to other fluids considered in hydraulics. Inertance effects are therefore usually negligible [21].

Range of Values Practical values of the airway's pneumatic parameters depend on age and the disease the respective patient suffers from. Figure 2.9 [14, slightly altered] depicts parameter ranges for patients categorised by age. Table 2.3 further quantifies

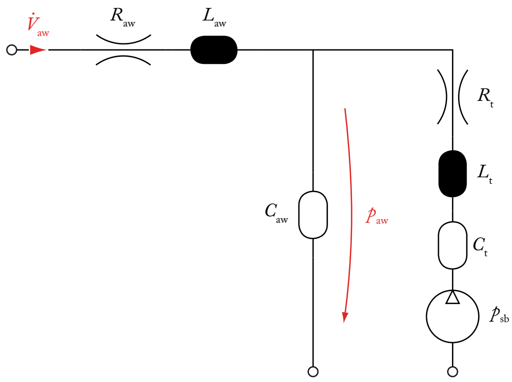

Figure 2.8: The DuBois Model of the Human Respiratory Tract

	Range of Values			
Quantity	Commonly Used Units		SI-Units	
R_{aw}	$2 \ldots 50$	$\frac{\text{mbar}}{\text{L/s}}$	$100{,}000 \ldots 5{,}000{,}000$	$\frac{\text{Pa}}{\text{m}^3/\text{s}}$
C_{aw}	$0.01 \ldots 0.1$	$\frac{\text{L}}{\text{mbar}}$	$0.01 \ldots 0.1 \cdot 10^{-5}$	$\frac{\text{m}^3}{\text{Pa}}$
$\dot{V}_{aw}$	$0 \ldots 300$	$\frac{L}{\text{min}}$	$0 \ldots 0.005$	$\frac{\text{m}^3}{\text{s}}$
p_{aw}	$0 \ldots 100$	mbar	$0 \ldots 100{,}000$	Pa

Table 2.3: Range of Values Regarding the Respiratory Tract and Single Compartment Model [32]

these ranges and provides a comparison between the commonly used units and SI-units.

2.3.2 Pathophysiology and Influence of Diseases on the Airways' Parameters

Apart from neuromuscular diseases, which require the support or complete take–over of the patient's respiratory function by a ventilation device, there are two main types of diseases associated with the human airways.

Diseases Causing Reduced Compliance (Restrictive Diseases) [28] A reduced compliance may be caused by

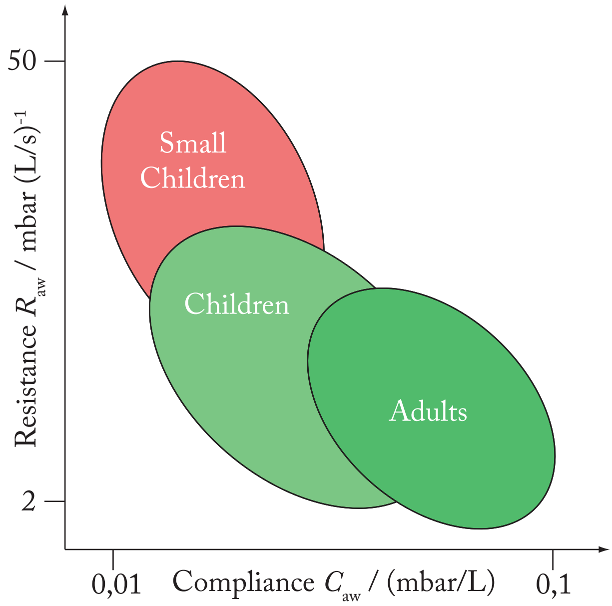

Figure 2.9: Visualisation and Categorisation of the Range of Values Regarding the Respiratory Tract and Single Compartment Model [14, slightly altered]

- Acute Respiratory Distress Syndrome (ARDS)[2],
- Pneumonia,
- Aspiration[3],
- Pulmonary Fibrosis[4],

amongst others. Either the available volume inside the lungs is reduced, or — more likely — the lungs become less elastic, which can be caused by scar tissue, for instance. To further safeguard a sufficient ventilation of the lungs, higher work of breathing is required. Patients suffering from one of the above diseases, therefore usually breathe faster and less deeply [28].

Diseases Causing Increased Resistance (Obstructive Diseases) [28] As becomes obvious from equation 2.30 (law of Hagen–Poiseuille), resistance scales by the inverse of the fourth power of the airways' diameter:

$$R_{\mathrm{aw}} \propto \frac{1}{d_{\mathrm{aw}}^4}.$$

[2]ARDS is the inflammation of the lung caused by a variety of direct and indirect issues.
[3]Aspiration denotes the unwanted intake of fluids or solids alien to the human airways.
[4]Pulmonary fibrosis is the pathological increase of connective tissue inside the lungs.

An increased resistance may be caused by [28]

- Asthma,
- Chronic Obstructive Pulmonary Disease (COPD),

or a functional stenosis (narrowing) of the airways, e.g. induced by a tubus.

Patient's suffering from obstructions usually breathe slowly, since resistance increases with higher flow.

2.4 Mechanical Ventilation

Mechanical ventilation is the full or partial support of gas exchange within the human airways. Spontaneous breathing is thus either fully replaced or assisted. In the most basic ways, this can be done by a physician manually operating a bag with a breathing mask attached. More sophisticated means employ automated mechanical ventilation devices, which are the subject of this thesis.

Traditionally, mechanical ventilators were distinguished as positive pressure and negative pressure ventilators, depending on the sign of the pressure applied relative to atmosphere. Negativ pressure is applied by lifting up the ribcage or contracting the diaphragm by means of underpressure. A famous example of those devices is the iron lung. Positive pressure ventilators ventilate by either invasive or non-invasive access to the airways (cf. figure 2.10).

Masks for non-invasive ventilation generally incorporate leakages, which have to be accounted for by the control algorithms and which provide a natural means for expiration. Invasive ventilation does not make used of masks, but applies flow or pressure via an endotracheal tube or a tracheotomy. Expiration valves are designed as a means to control time of expiration and the expiratory pressure or flow, as well as to provide a defined path for the expired gas.

For the context of this thesis, the term mechanical ventilators usually refers to automated positive pressure ventilation devices as explained above. Additionally this thesis predominantly focuses on invasive ventilation.

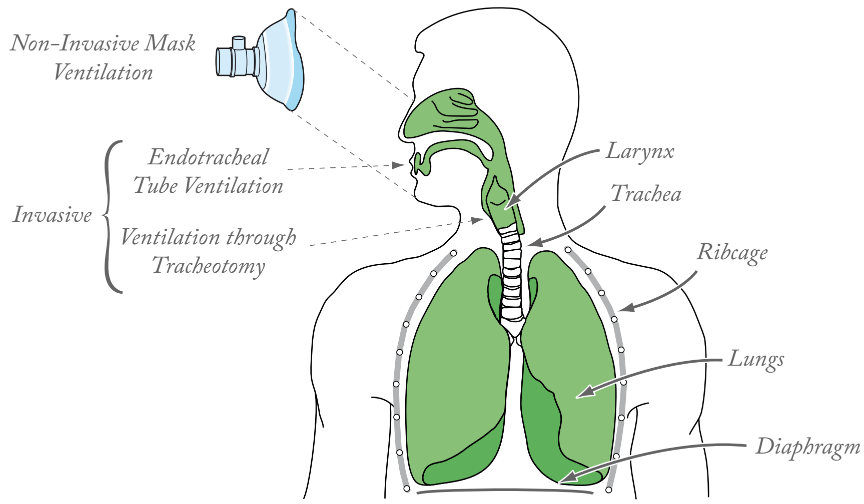

Figure 2.10: Rough Delineation of Anatomy and Non-Invasive and Invasive Access to the Human Airways

2.4.1 Aims of Mechanical Ventilation

Mechanical ventilators are life support devices to replace or partially support the respiratory function of patients. This is done in one or more of the following areas [8], [32]:

1. **Ventilation** facilitates gas exchange and thus eliminates CO_2, in order to achieve a desired arterial pH level,
2. **Pump support** assists breathing by support of the respiratory muscles, short- or long-term.
3. **Oxygenation** aims at increasing the amount of oxygen in the arterial blood.
4. **Protection** aims at preventing the human airways from obstruction or aspiration usually by selecting an appropriate patient interface.

Most generally, these goals are achieved by applying a defined pressure or volume flow at a defined level of oxygen concentration.

Modern mechanical ventilators can be classified into three main categories:

- ICU[5] Ventilators,
- Portable Ventilators,
- Homecare Ventilators.

Homecare devices should blend into the patient's personal life as seamlessly as possible for convenience, still maintaining effectiveness of therapy.

Whereas ICU ventilators generally are host to many different modes of ventilation, since they are stationary devices intended to cover all aspects of clinical applications, modern portable ventilators try to provide similar functionality under the constraint of maximised portability. The latter are used in various situations that place different requirements on their design [18]:

- Primary transfer from an accident scene,
- Secondary transfer between healthcare facilities (intra- or inter-hospital),
- Domiciliary ventilation,
- Improvised intensive care facilities, i.e. military field hospitals, civilian contingency planning.

Portable ventilators are the main focus of this thesis.

[5] Intensive Care Unit

2.4.2 Ventilation Control — Delimitation

Closed-loop ventilation control can be regarded as a two level hierarchical control system depicted by figure 2.11.

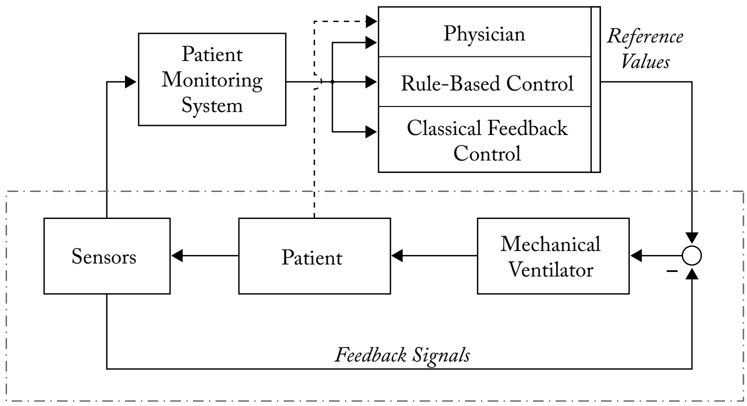

Figure 2.11: Two Level Hierarchical Closed-Loop Control System of Mechanical Ventilation

The inner, fast control loop — denoted by the dashed line — comprises the mechanical ventilator with a reference tracking controller. It operates on an *intrabreath basis*, maintaining ventilatory targets such as those explained in the following section within each single breathing interval [42]. The reference values are set by the outer control loop, which operates on an interbreath basis, adjusting parameters between single or multiple breaths. It can be driven by rule-based control, classical feedback control[6] and/or a physician, who — in addition to evaluating values provided by the patient monitoring system — is also able to infer the patient's state of health by word of mouth or visuals.

2.4.3 Parameters of Mechanical Ventilation

Closed-loop feedback control is subject to a set of parameters, which determine the controlled respiratory function. These will be briefly defined next.

Definition 2.13 (Ventilation Cycle [32]). *A ventilation cycle is the duration from the beginning of the inspiration to the end of the expiration. The total duration is the sum of the durations of inspiration T_{insp} and expiration T_{exp}:*

$$T_{\text{vc}} = T_{\text{insp}} + T_{\text{exp}} \tag{2.42}$$

[6]The term *classical feedback control* refers to driving the control error to zero by a mathematical approach. The control error is denoted the difference between reference signal and feedback signal.

Definition 2.14 (Frequency of Ventilation [32]). *The frequency of ventilation is the amount of breaths per time unit:*

$$f_{\mathrm{vc}} = \frac{1}{T_{\mathrm{vc}}} \tag{2.43}$$

Definition 2.15 (I:E Ratio [32]). *The ratio between the duration of inspiration and expiration defines the I:E ratio:*

$$\mathrm{I} : \mathrm{E} = \frac{T_{\mathrm{insp}}}{T_{\mathrm{exp}}} \tag{2.44}$$

Definition 2.16 (Tidal Volume and Minute Volume [32]). *The tidal volume V_{tidal} is the air volume introduced into the human airways with each ventilation cycle. The minute volume $\dot{V}_{\mathrm{mv}}$ is defined as the amount of volume ventilated per minute:*

$$\dot{V}_{\mathrm{mv}} = V_{\mathrm{tidal}} \cdot f_{\mathrm{vc}}, \tag{2.45}$$
$$\textit{with } \left[\dot{V}_{\mathrm{mv}}\right] = \frac{\mathrm{L}}{\mathrm{min}} \quad [f_{\mathrm{vc}}] = \frac{1}{\mathrm{min}}.$$

Definition 2.17 (Ventilatory Flow, Pressure and PEEP [32]). *The ventilatory flow and pressure are defined as the flow inside the human airways $\dot{V}_{\mathrm{insp}} = \dot{V}_{\mathrm{aw}}$ of inspired gas at the pressure $p_{\mathrm{insp}} = p_{\mathrm{aw}}$ relative to atmospheric pressure p_{amb}.*

The positive end-expiratory pressure p_{PEEP} is the pressure applied during expiration, against which the patient has to exhale.

Definition 2.18 (Fraction of Inspired Oxygen $\mathrm{F_{iO_2}}$ [32]). *The fraction of inspired oxygen $\mathrm{F_{iO_2}}$ denotes the percentage of oxygen inside the inspiratory gas, where*

$$21\,\mathrm{vol.\,\%} \leq \mathrm{F_{iO_2}} \leq 100\,\mathrm{vol.\,\%} \textit{ holds.}$$

2.4.4 Ventilation Modes

Names for ventilation modes are not standardised and vary between manufacturers, due to patent law, sales strategy and language differences. A three-level denomination system is proposed by [10], which prevents the mixing up of the inner and outer control loop described above. Only the main items relevant for this thesis will be pointed out.

Control Variables Ventilation can be pressure or flow controlled. Flow control implies volume control and vice versa, but the actual value, which is used for feedback enables to distinguish [10]. Both pressure and flow cannot be used for control at the same time, but only on an interbreath basis or in a switching control manner, which aims at limiting the maximum pressure or flow, respectively. A basic control algorithm will thus be refered to either as volume controlled (VCV) or pressure controlled (PCV). A ventilator's inner control system's capability to perform either VCV or PCV and bumplessly switch between these will enable it to perform any combinations on a breath-by-breath basis.

Figure 2.12 displays idealised graphs for both volume control and pressure control and explains the characteristic shapes.

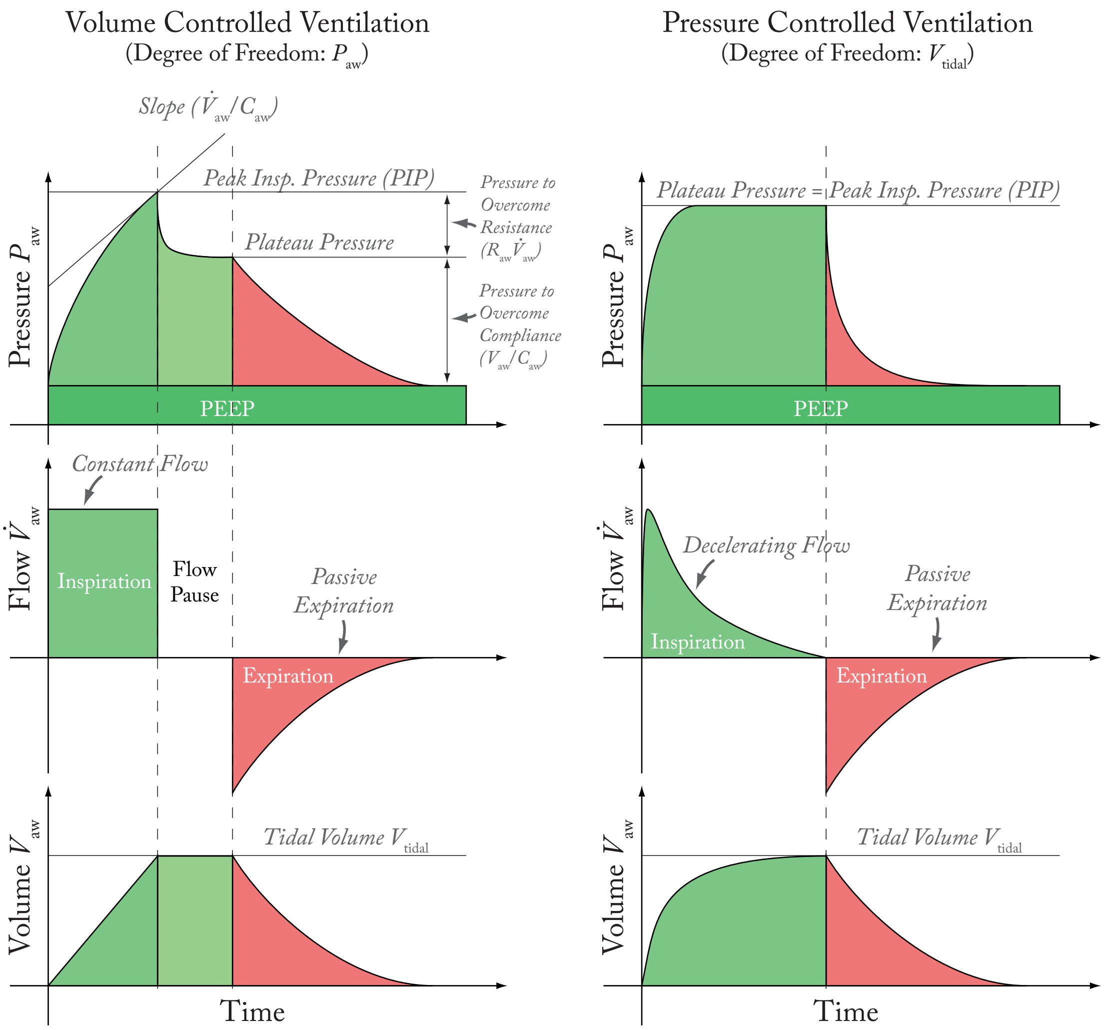

Figure 2.12: Volume Controlled (l.) and Pressure Controlled (r.) Ventilation Curves, [32, compiled and augmented]

Table 2.4 lists indicators and advantages of pressure controlled and volume controlled ventilation.

	Ventilation Mode by Control Variable	
	Volume Controlled	Pressure Controlled
Indicators	Reanimation (CPR), Simple and Safe	Postoperative, COPD, ARDS
Advantages	Simple, Safe (if pressure limited)	Pressure Limitation Equally Pressurised Lung Compartments, Better Oxygenation, Enables Leakage Ventilation, Patient Comfort

Table 2.4: Indicators and Advantages of Volume Controlled and Pressure Controlled Ventilation [32]

Spontaneous, Intermittent and Mandatory Ventilation [10] Continuous mandatory ventilation (CMV) means full ventilatory support: The patient's complete respiratory function is thus taken over by the mechanical ventilator.

Continuous spontaneous ventilation (CSV) triggers ventilatory support by detection of the patient's own effort. Both time and sizing of the breath are patient controlled.

Intermittent mandatory ventilation (IMV) is a combination of both spontaneous and mandatory ventilation. Spontaneous activity is allowed between mandatory breaths. If mandatory breaths are patient triggered, it is referred to as synchronised intermittent mandatory ventilation (SIMV).

Volume controlled ventilation prohibits spontaneous breathing activity, as the ventilation pressure denotes the degree of freedom.

From a ventilator design point of view it is important to allow for spontaneous breathing activity in case of pressure controlled ventilation.

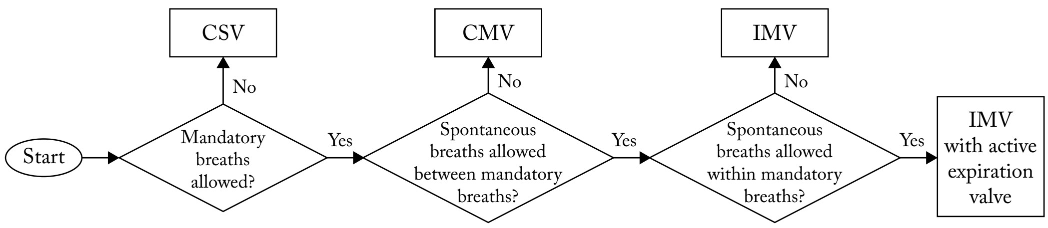

Figure 2.13: Distinction Graph between Continuous Spontaneous, Continuous Mandatory and Intermittent Mandatory Ventilation [10]

2.4.5 Dangers of Mechanical Ventilation

Higher than ambient oxygen levels during mechanical inspiration usually have the goal to prevent a decreased partial pressure of oxygen in the blood (hypoxemia). While, increasing the oxygen content in the blood (hyperoxemia) is a common treatment, it also has its drawbacks. [38] states, that an often seen problem resides in the misconception, that too much oxygen is better than too little. Recent reseach has shown, that both hypoxemia and hyperoxemia can be reasons for increased mortality. These results come in addition to the fact that oxygen in higher concentrations is toxic, because reactive oxygen intermediates can precipitate, causing lung injury. For $F_{iO_2} > 60\,\text{vol.}\,\%$ toxicity is increasing exponentially [28].

These facts give rise to the indication, that mechanical ventilators should be able to deliver the full spectrum of F_{iO_2}, while the ventilation remains in demand for reasonable treatment by the attending physician.

Further dangers result from mechanical injury, that may happen during mechanical ventilation. Pushing inspiratory pressure to levels higher or lower than the inflection points (cf. figure 2.14) can cause the so–called *barotrauma*[7] or *atelectasis*[8], respectively [32],[28].

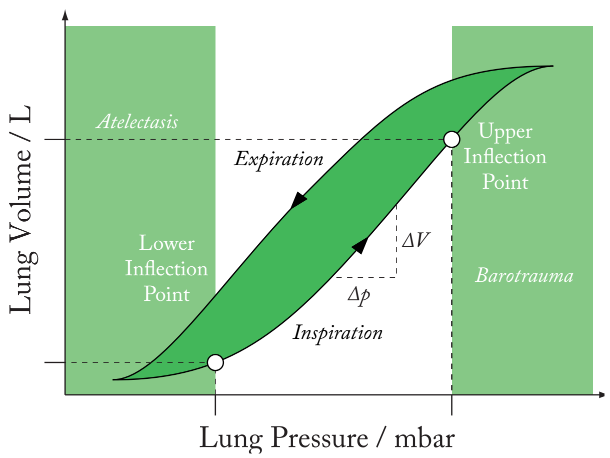

Figure 2.14: Schematic Pressure-Volume Curve During Ventilation and Risks of Barotrauma or Atelectasis [28, slightly altered]

As rectangularly shaped flow or pressure reference profiles are the norm (there is not enough evidence for an indication for sinusoidal, accelerating and decelerating flow [37]), in terms of control systems, the mechanical risks of ventilation can be avoided by imposing the constraint of little or no overshoot to step reference signals.

[7] A barotrauma happens, when the surrounding tissue cannot withstand the increased lung pressure.
[8] Atelectasis means the collapse of parts of the lung.

2.5 Control Theory

2.5.1 Continuous Time and Discrete Time Systems

Linear dynamic systems can be formulated as transfer functions $\mathbf{y}(t) = \mathbf{G}(s)\mathbf{u}(t)$ or state space models:

$$\dot{\mathbf{x}}(t) = \mathbf{A}\mathbf{x}(t) + \mathbf{B}\mathbf{u}(t)$$
$$\mathbf{y}(t) = \mathbf{C}\mathbf{x}(t) + \mathbf{D}\mathbf{u}(t)$$

Both representations are related to each other by

$$\mathbf{G}(s) = \mathbf{C}\left(s\mathbf{I} - \mathbf{A}\right)^{-1}\mathbf{B} + \mathbf{D}$$

While the above formulations represent continuous time behaviour of a system in time or frequency domain, sampled data systems are systems, whose behaviour is defined at discrete sampling intervals $t = k \cdot T_s$ only.

To transform a continuous time system into discrete time, e.g. zero order hold discretisation or a bilinear transformation known as the TUSTIN approximation can be used. Figure 2.15 gives an example of a continous time signal and its discrete counterparts obtained by both zero order hold and TUSTIN discretisation.

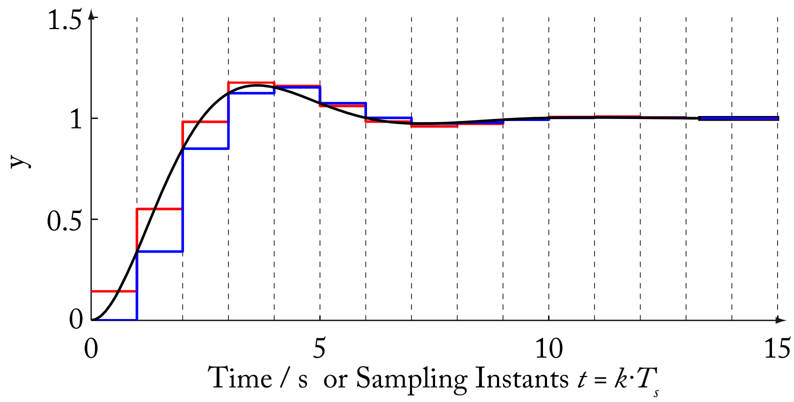

Figure 2.15: Comparison of TUSTIN and Zero Order Hold Discretisation, — Continuous Time Signal, — TUSTIN Approximation, — Zero Order Hold Approximation,

It becomes clear from figure 2.15, that the zero order hold discretisation more accurately describes the sampling of data at discrete time intervals. For this reason, zero order hold discretisation will be refered to as the standard discretisation technique throughout the thesis.

A TUSTIN approximation is obtained by substituting $s = \frac{2}{T_s}\frac{1-z^{-1}}{1+z^{-1}}$, whereas a zero order hold discretisation is given by sampling a signal at time instant $t = k \cdot T_s$ and holding it for the duration T_s. This latter *exact* discretisation is more easily given in terms of the transformation in state space [9]:

$$
\begin{aligned}
\mathbf{x}(k+1) &= \mathbf{\Phi x}(k) + \mathbf{\Gamma u}(k), \\
\mathbf{y}(k) &= \mathbf{Cx}(k) + \mathbf{Du}(k), \\
\text{where } \mathbf{\Phi} &= \mathrm{e}^{\mathbf{A}T_s} = \mathbf{I} + \mathbf{A}T_s + \mathbf{A}^2\frac{T_s^2}{2!} + \dots \\
\mathbf{\Gamma} &= \int_0^{T_s} \mathrm{e}^{\mathbf{A}t}\mathbf{B}\,\mathrm{d}t
\end{aligned}
$$

Again, both representations are related to each other by

$$\mathbf{H}(z) = \mathbf{C}\left(z\mathbf{I} - \mathbf{\Phi}\right)^{-1}\mathbf{\Gamma} + \mathbf{D}.$$

Tables exist, that facilitate direct transformation from continuous time LAPLACE domain into discrete time z domain [23]. Poles are mapped by $z = \mathrm{e}^{-T_s \cdot s}$, but care has to be taken with regard to the zeros. Discretising introduces $n - m$ sampling zeros, where n denotes the number of continuous time poles and m the number of continous time zeros. The excess zeros approach the zeros of the exact discretisation of an integrator of order $n - m$ for $T_s \to 0$.

The z-operator can be interpreted as if it were *shifting time*. Time delays can thus be easily formulated by

$$y(k - k_\mathrm{d}) = y(k) \cdot z^{-k_\mathrm{d}}.$$

Generalised Plant Representations Modern control theory often employs the description of dynamic systems in terms of generalised plants, which also include fictitious inputs $\mathbf{w}$ and outputs $\mathbf{z}$.

$$
\mathcal{P}(s) = \begin{cases} \dot{\mathbf{x}} &= \mathbf{Ax} + \mathbf{B}_{xw}\mathbf{w} + \mathbf{B}_{xu}\mathbf{u} \\ \mathbf{z} &= \mathbf{C}_{zx}\mathbf{x} + \mathbf{D}_{zw}\mathbf{w} + \mathbf{D}_{zu}\mathbf{u} \\ \mathbf{v} &= \mathbf{C}_{vx}\mathbf{x} + \mathbf{D}_{vw}\mathbf{w} + \mathbf{D}_{vu}\mathbf{u} \end{cases} \quad \equiv \quad \mathcal{P}(s) = \left[\begin{array}{c|c} \mathbf{A} & \begin{bmatrix} \mathbf{B}_{xw} & \mathbf{B}_{xu} \end{bmatrix} \\ \hline \begin{bmatrix} \mathbf{C}_{zx} \\ \mathbf{C}_{vx} \end{bmatrix} & \begin{bmatrix} \mathbf{D}_{zw} & \mathbf{D}_{zu} \\ \mathbf{D}_{vw} & \mathbf{D}_{vu} \end{bmatrix} \end{array}\right]
$$

Sometimes this same representation is also used for brevity and transfer function matrix and state space formulations are typically mixed.

[9] Difference in state space matrix or transfer function denomination will be dropped for the remainder of the thesis, where it is clear from the context.

2.5.2 Signal Norms and System Norms

Definition 2.19 (The $\mathcal{L}_2/l_2$ Norm [19])**.** *The $\mathcal{L}_2$ norm is defined as the integral over a signal's magnitude:*

$$\|\mathbf{y}(t)\|_2 = \left(\int_{-\infty}^{\infty} \mathbf{y}(t)^T \mathbf{y}(t) \mathrm{d}t \right)^{\frac{1}{2}}, \tag{2.46}$$

for continuous time systems. For discrete time systems, the norm is termed l_2 and the integral degenerates to a summation:

$$\|\mathbf{y}(k)\|_2 = \left(\sum_{k=-\infty}^{\infty} \mathbf{y}(k)^T \mathbf{y}(k) \right)^{\frac{1}{2}}. \tag{2.47}$$

The $\mathcal{L}_2/l_2$ norm of a signal can often be interpreted as the signals energy, as well as the root mean square value.

Definition 2.20 (The $\mathcal{H}_\infty$ Norm [23])**.** *The $\mathcal{H}_\infty$ norm is the maximum singular value, i.e. the maximum gain over all input directions, over all frequencies:*

$$\|\mathbf{G}(s)\|_\infty = \sup_w \bar{\sigma}\left(\mathbf{G}(j\omega)\right). \tag{2.48}$$

For discrete time systems the $\mathcal{H}_\infty$ norm is defined as

$$\|\mathbf{G}(z)\|_\infty = \sup_z \bar{\sigma}\left(\mathbf{G}(z)\right). \tag{2.49}$$

Figure 2.16 illustrates this.

In combination with the *small gain theorem*, this can be utilised to express a required constraint on the generalised plant with modelled bounded additive uncertainty $\Delta(j\omega)$. It can also be used to express design constraints in terms of shaping filters to achieve certain control objectives. Necessary definitions to understand how these objectives are associated with frequency responses of the closed-loop plant will be explained next.

2.5.3 Design Objectives and Sensitivity Functions

Figure 2.17 depicts a general control loop with negative feedback and defines all relevant signals. Sensitivity functions are a useful tool in frequency domain analysis to judge the closed-loop behaviour of a system. The are defined as follows [23]:

Definition 2.21 (Sensitivity Functions)**.** *The transfer function* $\mathbf{S}(s)$ (Sensitivity) *describes closed-loop behaviour according to* $\mathbf{e} = \mathbf{S}(\mathbf{r} - \mathbf{n} - \mathbf{d})$ *and is calculated as*

$$\mathbf{S}(s) = (\mathbf{I} + \mathbf{G}(s)\mathbf{K}(s))^{-1}. \tag{2.50}$$

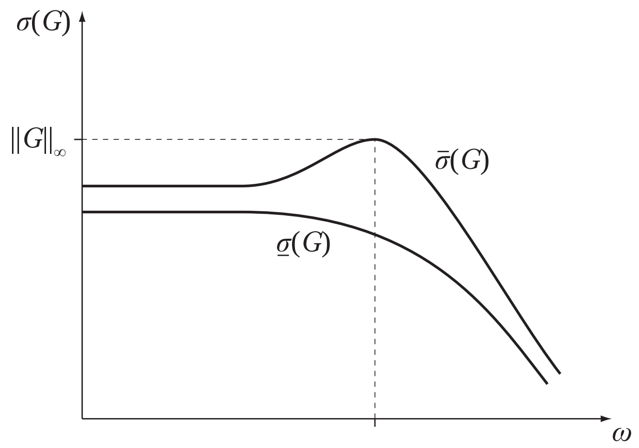

Figure 2.16: Visualisation of the $\mathcal{H}_\infty$ Norm in the Frequency Domain

The transfer function $\mathbf{T}(s)$ (Complementary Sensitivity) *describes closed-loop behaviour according to* $\mathbf{y} = \mathbf{T}(\mathbf{r} - \mathbf{n})$ *and is calculated as*

$$\mathbf{T}(s) = (\mathbf{I} + \mathbf{G}(s)\mathbf{K}(s))^{-1}\mathbf{G}(s)\mathbf{K}(s) = \mathbf{I} - \mathbf{S}(s). \tag{2.51}$$

The transfer function $\mathbf{KS}(s)$ (Control Sensitivity) *describes closed-loop behaviour according to* $\mathbf{u} = \mathbf{KS}(\mathbf{r} - \mathbf{n} - \mathbf{d})$ *and is calculated as*

$$\mathbf{KS}(s) = \mathbf{K}(s)\mathbf{S}(s) = \mathbf{K}(s)(\mathbf{I} + \mathbf{G}(s)\mathbf{K}(s))^{-1}. \tag{2.52}$$

The transfer function $\mathbf{SG}(s)$ (Input Sensitivity) *describes closed-loop behaviour according to* $\mathbf{y} = \mathbf{SGi}$ *and is calculated as*

$$\mathbf{SG}(s) = \mathbf{S}(s)\mathbf{G}(s) = (\mathbf{I} + \mathbf{G}(s)\mathbf{K}(s))^{-1}\mathbf{G}(s). \tag{2.53}$$

The same holds for discrete time systems. Desired closed-loop behaviour can be interpreted in terms of the sensitivity functions defined above and can be summarised as follows:

Ideal Reference Tracking Requires that $\mathbf{S}(s)$ is small, $\mathbf{T}(s)$ should be 1, respectively. Having this at low frequencies means good reference tracking for static reference inputs.

Disturbance Rejection Requires that $\mathbf{S}(s)$ is small.

Noise Attenuation Requires $\mathbf{T}(s)$ to be small. Noise rejection is generally wished for at higher frequencies. Thus $\mathbf{T}(s)$ should show low pass behaviour, attenuating the measurement noise frequency.

Control Effort Requires that $\mathbf{KS}(s)$ is reasonably bounded. $\mathbf{KS}(s)$ being small at higher frequencies also reduces excessive control action, i.e. oscillations.

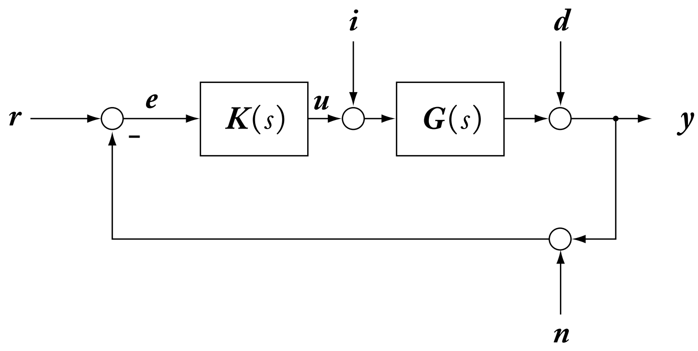

Figure 2.17: General Control Loop with Controller $\mathbf{K}(s)$, Plant $\mathbf{G}(s)$, Reference Input $\mathbf{r}(t)$, Control Error $\mathbf{e}(t)$, Controller Output $\mathbf{u}(t)$, Plant Output $\mathbf{y}(t)$, Input Disturbance $\mathbf{i}(t)$, Output Disturbance $\mathbf{d}(t)$ and Measurement Noise $\mathbf{n}(t)$

2.5.4 Controller Design Tools

$\mathcal{H}_\infty$-Norm Based Mixed Sensitivity Controller Design Controller design based on the $\mathcal{H}_\infty$ norm usually has the aim to achieve certain objectives on $\|\cdot\|_\infty$ subject to closed-loop stability. [19]

When refering to mixed sensitivity controller design, these objectives are to shape the sensitivities according to the criteria given above. Employing the $\mathcal{H}_\infty$ norm, this can be done by defining weights in the form of shaping filters, that pose constraints

$$\|\mathbf{W}(s)\mathbf{S}_{21}(s)\|_\infty < 1$$

on some sensitivity function $\mathbf{S}_{21}$ from input 1 to output 2. These inputs and outputs may well be fictitious. Figure 2.18 shows how the generalised plant for $\mathcal{H}_\infty$-norm based mixed sensitivity controller design is constructed if sensitivity $S(s)$, complementary sensitivity $T(s)$ and control sensitivity $K(s)S(s)$ are to be shaped by the respective filters $W_S(s)$, $W_T(s)$ and $W_{KS}(s)$.

The respective constraints on the closed-loop behaviour are

$$\left\| \begin{bmatrix} \mathbf{W}_S(s)\mathbf{S}(s) \\ \mathbf{W}_{KS}(s)\mathbf{K}(s)\mathbf{S}(s) \\ \mathbf{W}_T(s)\mathbf{T}(s) \end{bmatrix} \right\|_\infty < 1 \Leftrightarrow \|\mathbf{T}_{zr}(s)\|_\infty < 1.$$

If this constraint is posed this way, a maximum approximation error occurs, if the individual shaping constraints are equal in magnitude. This approximation error goes to zero, in frequency regions, where only one constraint is “active”, i.e. all the other magnitudes are small.

Table 2.5 lists typical first order shaping filters, with ω_{cl} denoting the desired closed-loop bandwidth.

	Frequency Response	
	Filter	Inverse Filter
Sensitivity $W_S(s) = \frac{\omega_\varepsilon}{M_S \omega_{\mathrm{cl}}} \frac{s+\omega_{\mathrm{cl}}}{s+\omega_\varepsilon}$ $0 < \omega_\varepsilon \ll \omega_{\mathrm{cl}}$	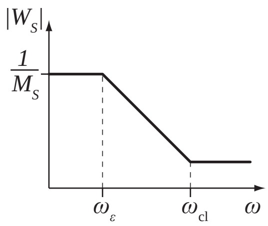	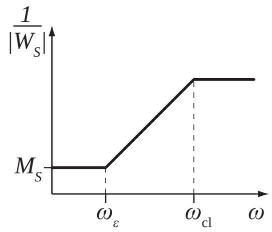
Control Sensitivity $W_{KS}(s) = \frac{c}{M_{KS}} \frac{s+\omega_{\mathrm{cl}}}{s+c\omega_{\mathrm{cl}}}$ $c \gg 1$	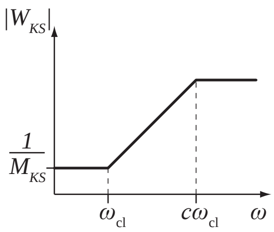	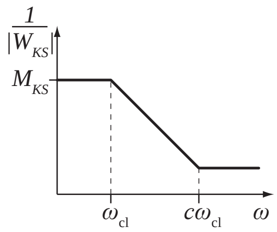
Complementary Sensitivity $W_T(s) = \frac{c}{M_T} \frac{s+\omega_{\mathrm{cl}}}{s+c\omega_{\mathrm{cl}}}$ $c \gg 1$	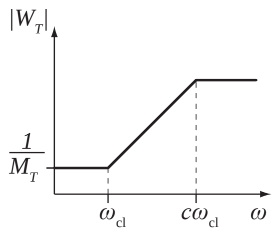	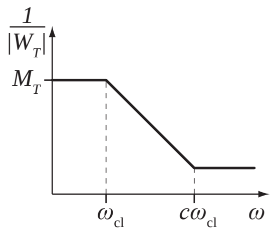

Table 2.5: Overview about Standard Shaping Filters for Mixed Sensitivity $\mathcal{H}_\infty$-Norm Based Controller Design [23], [29]

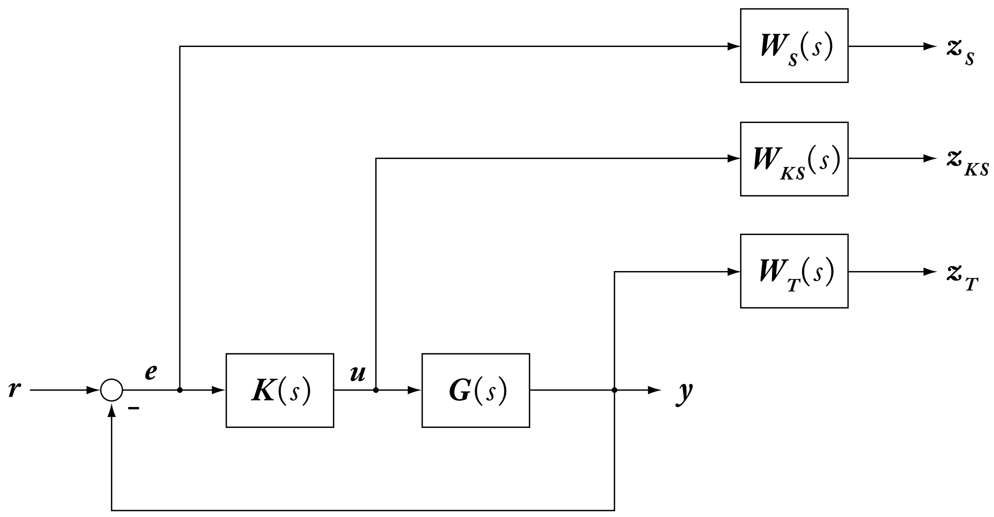

Figure 2.18: Construction of the Generalised Plant for $\mathcal{H}_\infty$-Norm Based Mixed Sensitivity Controller Design [23]

The $\mathcal{H}_\infty$ norm based design for sensitivity shaping can be solved by posing the problem as a linear matrix inequality (LMI). The LMI is given only for the continous time case for brevity.

Theorem 2.1 ($\mathcal{H}_\infty$ Performance for Continuous Time Systems [23])**.** $\|\mathbf{T}\|_\infty < \gamma$ *if and only if there exists a positive definite, symmetric matrix* $\mathbf{P}$ *that satisfies the linear matrix inequality*

$$\begin{bmatrix} \mathbf{AP} + \mathbf{PA}^T & \mathbf{B} & \mathbf{PC}^T \\ * & -\gamma\mathbf{I} & \mathbf{D}^T \\ * & * & -\gamma\mathbf{I} \end{bmatrix} < 0, \tag{2.54}$$

$$\textit{with } * \textit{ indicating symmetric completion.} \tag{2.55}$$

γ *denotes the* $\mathcal{H}_\infty$ *performance.*

The above theorem has to be expressed in terms of the closed-loop system, which involves a linearising change of variables and some algebra. How this is solved in detail can be read in [23]. MATLAB tools are readily available, which solve this problem in continous time. The solution is a controller with the same dynamic order as the plant. This may often be too complex for actual implementation. Furthermore, controller synthesis in continuous time with consequent discretisation of the controller demands for sampling frequencies of $\omega_s > 20 \ldots 30 \cdot \omega_{cl}$ and poses additional problems, with regard to explicitly taking into account time delayed plants.

Further theorems and tools, which directly apply to discrete time systems have been developed. One used in this thesis will be briefly explained next.

$\mathcal{H}_\infty$ Norm Based Design of Fixed Order Controllers Synthesis of fixed order controllers based on the $\mathcal{H}_\infty$ norm is an active field of research [51]. Solutions have been proposed based on bilinear matrix inequalities or iterative algorithms. A solution belonging to the latter is the MATLAB toolbox HIFOO , which has been developed to deal with the synthesis of $\mathcal{H}_\infty$ norm optimal controllers of dynamic orders lower than that of the plant, or even with controllers predefined in structure and order [9]. Additionally, constraints can be imposed for a family of plants, asking the algorithm to search for a single controller to robustly guarantee stability and performance with performance measure γ. The toolbox has been extended to carry out the design for discrete time systems as well (HIFOOD) [35].

The controller synthesis is carried out in two steps by gradient–based search techniques:

1. **Stabilisation** First a set of controllers $\mathbf{K}_i(s)$ or $\mathbf{K}_i(z)$, respectively, is sought, which stabilises the closed-loop system, thus guaranteeing robust stability. This is done by minimizing the maximum real part of the closed-loop eigenvalues.
2. **Optimisation** The closed-loop $\mathcal{H}_\infty$ norm is then optimised, in order to try and guarantee robust performance with performance measure γ.

With LMI based $\mathcal{H}_\infty$ controller synthesis described above, stability is implicit, due to the appearance of the LYAPUNOV stability equation in the LMI conditions. This is not the case with the gradient–based tool HIFOO, which is why the above two distinct steps are necessary.

Finding a robust low or fixed order controller is a non–convex problem. The gradient–based nature of the optimisation approach would thus make the tool prone to getting stuck in local minima. This is dealt with by multiple iterations with randomly choosen additional initial controllers to supplement the previous best solution. Reports have shown, that despite the local search approach, HIFOO leads to good results [5], [35].

2.5.5 Generalised LMI-Based Synthesis of Anti–Windup Compensation for Discrete Time Systems

Most common controller synthesis methods do not take actuator constraints into account. If controllers with (near) integral action are employed and a system is driven to its physical limits, a phenomenon called *integrator windup occurs*: While the system's actuator is constrained, integrators charge up, trying to no avail to enforce faster settling to the desired reference value. The system overshoots, because the integrators need additional time to discharge again. The left plot in figure 2.19 illustrates this. *Anti-windup* measures generally feed back the extent of controller action surpassing the constraints to the controller. Figure 2.20 displays a typical control loop with actuator saturation and anti-windup feedback.

While it makes intuitive sense to subtract $\delta = \mathbf{u} - \hat{\mathbf{u}}$ from the error signal entering a PID controller's integrator, controller's of arbitrary structure are more difficult to modify.

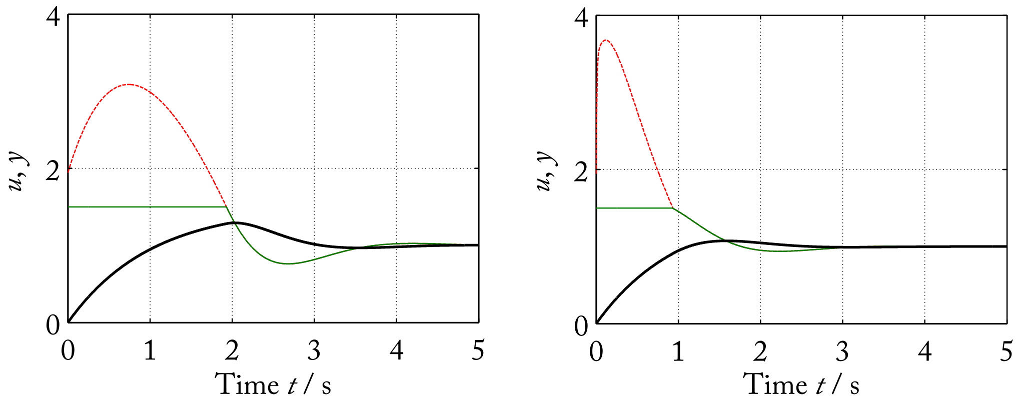

Figure 2.19: Exemplary Step Responses with (r.) and without (l.) Anti-Windup Control, —— System Response y, —— Constrained System Input $\hat{u}$, ---- Unconstrained System Input u

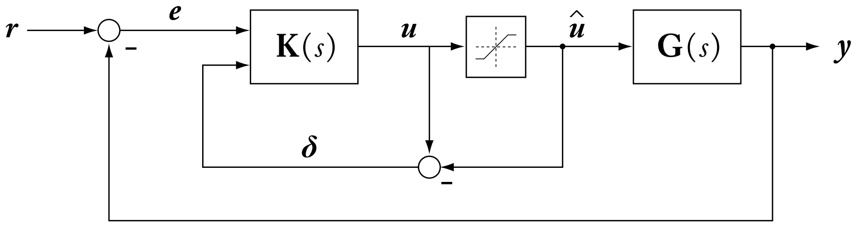

Figure 2.20: Typical Control Loop with Actuator Saturation and Anti-Windup Feedback

A general framework for the formulation of anti-windup designs, applicable to MIMO systems, is given in [26]. Amongst others, *high gain conventional anti-windup*, which forms an altered control error $\hat{\mathbf{e}} = \mathbf{e} - \alpha\delta, \alpha \gg 1$ and the above mentioned *anti-reset-windup* applied to PI/PID controllers are special cases of the described framework. A common approach is to first synthesise a nominal controller and afterwards augment it by some anti-windup scheme. [41] proposes such a scheme in the form of a LMI-based *explicit static anti-windup scheme* for discrete time systems, which has been used in this thesis and the relevant information for its application is given in the following theorem.

Theorem 2.2. *(Explicit Static Anti-Windup Synthesis for Discrete Time Systems) [41] Define the diagonal saturation* $\hat{\mathbf{u}} = \mathbf{\Psi}(\mathbf{u})$ *with sector condition* $\mathbf{u}^T\mathbf{W}(\mathbf{u} - \hat{\mathbf{u}}) \geq 0$, $\mathbf{W}$ *being an arbitrary positive definite diagonal matrix and the stable, strictly proper plant*

$$\mathcal{G}(z) = \left[\begin{array}{c|c} \mathbf{A}_g & \mathbf{B}_g \\ \hline \mathbf{C}_g & \mathbf{0} \end{array}\right] \tag{2.56}$$

with n_g states, n_u inputs and n_y outputs. Further define the nominal controller

$$\mathcal{K}(z) = \left[\begin{array}{c|c} \mathbf{A}_k & \mathbf{B}_k \\ \hline \mathbf{C}_k & \mathbf{D}_k \end{array}\right] \tag{2.57}$$

with order n_k. Also define the augmented explicit static anti-windup controller

$$\bar{\mathcal{K}}(z) = \left[\begin{array}{c|cc} \begin{bmatrix} \mathbf{A}_k & \mathbf{0} \\ \mathbf{0} & \mathbf{0} \end{bmatrix} & \begin{bmatrix} \mathbf{\Lambda}_1 \\ \mathbf{\Lambda}_2 \end{bmatrix} & \begin{bmatrix} \mathbf{B}_k \\ \mathbf{0} \end{bmatrix} \\ \hline \begin{bmatrix} \mathbf{C}_k & \mathbf{I} \end{bmatrix} & \begin{bmatrix} \mathbf{0} \end{bmatrix} & \begin{bmatrix} \mathbf{D}_k \end{bmatrix} \end{array}\right] \tag{2.58}$$

with order $n_k + n_u$ and additional input $\delta(k)$. The interconnection as given in figure 2.21

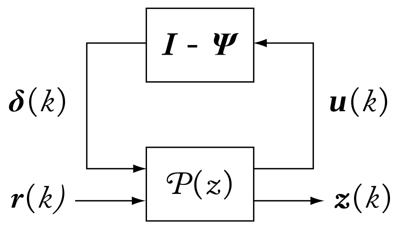

Figure 2.21: Generalised Interconnection of Generalised Plant and Saturation

formulated as a generalised plant

$$\mathcal{P}(z) = \begin{cases} \mathbf{x}(k+1) & = \mathbf{A}\mathbf{x}(k) + \mathbf{B}\delta(k) + \mathbf{B}_r\mathbf{r}(k) \\ \mathbf{u}(k) & = \mathbf{C}_u\mathbf{x}(k) + \mathbf{D}_u\delta(k) + \mathbf{D}_{ur}\mathbf{r}(k) \\ \mathbf{z}(k) & = \mathbf{C}_z\mathbf{x}(k) + \mathbf{D}_z\delta(k) + \mathbf{D}_{zr}\mathbf{r}(k) \end{cases} \tag{2.59}$$

with matrices

$$\mathbf{A} = \begin{bmatrix} \mathbf{A}_g - \mathbf{B}_g\bar{\mathbf{D}}_k\mathbf{C}_g & \mathbf{B}_g\bar{\mathbf{C}}_k \\ -\bar{\mathbf{B}}_k\mathbf{C}_g & \bar{\mathbf{A}}_k \end{bmatrix}, \quad \mathbf{B} = \mathbf{B}_\delta - \mathbf{B}_e\mathbf{\Lambda},$$
$$\mathbf{B}_\delta = \begin{bmatrix} -\mathbf{B}_g \\ \mathbf{0} \end{bmatrix}, \quad \mathbf{B}_e = \begin{bmatrix} \mathbf{0} \\ \mathbf{I} \end{bmatrix}, \quad \mathbf{B}_r = \begin{bmatrix} \mathbf{B}_g\bar{\mathbf{D}}_k \\ \bar{\mathbf{B}}_k \end{bmatrix},$$
$$\mathbf{C}_u = \begin{bmatrix} -\bar{\mathbf{D}}_k\mathbf{C}_g & \bar{\mathbf{C}}_k \end{bmatrix}, \quad \mathbf{D}_{ur} = \begin{bmatrix} \bar{\mathbf{D}}_k \end{bmatrix}, \quad \mathbf{C}_z = \begin{bmatrix} -\mathbf{C}_g & \mathbf{0} \end{bmatrix},$$
$$\mathbf{D}_{zr} = \begin{bmatrix} \mathbf{I} \end{bmatrix}$$

is globally stable for all $\mathbf{\Psi}$ and has a maximum induced l_2 gain performance of γ, if there exists a matrix $\mathbf{Q} = \mathbf{Q}^T > 0, \mathbf{Q} \in \mathbb{R}^{(n_g+n_k+n_u)\times(n_g+n_k+n_u)}$, a diagonal matrix $\mathbf{M} > 0, \mathbf{M} \in \mathbb{R}^{n_u \times n_u}$, an arbitrary matrix $\mathbf{X} := \begin{bmatrix} \mathbf{\Lambda}_1^T & \mathbf{\Lambda}_2^T \end{bmatrix}^T \mathbf{M} \in \mathbb{R}^{(n_k+n_u)\times n_u}$ and *scalars* $\gamma > 0$, $d > 0$, *such that the following LMIs with objective to minimize* γ *are satisfied:*

$$\begin{bmatrix} -\mathbf{Q} & * & * & * & * & * \\ \mathbf{0} & -\gamma\mathbf{I} & * & * & * & * \\ \mathbf{C}_u\mathbf{Q} & \mathbf{D}_{ur} & -2\mathbf{M} & * & * & * \\ \mathbf{C}_z\mathbf{Q} & \mathbf{D}_{zr} & \mathbf{0} & -\gamma\mathbf{I} & * & * \\ \mathbf{A}\mathbf{Q} & \mathbf{B}_r & \mathbf{B}_\delta\mathbf{M} - \mathbf{B}_e\mathbf{X} & \mathbf{0} & -\mathbf{Q} & * \\ \mathbf{0} & \mathbf{0} & \mathbf{M} & \mathbf{0} & \mathbf{0} & -d\mathbf{I} \end{bmatrix} < 0. \tag{2.60}$$

Refering to figure 2.19 again, the right hand side plot was generated by augmenting the controller with the help of above theorem.

Further theorems, that also consider non-static discrete time anti-windup controllers can be found in [46].

3 Concept Development

This chapter documents the thesis' conceptual phase. The morphological analysis has been chosen as a means to develop a feasible pneumatic structure for a novel ventilation device, preliminarily entitled MeduVent.

At first, the requirement profile for the pneumatic structure is given in a concise way, which actually already forms the first step of the morphological analysis. Section 3.2 expands on the analysis, providing a brief explanation of the method, defining the utilised parameters and stating the results in terms of a synthesis of different concepts. The closing section further evaluates these concepts and gives reasons for the final solution, which is adopted as a functional model and for controller synthesis.

The thesis will continue with the proof of concept in the forthcoming chapters.

3.1 Requirement Profile

The pneumatic structure to be designed has the aim to enhance applicability in the field compared to the MEDUMAT Transport with respect to operation in case of lacking oxygen supplies (cf. section 1.1). Concepts, i.e. their realisation as production models, should be able to provide...

- Support for both robust pressure and volume controlled based modes of ventilation,
- Support for robust control of PEEP,
- Economical use of resources (electric energy and oxygen supply)
- Control of the inspired fraction F_{iO_2} of oxygen within the full physically possible range (21 vol. % to 100 vol. %) for both pressure and volume controlled based modes of ventilation,
- Maintain ventilation functionality for $F_{iO_2} = 21\,\text{vol.}\,\%$ in case of depleted oxygen supplies.
- Light-weight and robust options for construction,
- Compliance with european norm for emergency and transport ventilators [12].

3.2 Morphological Analysis

3.2.1 Method

The general morphological analysis is a method to develop solutions based on the investigation of isolated subproblems invented by Fritz Zwicky [44]. Approaching the problem by this creativity method, lets the user deliberately detach himself from existing solutions. It is the aim to consider the problem at hand from a certain distance, leading to approaches that have previously been unaccounted for.

A complex problem is subdivided into different dimensions to form the *morphological box*.

The procedure according to [44] contains five steps:

1. Concise formulation of the requirement profile for a given problem.
2. Assessment of all parameters relevant for the solution.
3. Construction of the morphological box, including all potential solutions for each parameter.
4. Evaluation of the individual solutions.
5. Synthesis of configurations of solutions and practical application.

In this thesis, the morphological analysis has been used to the extent of two dimensions: Setting up desired *functions* and finding multiple *solutions* for each of them. In the synthesis step, these complementary or contrasting solutions to the individual functions have been combined in feasible ways, in order to derive a new pneumatic concept for the MeduVent ventilation device.

3.2.2 Parameters of the Analysis

From the requirement profile five major functions F1 to F5 have been isolated to construct a morphological box with:

F1 Ambient air source,

F2 Oxygen source,

F3 Realisation of pressure controlled ventilation modes,

F4 Realisation of volume controlled ventilation modes,

F5 PEEP pressure control.

These functions have been chosen, because they characterise the overall pneumatic structure of a ventilation device in just five aspects, while their formulation is closely related to the control of the ventilation.

3.2.3 Morphological Box

Table 3.1 shows the morphological box resulting from possible solutions to the individual functions.

Function	Solution S1	S2	S3	S4	S5	S6	S7
F1 Ambient Air Source	Venturi Injector	Blower (Pressure Source)	Pressurised Clinical Air Reservoir (Flow Source)	Compressor (Flow Source)	Piston Pump (Flow Source)	Double Action Bellow System (Flow Source)	Pneum. Driven Blower
F2 O_2 Source	Pressurised Gas (Flow Source)	N_2 Filtration (Semipermeable Membrane)	N_2 Adsorption (Molecular Sieve)	Gas Centrifuge	Electrolysis		
F3 Pressure Control	Fast Flow Control Valve	Pressure Divider Circuit	Directly by Pneumatic Source	Large Bore Valve			
F4 Flow Control	Flow Control Valve	Flow Divider Circuit	Directly by Pneumatic Source	Large Bore Valve	Fractional Feedback of Flow		
F5 PEEP Control	Leakage Blind	Switching Valves (Gas Pulses)	Controllable Pressure Divider (Prop. Valves)	Dedicated Pressure Source (Small Size Blower)	Main Flow/Pres. Source	Dedicated Flow Source (Small Size Compressor)	Electrically Actuated Patient Valve (Voice Coil)

Table 3.1: Morphological Box Depicting the Isolated Design Objectives and Principles of Solution. *Concept* Ia & Ib, *Concept* Ib only, *Concept* II, *Concept* III

Three major concepts — candidates to the implementation as functional model — have been synthesised from the individual functions. They are indicated by their respective markings.

In the following, the individual solutions for each function are briefly characterised and evaluated in terms of advantages and disadvantages.

3.2.4 Solutions to Functions

F1 — Ambient Air Source A source for ambient air has to function independently from the oxygen supply. The concept realised in the MEDUMAT Transport makes use of a venturi injector, which in principle uses the oxygen's expansion energy to draw in ambient air. Though this principle is efficient, it imposes a lower bound on F_{iO_2}. In terms of the MeduVent ventilation device, it can therefore only be regarded as an additional means to increase energy efficiency by unloading an active ambient air source.

Employing reservoirs of pressurised clinical air immediately raises the risk of depleted supplies during transport, while electrical energy is always more likely to be available.

Blower technology — in contrast to compressors — is very common to medical appliances. Most homecare devices rely on them and the experience gained over the time increases the efficiency obtained in the short–term over solutions that might promise higher efficiency after long–term research. A blower is an ideal pressure source as a first approximation. Given the fact, that — at the level of current knowledge — pressure controlled ventilation hosts more advantages and is more frequently indicated than volume controlled ventilation (cf. table 2.4), it is a suitable choice.

Other flow sources, like a double action bellow system is more suited to closed–loop anesthesia and requires a relatively large constructional volume, while piston pumps generate unacceptable pulsation.

Table 3.2 summarises the advantages and disadvantages of the respective solutions.

	Solution	Evaluation	
		Pro	Contra
S1	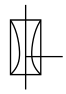 Venturi Injector	+ Uses O_2 expansion energy + Low constructional effort	- Limited lower F_{iO_2} bound - Passive, difficult control - Limited (O_2) flow, if injection channel closed
S2	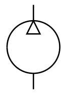 Blower (Pressure Source)	+ Ideal for pressure control + Low research effort + Multi-stage design increases efficiency	- Energy consumption - Relatively slow response
S3	 Pressurised Clinical Air Reservoir (Flow Source)	+ Ideal for flow control + Low research effort	- Stationary - Requires infrastructure
S4	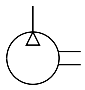 Compressor (Flow Source)	+ Ideal for flow control + Possibly higher efficiency	- High research effort (medical applications rare)
S5	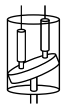 Piston Pump (Flow Source)		- Pulsation inacceptable
S6	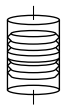 Bellow (Flow Source)	+ Experience from anesthesia + Semi–continuous flow if doubly actuated	- Bellow volume limited (not feasible for leakage or NIV systems) - Requires relatively large constructional space
S7	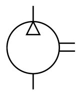 Pneumatically Driven Blower (Pressure Source)	+ Uses O_2 expansion energy	- Limited lower F_{iO_2} bound - Passive, difficult control - Mechanically complex

Table 3.2: Solutions to Function **F1** — Ambient Air Source

F2 — Oxygen Source Despite the fact, that an oxygen infrastructure in most developed countries is usually well established, alternatives to the dependence on pressurised oxygen from bottles or hospital supplies have been sought.

Oxygen concentrators used in homecare solutions employ molecular sieves to adsorb nitrogen from the ambient air to achieve oxygen concentrations of up to 96 %. Relatively high pressures are necessary, though, and flow rates are usually limited to be well under 10 L/ min.

Arising from the idea of non-dissipative oxygen sensors, the deprivation of ambient air from oxygen by a semi-permeable membrane (mechanical filtration) is thinkable as well. This principle is already employed for the filtration of helium in oxygen rebreather diving equipment. However, no existing research with regard to nitrogen is known to the author.

The same goes for adopting gas centrifuges to the needs of oxygen enrichment. A gas centrifuge can separate components of gas mixtures by molecular weight and is primarily used to separate uranium 235 from uranium 238 in the process of the enrichment of uranium. Numerous adverse requirements makes this unfeasible for ventilation purposes.

Electrolysis in solid oxide electrolysis cells can be used for oxygen regenerative air revitalisation systems as employed in space engineering [33]. Energy demand prohibits this approach, though.

Table 3.3 again summarises the advantages and disadvantages of the respective proposed solutions.

		Evaluation	
	Solution	Pro	Contra
S1	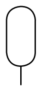 Pressurised Gas (Flow Source)	+ Ideal for flow control + Existing technology and infrastructure	- Limited supplies
S2	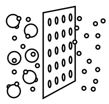 N_2 Adsorption by Molecular Sieve	+ Unlimited supply + Existing technology (O_2 concentrators)	- Low flow rates only - High pressures over sieve
S3	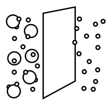 N_2 Filtration by Semi-permable Membrane	+ Unlimited supply	- Low flow rates only - High amount of research necessary
S4	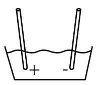 Electrolysis	+ Unlimited supply	- High energy consumption
S5	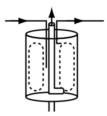 Gas Centrifuge	+ Unlimited supply	- High energy consumption - Low efficiency

Table 3.3: Solutions to Function **F2** — Oxygen Source

F3 — Pressure Control and F4 — Volume Control Means to provide good quality of pressure and volume control generally depend on the possibilities to convert the pneumatic power sources chosen into the respective need of the ventilation modes.

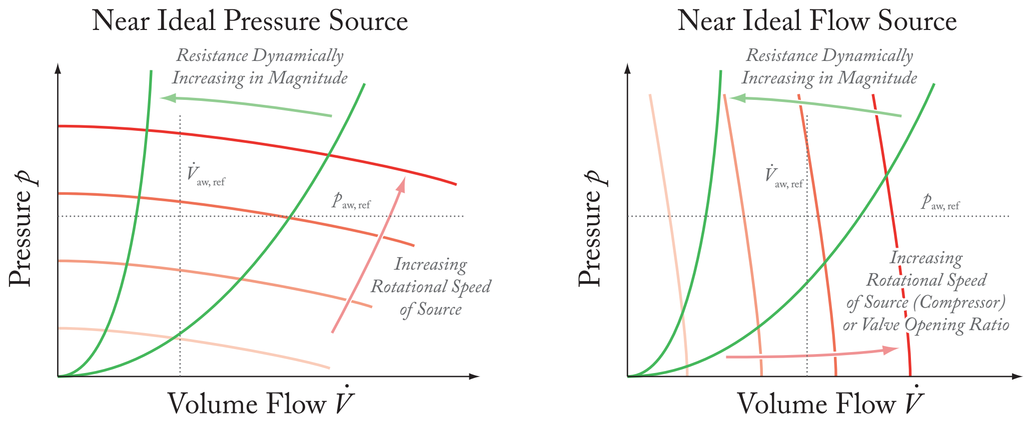

Figure 3.1: Comparison of Near Ideal Pressure and Flow Source and Schematic Visualisation of Dynamically Varying System Characteristic

Volume controlled ventilation using a near ideal pressure source, requires highly dynamic control of the source. Figure 3.1 compares how operating points evolve as the intersection of a dynamically varying system characteristic and a near ideal pressure or flow source. It becomes obvious, that a near ideal pressure source — i.e. a blower — would therefore

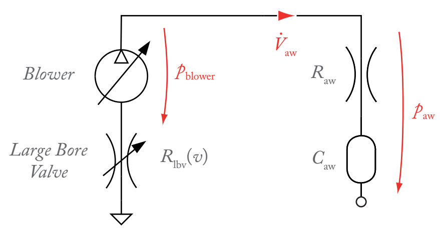

Figure 3.2: Basic Pneumatic Network Topology for Using a Blower in Conjunction with a Large Bore Valve for Flow Control

benefit from a large bore valve in series, which converts pressure energy to flow energy by controlling the opening ratio (cf. figure 3.2). Assuming that the valve's resistance is dominating the system characteristic during the dynamic control phase,

$$R_{\text{lbv}} \gg |\underline{Z}_{\text{aw}}(s)| = \left| R_{\text{aw}} + \frac{1}{sC_{\text{aw}}} \right|, \quad s > 0$$

flow can be controlled by observing,

$$\dot{V}_{\text{aw}} = \frac{p_{rmblower}}{R_{\text{lbv}}} = f(R_{\text{lbv}}).$$

The reciprocal reasoning is valid, when an attempt is made to employ a flow source for pressure control, except that the valve should be put in parallel to the source.

Using the valve as the main actuator for pressure control, while still using a pressure source, on the other hand, is theoretically feasible, as much faster dynamics and a lower energy consumption of the valve can be assumed. This generates pneumatic losses, which may be unwanted for, though. These losses, however, might be acceptable, if high ventilation frequencies, e.g. in pediatrics, are necessary and it is both more energy efficient and beneficial in terms of control quality to keep a blower at a near constant level.

Flow divider or pressure divider circuitry mark two more basic principles of converting pneumatic power sources. They come at the risk of producing losses in the amount of gas transported, though.

These losses could be reduced by feeding back portions of the flow to recirculate, which is restricted by the amount of cooling necessary for the pneumatic power source.

Tables 3.4 and 3.5 list the advantages and disadvantages of the respective proposed solutions for both pressure control and volume control related topological solutions.

	Solution	Evaluation	
		Pro	Contra
S1	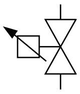 Fast Flow Control Valve	+ Existing technology	- Requires high pressure at inlet - Highly dynamic pressure control
S2	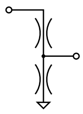 Pressure Divider Circuit	+ High quality of control	- Losses of gas
S3	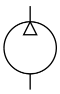 Directly by Pneumatic Source	+ High quality of control for native pressure sources	- Lowered efficiency due to many changes in source duty cycles
S4	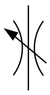 Large Bore Valve	+ Low response time + Low energy consumption	- Pneumatic losses - Need for highly dynamic pressure control

Table 3.4: Solutions to Function **F3** — Pressure Control

	Solution	Evaluation	
		Pro	Contra
S1	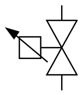 Fast Flow Control Valve	+ Existing technology + Well suited to flow control under supercritical flow conditions	- Requires high pressure at inlet
S2	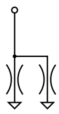 Flow Divider Circuit	+ High quality of control	- Losses of gas
S3	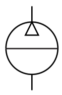 Directly by Pneumatic Source	+ High quality of control for native flow sources	- Lowered efficiency due to many changes in source duty cycles
S4	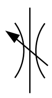 Large Bore Valve	+ Low response time + Low energy consumption + Well suited for conversion of pressure to flow source	- Pneumatic losses
S4	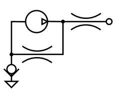 Fractional Feedback of Flow	+ Potentially no losses + Well suited for conversion of pressure to flow source	- Pneumatic losses - Heat is trapped in feedback

Table 3.5: Solutions to Function **F4** — Flow Control

F5 — PEEP Control The pneumatic design of the MEDUMAT Transport employs are very small orifice — an intentional leakage blind — to convert a small flow to a pressure, which is then transmitted via a pilot line to the pneumatically actuated expiration valve, resembling a pilot-to-close check valve. A related concept makes use of switching valves, which either open to charge or to discharge a small compliance. This cost effective solution is difficult to control in terms of classical control systems approaches, though.

Solutions making use of dedicated pneumatic sources are left out from the discussion, but are listed in table 3.6 for completeness. This is done, because during the analysis, it has been observed, that means of controlling PEEP can largely be developed independently from volume or pressure control. If the main pneumatic power sources are employed in contrast to dedicated ones, it is again a question of effectively converting flow or maintaining pressure.

Furthermore, another general question about PEEP control deals with whether the expiration valve should be located near the patient or inside the ventilation device's housing. This is partly related to the chosen principle for PEEP control, but does not contribute to the main aspects of this thesis. Again, for completeness table 3.7 lists advantages and disadvantages related to the placement of the expiration valve.

		Evaluation	
	Solution	Pro	Contra
S1	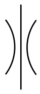 Leakage Blind	+ Existing technology + Conversion of flow to pressure	- Minimal gas losses
S2	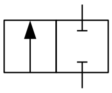 Switching Valves	+ Existing technology + Fast response + Cost effective	- Difficult control
S3	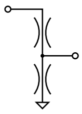 Controllable Pressure Divider	+ High quality of control	- Patented solution
S4	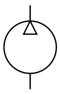 Main Pneumatic Power Source	+ Simplicity	- Frequent load cycles
S5	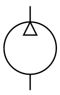 Dedicated Pressure Source	+ High quality of control + Independent from inspiratory control + Low energy consumption of the source	- Additional actuator - Main pneumatic sources inactive during expiration
S6	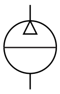 Dedicated Flow Source	+ Independent from inspiratory control + Low energy consumption of the source	- Not well suited for pressure control - Additional actuator - Main pneumatic sources inactive during expiration
S7	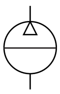 Electrically Actuated Patient Valve (Voice Coil)	+ Dedicated and direct actuation	- High energy consumption - Additional actuator - Main pneumatic sources inactive during expiration

Table 3.6: Solutions to Function **F5** — PEEP Control

	Evaluation	
Solution	Pro	Contra
Expiratory Valve Inside Housing	+ Many options for valve control: electric, pneumatic + Easy integration of leakage ventilation	- Increased hose compliance due to double tube ventilation hose - Quadratically increased hose resistance if tube area decreases - Contamination by patient's expired gas; filter needed
Expiratory Valve Near Patient	+ Single tube ventilation hose + Reduced ventilation hose compliance and resistance	- PEEP pilot pressure signal delayed by speed of sound - Accumulation of oxygen near patient and in patient's clothes - weight raises danger of extubation, especially with infants

Table 3.7: Advantages and Disadvantages of Possible Expiratory Valve Placements

3.3 Candidate Evaluation

The main concepts extracted from the morphological box have already partly undergone an evaluation, since only combinations of solutions have been selected, that were definitely able to deliver the full spectrum of oxygen concentrations. As a further step, the candidate concepts chosen are evaluated based on a condensed requirement profile given by the items:

E1 Energy and resource efficiency,

E2 Potential for high quality of control (PCV, VCV, PEEP),

E3 Research and constructional effort, robustness.

3.3.1 Common Principles

As becomes obvious from the morphological box given in table 3.1, the synthesised candidate concepts share a number of principles. The core idea, that has been decided to investigate consists of employing a blower in conjunction with a large bore valve, to make sure that quality of control for both volume controlled ventilation and pressure controlled ventilation is high. In addition, prepressurised oxygen together with a fast proportional flow control valve is regarded as the most realistic oxygen source. It can cater to the prevailing demands in emergency medicine, both in terms of flow capabilities, disposability and research effort.

As discussed previously, PEEP control can be designed to be largely independent from the power sources and control principles employed for the inspiration phase. However, it is deemed desirable to first investigate solutions that do without additional actuators and assess the quality of control thus obtained. Therefore, all concepts rely on controlling PEEP via a blind, a solution established in the MEDUMAT Transport . It is assumed and subject to verification, that this principle is feasible in all ventilatory situations with respect to the proposed MeduVent designs as well.

For lack of non-consuming and sufficiently reliable F_{iO_2} sensors, no dedicated F_{iO_2} sensor is used for feedback. Instead, the oxygen concentration is calculated from the respective flows. To reduced losses, the oxygen flow is measured on a high pressure level ($\approx 3\,\mathrm{bar}$) in front of the proportional valve, rendering the pressure drop over the sensor insignificant.

Excess and emergency pressure valves are common to all designs as well, making sure, that the patient is both protected from pressures exceeding $100\,\mathrm{mbar}$ and enabled to draw in additional air, in case of system failure.

3.3.2 Concept I

The pneumatic structure is based on a modular design: It essentially consists of two ventilation devices, one of which can provide $F_{iO_2} = 100\,\text{vol.}\,\%$, while the other can provide $F_{iO_2} = 21\,\text{vol.}\,\%$. They are joined at a mixing chamber with a PEEP blind attached to it. The large bore valve is put in front of the blower, as a decrease of up to 20 % in power consumption can be expected for particular blower designs, in case of a totally closed valve. This has been verified experimentally. To ensure a sufficient cooling flow, a fixed leakage is introduced at the blower outlet.

A pneumatic network topology of concept Ia is given in figure 3.3.

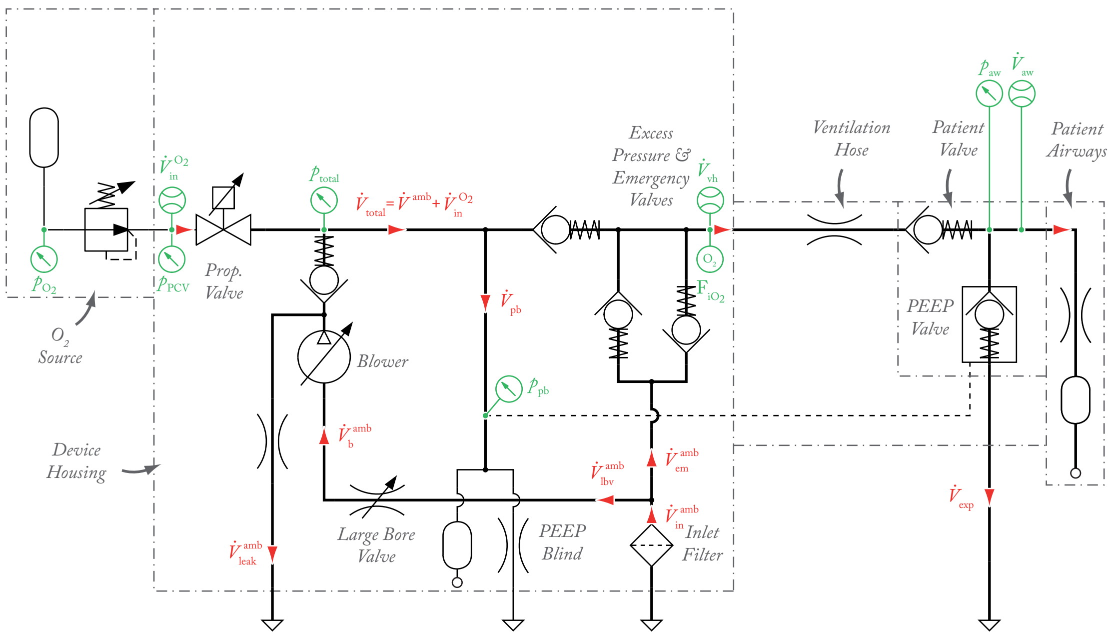

Figure 3.3: Pneumatic Network Topology of Concept Ia

In terms of control, sensors providing feedback for airway pressure p_{aw}, PEEP blind pressure p_{pb}, inspiratory flow $\dot{V}_{\mathrm{vh}}$ and oxygen flow $\dot{V}_{\mathrm{in}}^{\mathrm{O_2}}$ are sufficient. Any further sensors are used for monitoring purposes and alarms. Pressure control is assumed to be largely independent from the oxygen flow in the air mix, maintaining beneficial dynamic properties. However, a check valve is necessary to prevent oxygen flowing towards the blower in case of $F_{iO_2} = 100\,\text{vol.}\,\%$, or when the oxygen flow's dynamic pressure exceeds the pressure built up by the blower. PEEP control is held variable to be executed by both the blower, the large bore valve or the oxygen valve. To investigate feasibility, using only the large bore valve is considered in this thesis. This promises a faster response time and relative independence from the blower speed during expiration.

The effort to realise this concept is kept intentionally low. Apart from the large bore valve, the individual technologies and components employed can already be found in other devices produced by WEINMANN, effectively merging principles of homecare and emergency devices.

An extension — denoted concept Ib (cf. figure 3.4) — is suggested by adding a venturi injector, which can draw in air from the ambience. The inlet is connected to the large bore valve's outlet, in order to be able to cut off flow completely, rendering an additional valve to bypass the venturi injector unnecessary. This extension comes at the expense of a potential increase in control effort, for the oxygen source and ambient air source are coupled.

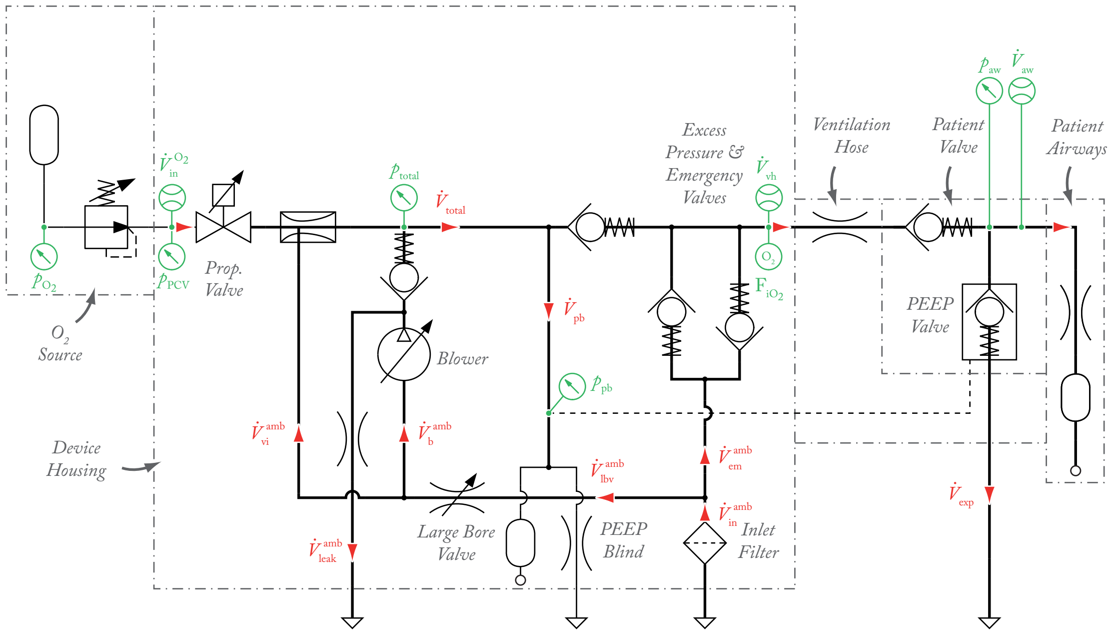

Figure 3.4: Pneumatic Network Topology of Concept Ib

3.3.3 Concept II

A second concept makes use of a 3-2 way large bore valve. Figure 3.5 depicts the network topology, which — with respect to the oxygen flow control — is similar to the first concept.

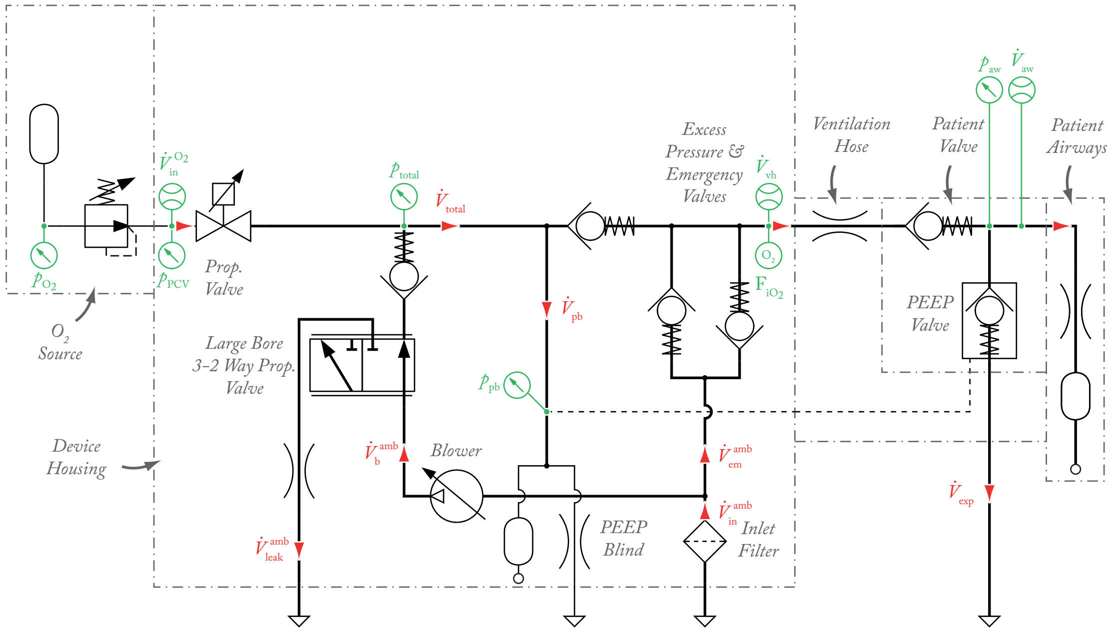

Figure 3.5: Pneumatic Network Topology of Concept II

The basic idea consists in dividing the total ambient flow between a leakage and the patient. Under the assumption, that

$$R \approx R_{\text{leak}} \approx |\underline{Z}_{\text{aw}}(s)| = \left| R_{\text{aw}} + \frac{1}{sC_{\text{aw}}} \right|, \quad s > 0 \tag{3.1}$$

holds, i.e. the leakage resistance is properly dimensioned. The total resistance of the simplified network in terms of the ratio $\rho = \frac{R_{\text{lbv,max}}}{R}$ is given by

$$R_{\text{total}} = \sqrt{R} \cdot \frac{\sqrt{\left(\frac{R_{\text{lbv,max}}}{R \cdot v^2} + 1\right) \cdot \left(\frac{R_{\text{lbv,max}}}{R \cdot (1-v)^2} + 1\right)}}{\sqrt{\frac{R_{\text{lbv,max}}}{R \cdot v^2} + 1} + \sqrt{\frac{R_{\text{lbv,max}}}{R \cdot (1-v)^2} + 1}} = \sqrt{R} \cdot \frac{\sqrt{\left(\frac{\rho}{v^2} + 1\right) \cdot \left(\frac{\rho}{(1-v)^2} + 1\right)}}{\sqrt{\frac{\rho}{v^2} + 1} + \sqrt{\frac{\rho}{(1-v)^2} + 1}}, \tag{3.2}$$

where $R_{\text{lbv}}(v) = \dfrac{R_{\text{lbv,max}}}{v^2}$ denotes the resistance of each of the valve's branches.

A simplified pneumatic structure only concerning the ambient flow is given in figure 3.6 (r.).

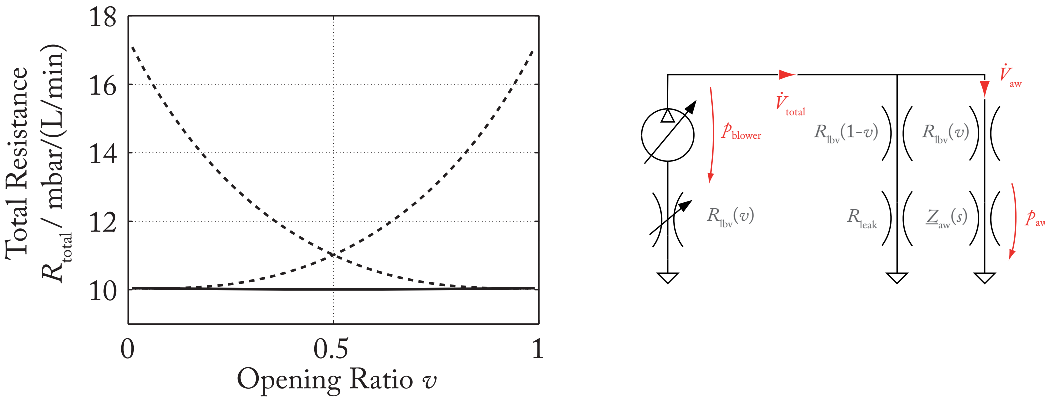

Figure 3.6: —— Total Resistance R_{total} versus Large Bore Valve Opening Ratio v under the Assumption that $\rho \approx 10^2$, ---- Total Resistance R_{total}, where $R_{\text{leak}}/\,|\underline{Z}_{\text{aw}}(s)| \approx 1/200$ or ≈ 200, respectively (l.), Simplified Ambient Air Flow Pneumatic Network Topology of Concept II (r.)

Assuming a ratio $\rho \approx 10^2$, the plot 3.6 (l.) clearly indicates, that the opening ratio v only has minimal influence on the total resistance calculated by equation 3.2. If assumption 3.1 does not hold, the plot also shows, that the variation on the total resistance is significantly limited.

The above considerations give rise to a VCV control scheme, where the blower is actuated to provide a total flow, which is the sum of necessary cooling flow and patient reference flow:

$$\dot{V}_{\text{total}} = \dot{V}_{\text{leak}} + \dot{V}_{\text{aw,ref}}$$

The large bore valve is controlled to divide the total flow in the respective branches.

In this scheme a significant drawback resides in the fact, that at the end of inspiration, the blower motor either has to be actively braked, or the large bore valve has to direct all flow to the environment, away from the patient. A combination of both approaches is possible, still — with respect to energy efficiency — free blowing is highly undesirable.

3.3.4 Concept III

The third concept marks an attempt at effectively integrating the blower into the oxygen flow path. To prevent oxygen losses and — because a certain cooling flow is to be maintained through the blower — a portion of the flow is fed back to recirculate. However, active cooling might be necessary, as the feedback flow's temperature goes up.

Accurately controlling for the desired F_{iO_2} also proves to be more difficult, for the feedback flow's oxygen concentration is unknown. This poses the issue of developing and installing a reliable, dedicated F_{iO_2} sensor.

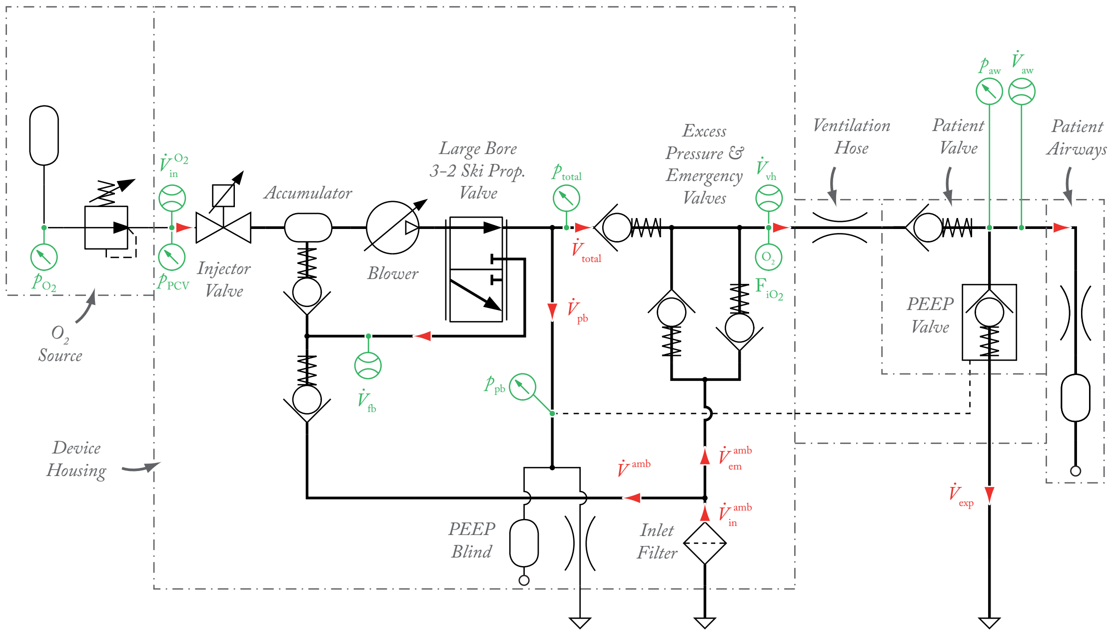

Figure 3.7: Pneumatic Network Topology of Concept III

3.3.5 Comparison with Competitive Products

Prior to the morphological analysis, different competitive products have been analysed with regard to their specific pneumatic structure. Only products, whose specifications announce, that are capable of operating without oxygen supply have been considered. The PulmoneticSystems LTV1000/1200 , Dräger Carina and the Airox LegendAir are a selection of devices, with which the previously introduced concepts are now briefly compared. Mandatory pneumatic elements, such as an excess pressure valve or an emergency valve, have been neglected in the schematics. Furthermore, the degree of detail and accuracy is limited by the information available in the respective user manuals.

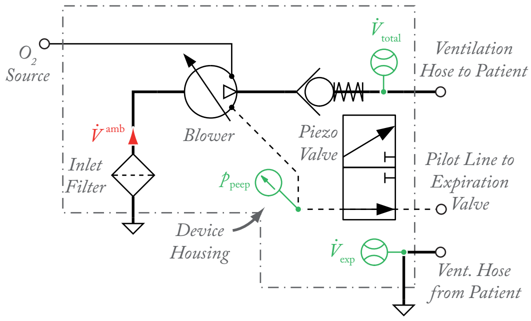

Figure 3.8: Simplified Pneumatic Network Topology of the Airox LegendAir Homecare Ventilation Device, Adapted to this Thesis' Pneumatic Symbol Nomenclature from [3]

Airox LegendAir The Airox LegendAir is a homecare ventilation device. Therefore, it is only capable of having a low pressure O_2 supply attached to it. F_{iO_2} measurement is optional and as can be infered from the manual [3], is not subject to control. The manual is not accurate, as to where exactly the ambient air and oxygen flows are mixed. The same goes for the expiration pilot line attached to the blower. The blower is controlled during inspiration and expiration. During expiration, the piezo valve controls the so–called *"blowby"*: A remaining flow is maintained and controlled by the valve to guarantee cooling and prevent the expired gas from entering the ventilation hose again [3].

Figure 3.8 displays a simplified pneumatic network topology adapted from [3].

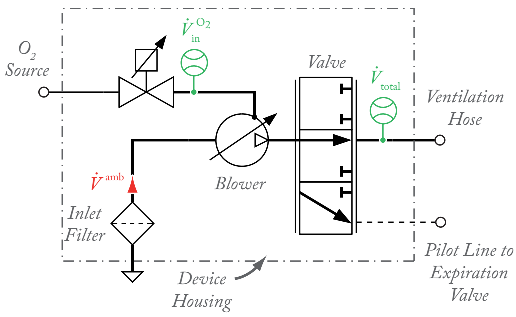

Figure 3.9: Simplified Pneumatic Network Topology of the Dräger Carina NIV—ICU Ventilation Device, Adapted to this Thesis' Pneumatic Symbol Nomenclature

Dräger Carina The Dräger Carina is a ventilation device originally intended for clinical non–invasive ventilation. The product brochure also claims, that it is capable of performing invasive ventilation [16]. The device hosts both a low–pressure and a high–pressure oxygen inlet (simplified in figure 3.9) and employs a dedicated oxygen differential pressure flow measurement. The operating manual [15] states, that gas mixture happens inside the blower. Flow is said to be controlled directly by the blower, which is possible due to its very low moment of inertia. A valve can be operated externally to switch between a pilot line controlled expiration valve and leakage ventilation. Figure 3.9 shows a rendition of the device's pneumatic structure [15].

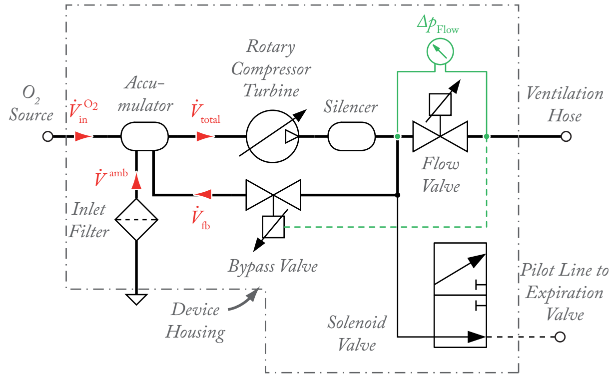

Figure 3.10: Simplified Pneumatic Network Topology of the PulmoneticSystems LTV1000/1200 Transport Ventilation Device, Adapted to this Thesis' Pneumatic Symbol Nomenclature from [36]

PulmoneticSystems LTV1000/1200 The PulmoneticSystems LTV1000/1200 is the only actual transport ventilation device considered here. It hosts an internal oxygen blender and mixes ambient air and oxygen in an accumulator in front of a "rotary compressor turbine". This turbine adds energy to the mixed gas for pressure and flow control. The flow valve after the silencer lets ventilation gas flow towards the patient. Excess flow is diverted and fed back to the accumulator. The bypass valve is controlled in order to maintain a positive pressure drop over the flow valve, yet it also has the objective to "ensure that excess energy is not wasted" [36]. The flow valve is of proportional nature and is characterised, such that it also functions as a flow meter based on differential flow measurement.

A solenoid valve is used to control the expiration valve pilot pressure.

Comparison with the Concepts Concept Ia is significantly different to all competitor's products described above: It employs less actuators than the LTV1000/1200, but adds the large bore valve in comparison to the Airox LegendAir to account for higher quality demands on flow control in emergency ventilation devices. The large bore valve at the blower inlet possibly increases energy efficiency, an issue the popular LTV1000/1200 is facing [11]. In addition, the approach employed with both concepts I and II completely separates ambient air and oxygen flow control, whereas the LTV1000/1200 has a valve placed in paths conducting the gas mixture.

The constant leakage enables to maintain cooling flow if correctly dimensioned, while it remains unclear, how possible heat problems are coped with by the LTV1000/1200 or Dräger Carina design.

Concept III is based on the LTV1000/1200 design, but makes an attempt at reducing the number of actuators, by employing a single 3–2 way large bore valve.

3.3.6 Conclusion

Based on the aforementioned condensed items to assess the candidate concepts' potential performances in terms of control, effort and efficiency, an evaluation matrix is given in figure 3.11. A significant amount of uncertainty encompasses the assessment, but a crude

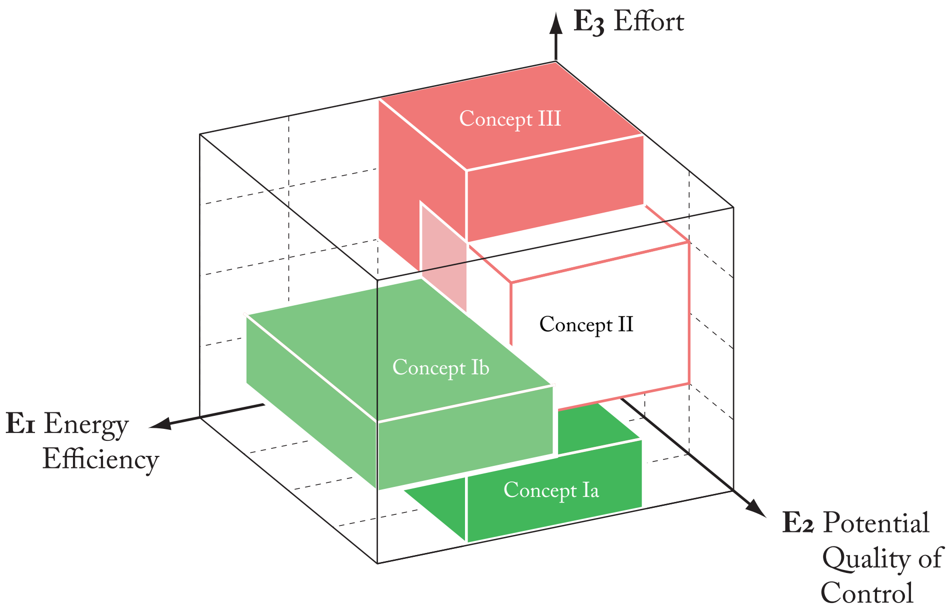

Figure 3.11: Evaluation Matrix Assessing the Candidate Concepts' Potential Performances

relative comparison can be drawn from the graphic. Naturally, uncertainty is largest, where potential effort is highest. This has been tried to reflect in the size of the boxes.

Concept Ib promises the best performance, but poses additional effort due to the inclusion of the venturi injector. As a first step, though, and based on this evaluation and the previous discussion of the concepts, concept Ia will be chosen as a functional model to be constructed, nonlinearly modelled and controlled for a thorough practical investigation of its viability and performance as a novel mechanical ventilator design.

4 Nonlinear Plant Modelling

It is this chapter's intention to document the plant's modelling and provide the relevant equations and principles. The chapter is structured to present the individual components' modelling separately from section 4.1 to 4.9. The following section 4.10 is dedicated to describe the methodology applied to synthesise a nonlinear overall state space model for simulation. The final section deals with simulation and validation issues.

4.1 Blower

4.1.1 Brushless Direct Current Motor Model

BLDC[1] motors employ the principle of rotating the magnetic field induced by current through the stator windings by electronic commutation, hence they are also called EC[2] motors. Thus, with BLDC motors, the rotor is a permanent magnet and the current in the stator windings is changed by electronic control, instead of having the armature current commutated to swap polarity while rotating in the center of a permanent magnet stator. This results in good dynamic performance and ease of controllability. The brushless technology is free of wear and maintenance [22].

Figure 4.1 depicts a model circuit of a typical BLDC motor. For simplicity phase resistances and inductances are assumed to be identical, as well as mutual inductance M is assumed to be covered by $L = \tilde{L} - M$.

The commutation is assumed to always let the voltage v_{mot} be applied to two phases in series and to be a square–wave commutation in nature. The commutation is not to be modeled, such that for the stator winding current $i = i_{\mathrm{a}} = i_{\mathrm{b}} = i_{\mathrm{c}}$ holds. Thus the circuitry can be simplified to figure 4.2.

[1]BLDC — Brushless Direct Current
[2]EC — Electronically Commutated

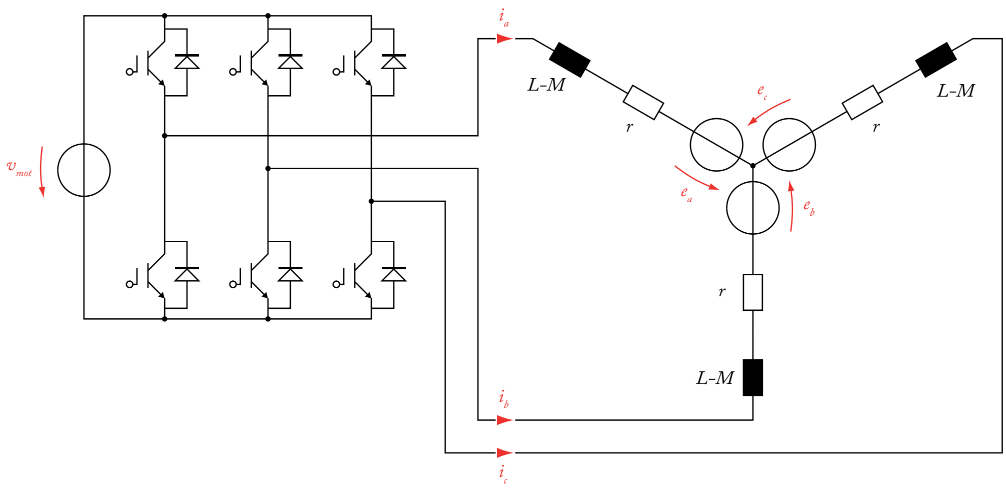

Figure 4.1: Model Circuit of a Typical BLDC Motor in Star–Connection [31, slightly altered]

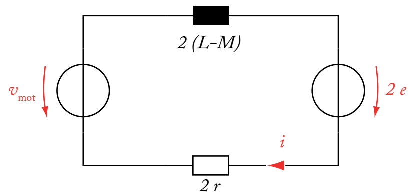

Figure 4.2: Simplified Model Circuit of a Typical BLDC Motor in Star–Connection

The electrical dynamic equation of the electric circuitry therefore follows the same structure, a conventional DC motor could be described with:

$$v_{\text{mot}} = 2L \cdot \mathrm{d}i/\mathrm{d}t + 2r \cdot i + 2 \cdot e, \tag{4.1}$$

with v_{mot} as the (controllable) motor supply voltage,
L as the phase inductance,
r as the phase resistance,
i as the winding current,
e as the voltage resulting from back–electromagnetic force.

The mechanical dynamics are governed by the same differential equation as if applied to conventional DC motors, as well:

$$
\begin{aligned}
T_{\text{mech}} &= J \cdot \dot{\omega} + b \cdot \omega, \\
&\text{with } T_{\text{mech}} \text{ as mechanical torque exerted by the motor,} \\
&\quad J \text{ as the mechanical moment of inertia,} \\
&\quad \omega \text{ as the motor's rotational speed,} \\
&\quad b \text{ as the mechanical damping coefficient.}
\end{aligned} \tag{4.2}
$$

Mechanical power is computed by

$$
\begin{aligned}
P_{\text{mech}} &= \eta_{\text{mot}} \cdot v_{\text{mot}} \cdot i, \\
&\text{with } \eta_{\text{mot}} < 0.88 \text{ as the motor's coefficient of efficiency [30],}
\end{aligned} \tag{4.3}
$$

and proportionality of torque with respect to current is established by

$$
\begin{aligned}
T_{\text{mech}} &= \frac{P_{\text{mech}}}{\omega} = \eta_{\text{mot}} \cdot k_{\text{m}} \cdot i, \\
&\text{with } k_{\text{m}} \text{ as the motor's characteristic torque constant.}
\end{aligned} \tag{4.4}
$$

This is due to the back–EMF[3] voltage being proportional to the rotational speed via

$$
\begin{aligned}
e &= k_{\text{e}} \cdot \omega, \\
&\text{with } k_{\text{e}} \text{ as the motor's characteristic back-EMF constant.}
\end{aligned} \tag{4.5}
$$

The resulting linear parameter-varying state–space representation yields:

$$
\underbrace{\begin{bmatrix} \dot{i} \\ \dot{\omega} \end{bmatrix}}_{\dot{\mathbf{x}}_{\text{BLDC}}} = \underbrace{\begin{bmatrix} -\frac{r}{L} & -\frac{k_{\text{e}}}{L} \\ \frac{\eta_{\text{mot}} k_{\text{m}}}{J} & -\frac{b}{J} \end{bmatrix}}_{\mathbf{A}_{\text{BLDC}}} \cdot \underbrace{\begin{bmatrix} i \\ \omega \end{bmatrix}}_{\mathbf{x}_{\text{BLDC}}} + \underbrace{\begin{bmatrix} \frac{1}{2L} \\ 0 \end{bmatrix}}_{\mathbf{B}_{\text{BLDC}}} \cdot v_{\text{mot}} \tag{4.6}
$$

$$
\underbrace{\begin{bmatrix} i \\ n \end{bmatrix}}_{\dot{\mathbf{y}}_{\text{BLDC}}} = \underbrace{\begin{bmatrix} 1 & 0 \\ 0 & \frac{60}{2\pi} \end{bmatrix}}_{\mathbf{C}_{\text{BLDC}}} \cdot \underbrace{\begin{bmatrix} i \\ \omega \end{bmatrix}}_{\mathbf{x}_{\text{BLDC}}} . \tag{4.7}
$$

As the motor is not going to be actively braked, a lower bound of 0 A is to be imposed on the current i_{mot}. Furthermore, the energy supply is set to saturate at 2.5 A, which also has to be taken into account. Figure 4.3 illustrates the state space model of the BLDC motor with state saturation and figure 4.4 shows a simulated step response of the blower motor model.

Also shown in figure 4.4 is a first order approximation of the BLDC motor model, which will later be used for controller synthesis.

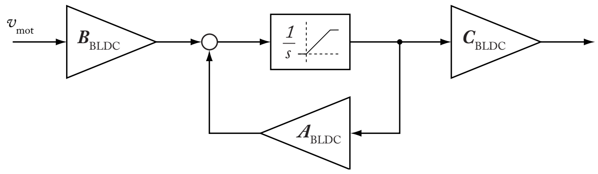

Figure 4.3: State Space Model of BLDC Motor with State Saturation

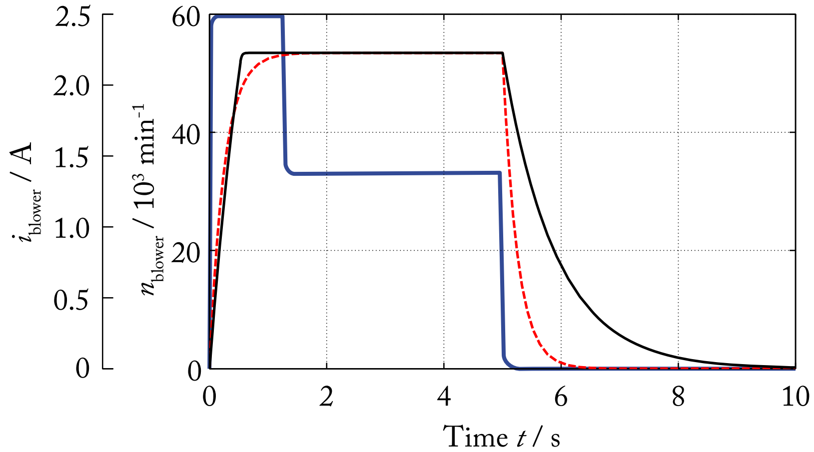

Figure 4.4: Simulated Step Response of the Blower BLDC Motor, —— BLDC Motor Model with Integrator Saturation, - - - - First Order Approximation, —— Simulated Motor Current

4.1.2 Static Characteristics

A blower's static characteristics usually follow a curve similar to figure 4.5.

As a first approximation, the entirety of the blower is modelled as an ideal pressure source with an additional throttle under turbulent flow conditions. Applying the BERNOULLI equation 2.24 and the equation for turbulent flow through orifices 2.32 accounts for the static characteristics being expressed by:

$$\begin{aligned} \Delta p_{\text{blower}} &= \Delta p_{\text{blower}}^{\text{ideal}} - \Delta p_{\text{blower}}^{\text{thr}}, \\ \text{with } \Delta p_{\text{blower}}^{\text{ideal}} &= \frac{1}{2}\varrho_{\text{out}}\left(\frac{u}{r_{\text{b}}}\right)^2, \\ \Delta p_{\text{blower}}^{\text{thr}} &= \frac{1}{2}\varrho_{\text{out}}\frac{C_{\text{b}}^{\text{thr}}}{A_{\text{b}}^{\text{thr}}}\dot{V}_{\text{blower}}^2. \end{aligned} \tag{4.8}$$

[3]EMF — Electromagnetic Force

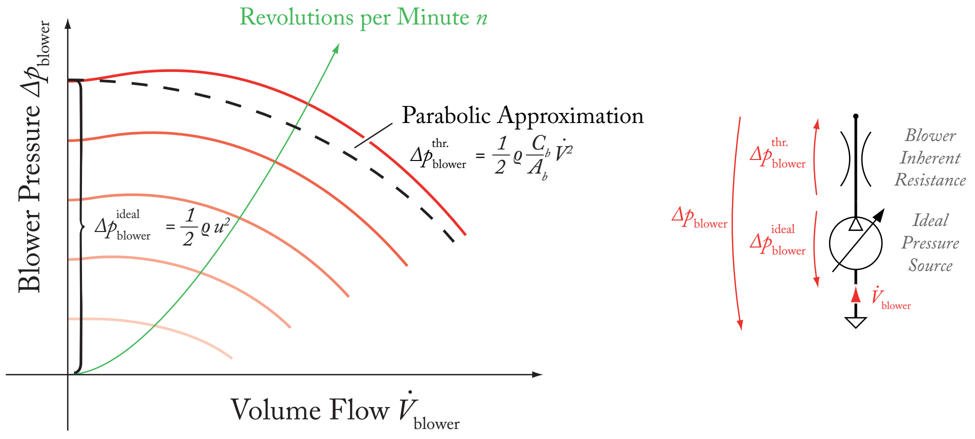

Figure 4.5: Typical Static Characteristics of a Blower Depending on Rotational Speed and Volume Flow

The throttle's flow coefficient $C_{\text{b}}^{\text{thr}}$, the characteristic throttle area $A_{\text{b}}^{\text{thr}}$, as well as the characteristic fan area radius r_{b} can be determined experimentally as concentrated parameters.

Data for the blowers employed in WEINMANN homecare ventilation devices is available and a multiple linear regression has been done to determine the coefficients r_{blower} and R_{blower}. A normalisation with respect to standard conditions density further enables to model the influence of ambient pressure on the blower performance:

$$p_{\text{blower}} = \frac{1}{2}\varrho_{\text{out}} \cdot \left(r_{\text{blower}} \cdot n^2 - R_{\text{blower}} \cdot \dot{V}^2_{\text{blower}}\right). \tag{4.9}$$

Figure 4.6 depicts the measured performance characteristics of the blower employed.

4.1.3 Integration

Figure 4.7 depicts the integration of the individual elements of the blower model described above. It also indicates the integration of the model into the overall pneumatic system, which happens via the signals p_{blower} functioning as an input to the pneumatic network and $\dot{V}_{\text{blower}} = \dot{V}^{\text{amb}}_{\text{lbv}}$ — the resulting volume flow through the large bore valve and blower. Ambient parameters, as well as the blower pressure, influence the density at the blower outlet.

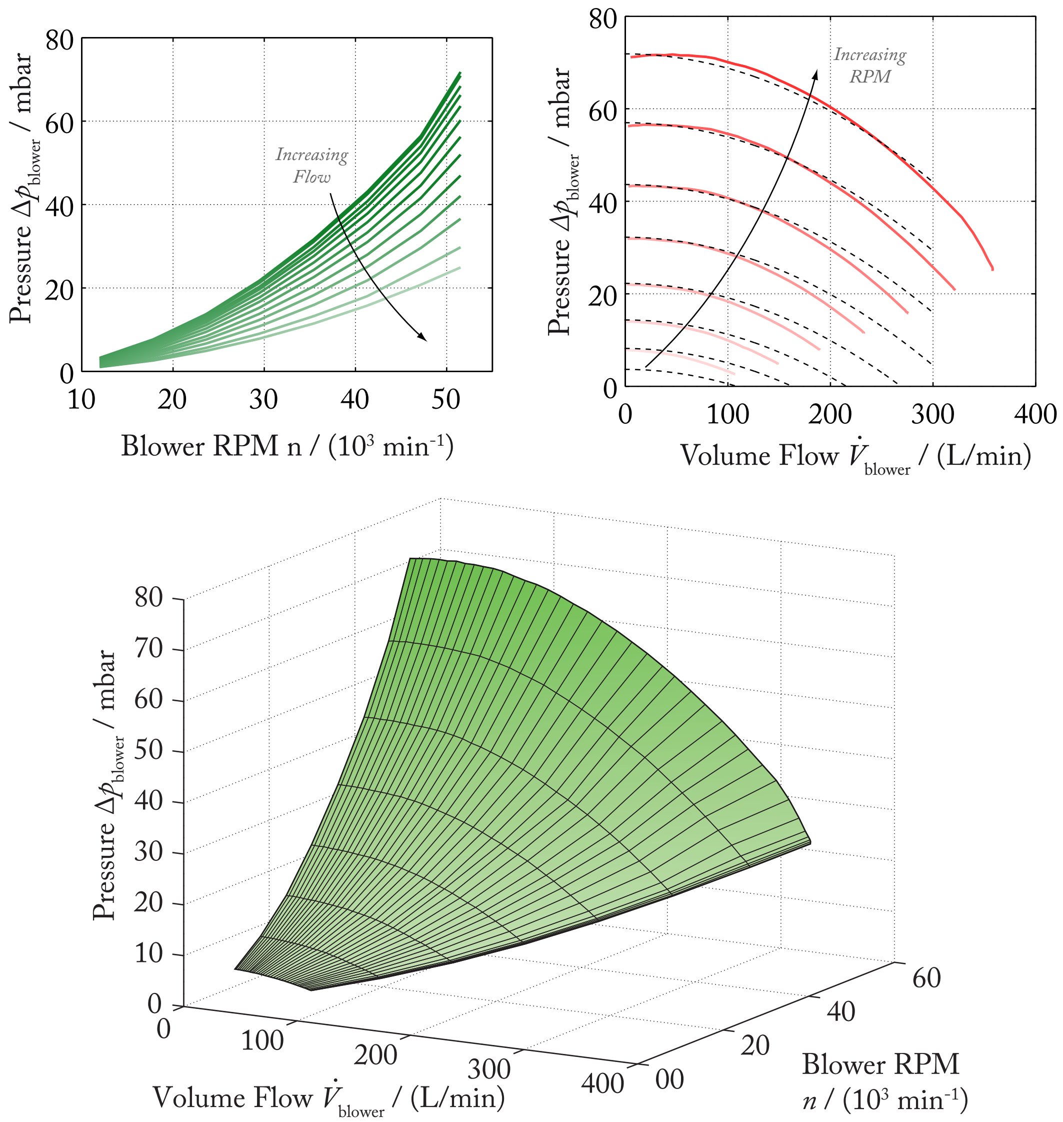

Figure 4.6: Measured and Calculated Static Characteristics of Employed Blower, Colored Lines and the Three–Dimensional Plot Indicate Measured Data, ---- Characteristics Calculated by Equation 4.9

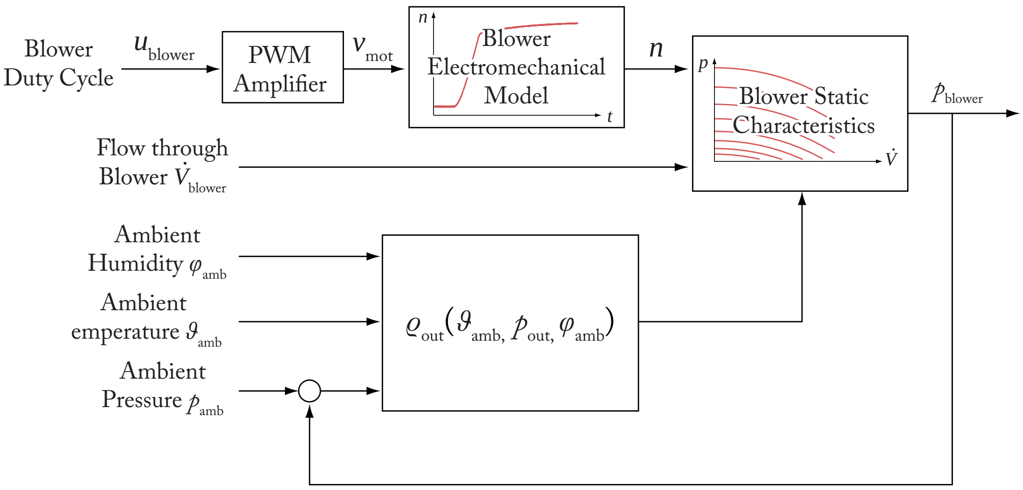

Figure 4.7: Block Diagram Indicating the Integration of Individual Model Elements of the Overall Blower Model

4.2 Proportional Large Bore Valve

The large bore proportional valve's conductance G_{lbv} is modelled utilising equation 2.35 for turbulent flow through sharp-edged orifices. Figure 4.8 compares measured values and the characteristic curve created by the model equation. The measurements have been conducted by applying constant pressure drops for defined opening ratios, while measuring flow. Calculation of conductance values by the quotient

$$G_{\text{lbv,meas}} = \frac{\dot{V}^2_{\text{lbv,meas}}}{\Delta p_{\text{lbv,meas}}} \tag{4.10}$$

resulted in characteristics independent of flow and pressure.

A constant offset $G_{\text{lbv,leak}} = G_{\text{lbv,meas}}|_{v=0}$ has been extracted from the measured data to respect leakages.

The final equation for modelling the large bore valve goes as follows:

$$\dot{V}^2_{\text{lbv}} = \Delta p_{\text{lbv}} \left(G_{\text{lbv}}(v) + G_{\text{lbv,leak}} \right) \qquad v = \frac{a_{\text{lbv, current}}}{a_{\text{lbv, opened}}} \in [0 \dots 1] \tag{4.11}$$

$$\text{with } G_{\text{lbv}}(v) = 2\frac{\alpha^2 a^2_{\text{lbv}}}{\varrho_{\text{out}}} \cdot \tilde{v}^2(v) \tag{4.12}$$

$$G_{\text{lbv,leak}} = 0.1602 \frac{(\mathrm{L/\,min})^2}{\mathrm{mbar}} \text{ as the leakage conductance,}$$

where $\alpha = 0.611$ for potential flow at ideally sharp-edged orifices,

$a_{\text{lbv}} = a_{\text{lbv, opened}} \approx 160\,\mathrm{mm}^2$ as the area for fully the opened valve,

ϱ_{out} as the air density at the large bore valve outlet.

Because v has been treated as if the opening area were proportional to the opening angle, the function $\tilde{v}(v)$ is introduced to accommodate the deviation from the ideal quadratic relation and thus improve the fit.

Figure 4.9 displays data stored in a lookup table, used to shift the characteristic curve. For the lower opening ratios, the deviation resembles a square root function, showing that the valve actually behaves linear in that area. The curve then enters a linear regime, indicating a constant bias of approximately 0.1 (note the dashed lines). At $v \approx 0.9$ the valve saturates.

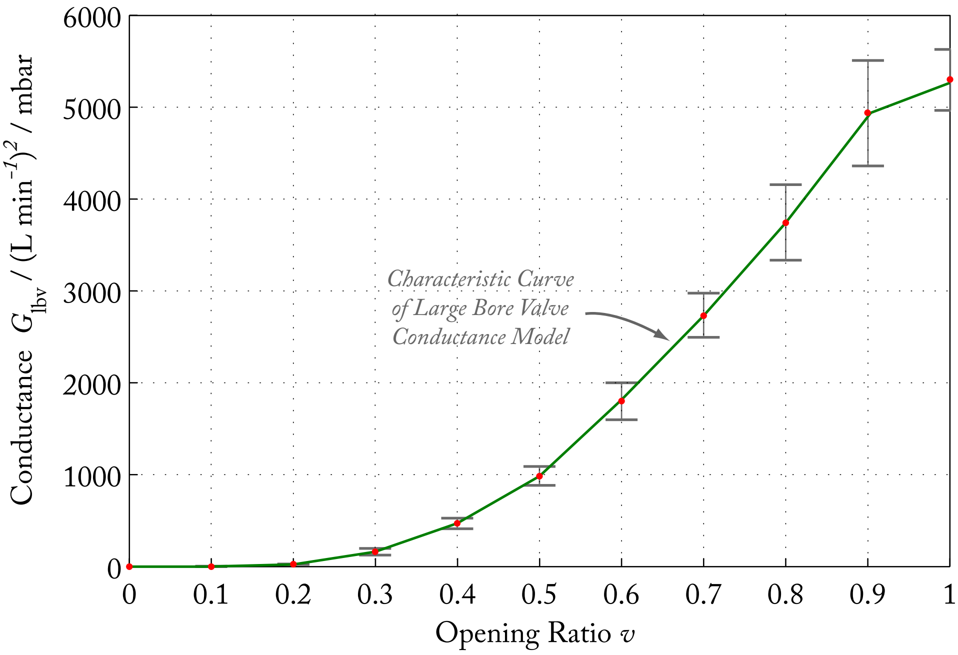

Figure 4.8: Large Bore Valve Conductance versus Opening Ratio, • Mean of Measured Values, ⌶ 2σ Standard Deviation Interval of Measured Values, — Approximation by Model

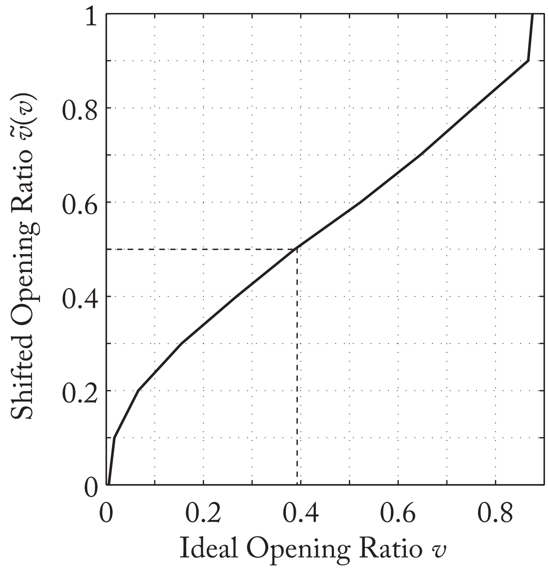

Figure 4.9: Deviation of Ideal Large Bore Valve Opening Ratio from Actual Opening Ratio

N	$p_{\mathrm{pcv,in}}/\,\mathrm{bar}$	Coefficients $k_1^N/\,\frac{\mathrm{mbar}}{\mathrm{L/\,min}}$	$k_2^N/\,\frac{\mathrm{mbar}}{(\mathrm{L/\,min})^2}$	$k_3^N/\,\frac{1}{(\mathrm{L/\,min})^2}$
1	2.7	41.169	0.271	20.989
2	3.0	41.115	0.252	21.129
3	4.5	22.141	0.072	11.456
4	6.0	14.659	0.032	7.676

Table 4.1: Look-Up Table Coefficients for the Static Pressure Control Valve Model [20]

4.3 Pressure Control Valve

The pressure control valve is a passive proportional controller, with the aim to regulate for a constant output pressure $p_{\mathrm{pcv,ref}} = 2.5\,\mathrm{bar}$. Due to its comparably fast dynamics, only a static model is used for simulation to incorporate the pressure control valve's steady state error into the simulation [20].

Deviations from the reference pressure occur due to increased flow $\dot{V}_{\mathrm{pcv}}$ and due to decreased inlet pressure $p_{\mathrm{pcv,in}}$:

$$p_{\mathrm{pcv,out}} = p_{\mathrm{pcv,out}}(p_{\mathrm{pcv,in}}, \dot{V}_{\mathrm{pcv}}). \tag{4.13}$$

Measurements and least squares approximations have been done in [20] based on different inlet pressures $p^N_{\mathrm{pcv,in}}, N = 1, \ldots, 4$. Results were fit to the functions

$$p_{\mathrm{pcv,out}} = k_1^N \cdot \dot{V}_{\mathrm{pcv}} - k_2^N \cdot \dot{V}^2_{\mathrm{pcv}} + 2.5\mathrm{e}^{-k_3^N \cdot \dot{V}_{\mathrm{pcv}}} \tag{4.14}$$

The results are implemented in terms of a 2–dimensional look-up table as depicted in figure 4.10. The coefficients k_l^N are given in table 4.1.

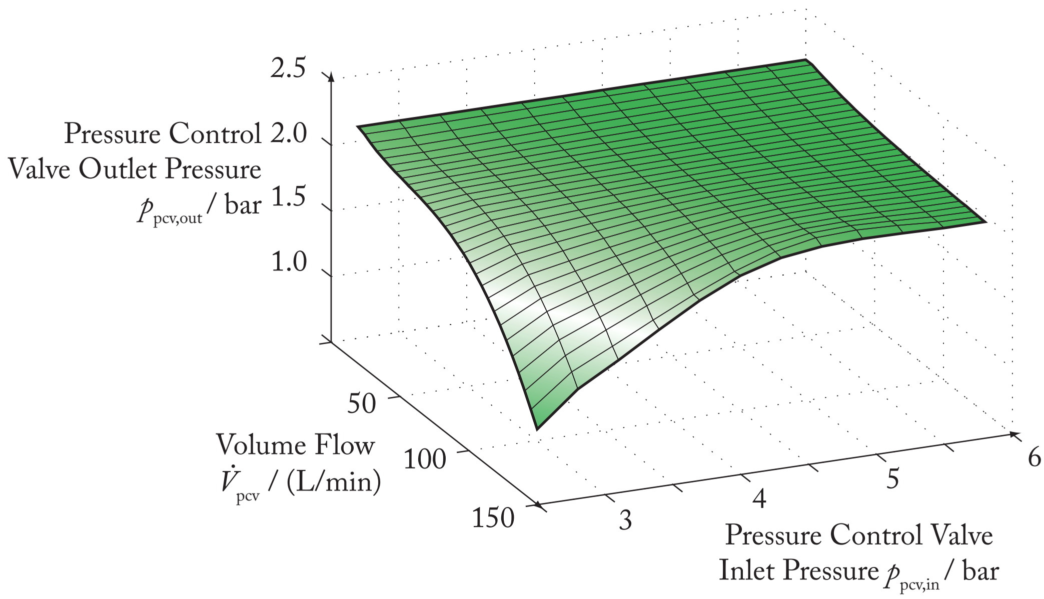

Figure 4.10: Static Characteristics of the Pressure Control Valve with Respect to Volume Flow and Inlet Pressure

4.4 Proportional Oxygen Inlet Valve

The oxygen inlet valve used in the functional model has been modelled in detail in [20]. It has been shown, that supercritical flow conditions always hold, except for a negligible error. This makes the proportional oxygen valve a near ideal mass flow source.

An important result of [20] exists in the static relation between volume flow $\dot{V}_{\text{in}}^{O_2}$ and valve opening ratio v_{ov}:

$$\dot{V}_{\text{in}}^{O_2}(v_{\text{ov}}) = 0.484\pi \cdot D_{\text{ov}} \cdot \frac{p_{\text{pcv,out}} + p_{\text{amb}}}{p_{\text{pb}} + p_{\text{amb}}} \cdot \sqrt{2 \cdot R_{\text{amb}} T_{\text{amb}}} \cdot h_{\text{ov,max}} \cdot v_{\text{ov}}, \tag{4.15}$$

with $D_{\text{ov}} = 4.0 \cdot 10^{-3}\,\text{m}$ as the valve's membrane diameter,
p_{amb} as the ambient pressure,
p_{pb} as the pressure after the oxygen valve,
R_{amb} as the ambient universal gas constant,
T_{amb} as the ambient temperature,
$\Delta h_{\text{ov,max}} = 2.0 \cdot 10^{-4}\,\text{m}$ as the valve's maximum armature lift.

A feedforward control algorithm corrects for changes of the static valve characteristic due to T_{amb} and p_{amb}, which is already implemented in the MEDUMAT Transport . The influence of p_{pb} is deemed negligible, since $p_{\text{pcv,out}} \gg p_{\text{pb}}$.

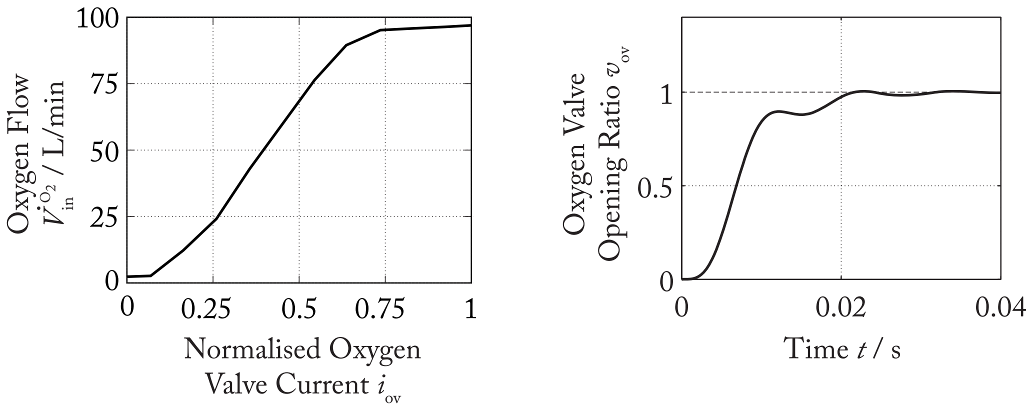

Figure 4.11: Static Characteristic of Measured Oxygen Valve Flow versus Measured Normalised Current (l.) and Simulated Oxygen Valve Opening Ratio Step Response (r.)

The dynamic behaviour is modelled by a linear transfer function $G_{v_{\mathrm{ov}},i_{\mathrm{ov}}}(s)$,which is composed from

$$G_{v_{\mathrm{ov}},i_{\mathrm{ov}}}(s) = G_{v_{\mathrm{ov}},F_{\mathrm{mag}}}(s) \cdot G_{F_{\mathrm{mag}},i_{\mathrm{ov}}}(s), \tag{4.16}$$

$$\text{with } G_{v_{\mathrm{ov}},F_{\mathrm{mag}}}(s) = \frac{V_{\mathrm{ov}}(s)}{F_{\mathrm{mag}}(s)} = \Delta F_{\mathrm{mag,max}} \cdot \frac{\omega_{\mathrm{ov}}^2}{s^2 + 2\zeta_{\mathrm{ov}}\omega_{\mathrm{ov}} \cdot s + \omega_{\mathrm{ov}}^2},$$

as the transfer function from magnetic force to opening ratio,

$$G_{F_{\mathrm{mag}},i_{\mathrm{ov}}}(s) = \frac{F_{\mathrm{mag}}(s)}{I_{\mathrm{ov}}(s)} = \frac{\Delta i_{\mathrm{ov,max}}}{\Delta F_{\mathrm{mag,max}}} \cdot \frac{1}{(1 + s \cdot \tau_{\mathrm{ov},1})(1 + s \cdot \tau_{\mathrm{ov},2})},$$

as the transfer function from normalised current to magnetic force,

where $\Delta F_{\mathrm{mag,max}}$ is cancelling out,

$\omega_{\mathrm{ov}} = 545 \frac{\mathrm{rad}}{\mathrm{s}}$ is the mechanical system's natural frequency,

$\zeta_{\mathrm{ov}} = 0.2$ is the mechanical system's damping coefficient,

$\Delta i_{\mathrm{ov,max}} = 380\,\mathrm{mA} - 130\,\mathrm{mA}$ is the linear span of current inputs,

$\tau_{\mathrm{ov},1} = 4.88\,\mathrm{ms}$,

$\tau_{\mathrm{ov},2} = 2.34\,\mathrm{ms}$ are the electrical system's time constants.

A step response of $G_{v_{\mathrm{ov}},i_{\mathrm{ov}}}(s)$ is shown in figure 4.11 (r.) [20]. The valve's static characteristic of flow $\dot{V}_{\mathrm{in}}^{O_2}$ with respect to normalised valve current i_{ov} is given in figure 4.11 (l.).

4.5 Check Valves

Several check valves have been incorporated into the pneumatic network. Their characteristic's have been determined in [20] and follow

$$p_{\mathrm{cv}} = R_{\mathrm{cv,lam}} \cdot \dot{V}_{\mathrm{cv}} + R_{\mathrm{cv,turb}} \cdot \dot{V}_{\mathrm{cv}}^2 \tag{4.17}$$
$$\text{with } R_{\mathrm{cv,lam}} = 0.1667 \frac{\mathrm{mbar}}{\frac{\mathrm{L}}{\mathrm{min}}}$$
$$R_{\mathrm{cv,turb}} = 2.3068 \cdot 10^{-5} \frac{\mathrm{mbar}}{(\frac{\mathrm{L}}{\mathrm{min}})^2}$$

Figure 4.12 illustrates the construction and defines flow and pressure nomenclature.

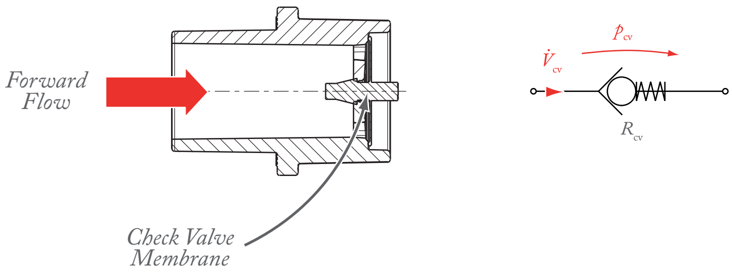

Figure 4.12: Check Valve Constructional Drawing [48] and Modelling Circuit

4.6 Ventilation Hose

The inspiratory flow is fed through a flexible ventilation hose. Due to its elasticity and the comparably large volume it contains, the ventilation hose is modelled as a pneumatic low pass with resistance and compliance (cf. figure 4.13). The ventilation hose's dynamics

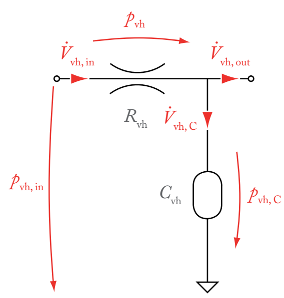

Figure 4.13: Model of the Ventilation Hose as a Pneumatic Low Pass

Quantity	Type of Ventilation Hose			
	Reusable		Single–Use	
R_{vh}	$2.4691 \cdot 10^{-4}$	$\frac{\mathrm{mbar}}{(\mathrm{L/\,min})^2}$	$1.0884 \cdot 10^{-4}$	$\frac{\mathrm{mbar}}{(\mathrm{L/\,min})^2}$
C_{vh}	$1.6 \cdot 10^{-3}$	$\frac{\mathrm{L}}{\mathrm{mbar}}$	$2.3 \cdot 10^{-3}$	$\frac{\mathrm{L}}{\mathrm{mbar}}$

Table 4.2: Ventilation Hose Parameters [20]

are governed by

$$\begin{aligned} p_{\mathrm{vh,in}} &= p_{\mathrm{vh}} + p_{\mathrm{vh,C}}, \\ p_{\mathrm{vh,C}} &= \frac{1}{C_{\mathrm{vh}}} \cdot V_{\mathrm{vh,C}}, \\ p_{\mathrm{vh}} &= R_{\mathrm{vh}} \cdot \dot{V}^2_{\mathrm{vh,in}}, \\ \dot{V}_{\mathrm{vh,out}} &= \dot{V}_{\mathrm{vh,in}} + \dot{V}_{\mathrm{vh,C}}. \end{aligned}$$

Resistance characteristic curves and compliance estimates have been determined in [20] for two types of ventilation hoses — single–use and reusable hoses. Table 4.2 reproduces the results in terms of concentrated parameters assuming turbulent flow. Experimental measurements in [20] showed, that time constants range between $\tau_{\mathrm{vh,su}} \in [0.8 \ldots 2.3\,\mathrm{ms}]$ and $\tau_{\mathrm{vh,mu}} \in [0.3 \ldots 0.8\,\mathrm{ms}]$ for the single–use and reusable ventilation hoses, respectively.

Due to the fact, that pressure is transmitted by the speed of sound, a time-delay is introduced by

$$p_{\mathrm{vh,C}}(t - t_{\mathrm{vh,d}}) = p_{\mathrm{vh,in}}(t). \tag{4.18}$$

With the speed of sound of $a = 343.2\,\frac{\mathrm{m}}{\mathrm{s}}$ and an assumed length of $2 \ldots 3\,\mathrm{m}$ this accounts for a time delay of $t_{\mathrm{vh,d}} \approx 5.8 \ldots 8.7\,\mathrm{ms}$.

4.7 PEEP Blind

The PEEP blind is a small orifice, through which the mixing chamber can discharge and equalise with ambience. This orifice is a component already used in the MEDUMAT Transport and its resistance value is known [20]:

$$\begin{aligned} \Delta p_{\mathrm{pb}} &= R_{\mathrm{pb}} \cdot \dot{V}^2_{\mathrm{pb}}, \\ \text{with } R_{\mathrm{pb}} &= 51.6529 \frac{\mathrm{mbar}}{(\mathrm{L/\,min})^2}. \end{aligned} \tag{4.19}$$

A dimensional drawing and the pneumatic circuitry, which considers the PEEP blind in conjunction with the mixing chamber's compliance, is given in figure 4.14.

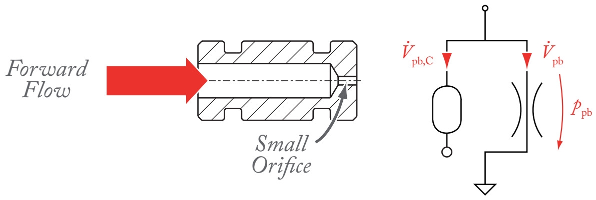

Figure 4.14: Dimensional Drawing of the PEEP Blind [48] and the Model Pneumatic Circuitry also Considering the Mixing Chamber's Compliance

The mixing chamber's compliance is determined experimentally by measuring the pressure p_{pb} during discharge. An exemplary curve is given in figure 4.15. The dashed lines indicate the approximate duration of discharge as $\Delta t_{peep} \approx 50\,\text{ms}$. The time constant $\tau_{peep} \approx 35\,\text{ms}$ is identified from p_{pb} having decreased by 63.2 %, thus assuming first order dynamic behaviour. Eventually an approximate compliance is determined by varying the parameter C_{pb} and comparing nonlinear simulation results with the measurement. The value is identified to $C_{pb} \approx 5 \ldots 7 \cdot 10^{-5}\,\text{L/mbar}$, which corresponds to applying equation 2.36 with an estimated mixing chamber volume of $V_{pb} \approx 70\,\text{mL}$

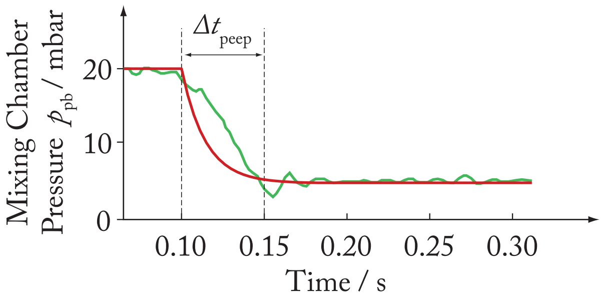

Figure 4.15: Measurement of Discharge via the PEEP Blind, —— Measured Discharge Curve, —— Simulated Discharge Curve

4.8 Patient Valve

The expiration valve acts as an almost ideal pressure controller, with which a controlled expiration with or without positive end-expiratory pressure p_{peep} is realised: A membrane is installed on top of the expiratory outlet. The pilot pressure p_{pilot}, which equals the pressure drop over the PEEP blind (cf. section 4.7), results in a force closing the expiratory path, whereas the patient's airway pressure results in an opening force. The ratio of areas r_{peep} of both sides of the membrane determines a characteristic ratio of pressures for enabling expiration against a certain PEEP. An additional check valve prevents the expiratory flow $\dot{V}_{\mathrm{exp}}$ from reentering the ventilation hose.

Figure 4.16 depicts both a constructional drawing and the pneumatic circuit by which the patient valve is modelled.

The PEEP is modelled by the following equation:

$$\begin{aligned} p_{\mathrm{peep}} &= G_{\mathrm{peep}}^{-1} \cdot \dot{V}_{\mathrm{exp}} + r_{\mathrm{peep}} \cdot p_{\mathrm{pilot}} \\ \text{with } G_{\mathrm{peep}} &= \begin{cases} 0.0392 \frac{\mathrm{L/\,min}}{\mathrm{mbar}} & \text{, for } p_{\mathrm{aw}} > r_{\mathrm{peep}} \cdot p_{\mathrm{pilot}} \\ 0 \frac{\mathrm{L/\,min}}{\mathrm{mbar}} & \text{, for } p_{\mathrm{aw}} < r_{\mathrm{peep}} \cdot p_{\mathrm{pilot}} \end{cases} \\ r_{\mathrm{peep}} &= 1.7 \\ p_{\mathrm{pilot}}(t - t_{\mathrm{pilot,d}}) &= p_{\mathrm{pb}}(t) \end{aligned} \tag{4.20}$$

With the speed of sound of $a = 343.2 \frac{\mathrm{m}}{\mathrm{s}}$ and an assumed length of $2 \ldots 3\,\mathrm{m}$ this accounts for a time delay of $t_{\mathrm{pilot,d}} \approx 5.8 \ldots 8.7\,\mathrm{ms}$.

In the above formulation $G_{\mathrm{peep}} \to 0$ will result in a singularity, which is automatically avoided in the complete system description. Section 4.10 will expand on this. Furthermore, it should be noted, that the patient valve's characteristic can be approximated by linear (laminar) behaviour, which has been shown in [20].

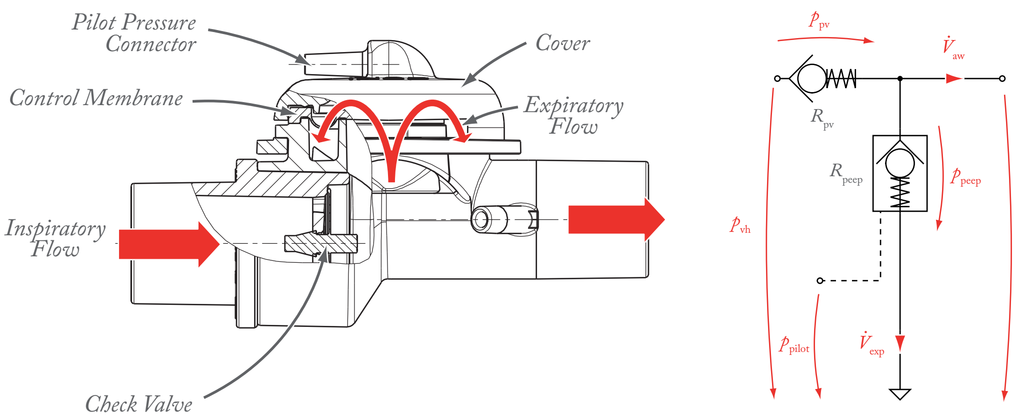

Figure 4.16: Patient Valve Constructional Drawing [48] and Modelling Circuit

4.9 Patient Airways

The patient's airways are modelled according to the single compartment model introduced in section 2.3. It is augmented by a pressure source, which simulates the patient's spontaneous breathing activity (cf. figure 4.17). Laminar flow is assumed with the pa-

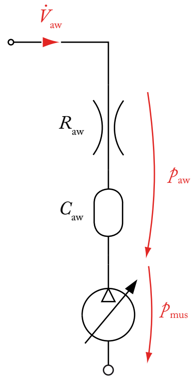

Figure 4.17: Model of the Patient's Airways According to the Single Compartment Model

tient's airways, which results in the following differential equation governing the patient's airway pressure:

$$p_{\mathrm{aw}} = R_{\mathrm{aw}} \cdot \dot{V}_{\mathrm{aw}} + \frac{1}{C_{\mathrm{aw}}} \cdot V_{\mathrm{aw}}. \tag{4.21}$$

Taking into account spontaneous breathing, the airway pressure becomes

$$\tilde{p}_{\mathrm{aw}} = p_{\mathrm{aw}} + p_{\mathrm{mus}}. \tag{4.22}$$

Realistic values for the airways' resistance and compliance are given in section 2.3.

4.10 Pneumatic Network

The pneumatic network is simulated as two superimposed subsystems, as to reflect ambient air and oxygen volume flows. Check valves and the expiration valve introduce topology switches, which are accouted for by first deriving dynamic equations for inspiration and expiration separately. The following principles are applied to model the complete network:

Pseudo–Linear Modelling The pneumatic network equations will be formulated by mesh and node equations as if it were a linear network. The nonlinearities introduced by turbulent flow conditions are then taken into account by

$$\Delta p = R(\dot{V}) \cdot \dot{V}, \\ \text{with } R(\dot{V}) = R \cdot |\dot{V}|.$$

System gains are continuously updated according to the system's current flow magnitudes.

Superposition The linear representations of subnetworks belonging to single pneumatic power sources or ventilation gas types, respectively, are superimposed. Still, flow dependent resistances change according to the total flow, e.g.

$$\begin{aligned} \Delta p &= \Delta p^{\mathrm{I}} + \Delta p^{\mathrm{II}}, \\ \text{with } \Delta p^{\mathrm{I}} &= R(\dot{V}) \cdot \dot{V}^{\mathrm{I}}, \\ \Delta p^{\mathrm{II}} &= R(\dot{V}) \cdot \dot{V}^{\mathrm{II}}, \\ R(\dot{V}) &= R \cdot |\dot{V}^{\mathrm{I}} + \dot{V}^{\mathrm{II}}|. \end{aligned}$$

and superscripts $^{\mathrm{I}}$ and $^{\mathrm{II}}$ indicating subnetworks 1 and 2.

Switched Systems To appropriately model the influence of the check valves on the system's behaviour, pressure drop over check valves will be formulated in terms of conductance: $G\Delta p = \dot{V}$. If the respective conditions require a valve to stop flow, $G = 0$ holds. The system is therefore modelled as an linear–parameter–varying (LPV) in the broadest sense of its definition: The system depends linearly on its states and inputs and nonlinearly (softly or hard) on a set of parameters, denoted θ [4].

4.10.1 Inspiration

Subnetwork 1 — Blower Figure 4.18 displays the pneumatic subnetwork for the blower pneumatic power source during the inspiratory phase. The topology incorpo-

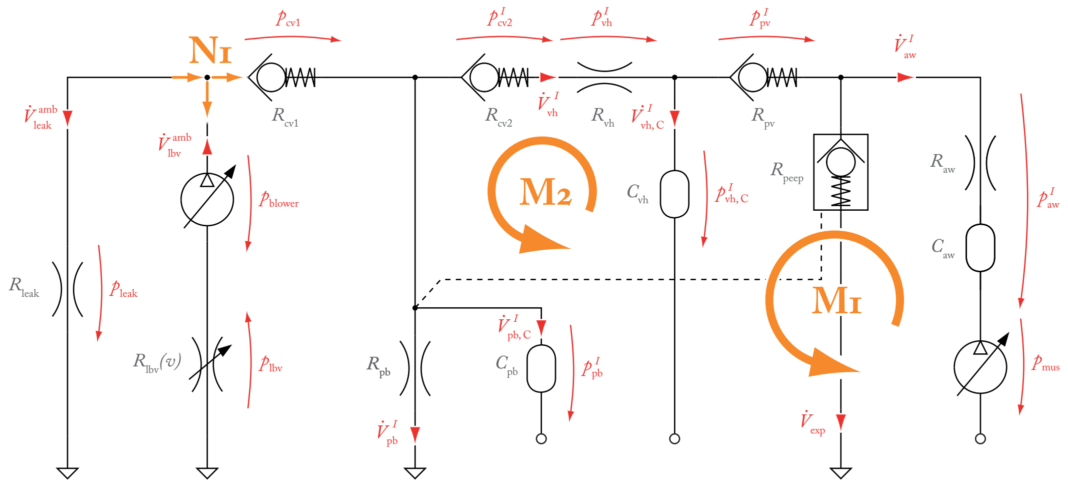

Figure 4.18: Pneumatic Subnetwork 1 for the Blower Pneumatic Power Source during Inspiration

rates three energy storages (compliances). Correspondingly three equations model the dynamic behaviour. The following mesh and node equations have been selected:

$$p^{\mathrm{I}}_{\mathrm{vh,C}} - p^{\mathrm{I}}_{\mathrm{aw}} - p^{\mathrm{I}}_{\mathrm{pv}} - p_{\mathrm{mus}} = 0 \qquad (\mathrm{M1}^{\mathrm{I}}_{\mathrm{insp}})$$
$$p^{\mathrm{I}}_{\mathrm{pb}} - p^{\mathrm{I}}_{\mathrm{vh,C}} - p^{\mathrm{I}}_{\mathrm{vh}} - p^{\mathrm{I}}_{\mathrm{cv,2}} = 0 \qquad (\mathrm{M2}^{\mathrm{I}}_{\mathrm{insp}})$$
$$\dot{V}^{\mathrm{amb}}_{\mathrm{lbv}} - \dot{V}^{\mathrm{amb}}_{\mathrm{leak}} - \dot{V}^{\mathrm{I}}_{\mathrm{vh,C}} - \dot{V}^{\mathrm{I}}_{\mathrm{aw}} - \dot{V}^{\mathrm{I}}_{\mathrm{pb}} - \dot{V}^{\mathrm{I}}_{\mathrm{pb,C}} = 0. \qquad (\mathrm{N1}^{\mathrm{I}}_{\mathrm{insp}})$$

The ambient air flows can be expressed in terms of the blower pressure (while check valve 1 is being neglected for simplicity), which marks another mesh equation used to eliminate the ambient air flow:

$$\dot{V}^{\mathrm{amb}}_{\mathrm{lbv}} = (p_{\mathrm{blower}} - p^{\mathrm{I}}_{\mathrm{pb}}) \cdot G_{\mathrm{lbv}}(v), \qquad (4.23)$$

It has been chosen to express $\dot{V}^{\mathrm{amb}}_{\mathrm{lbv}}$ in this way, such as to introduce the blower pressure input to the system and obtain a simpler formulation, since $p^{\mathrm{I}}_{\mathrm{pb}}$ can easily be expressed by the compliance's stored volume $V^{\mathrm{I}}_{\mathrm{pb,C}}$, a natural choice for a system state. The leakage flow can be expressed by

$$\dot{V}^{\mathrm{amb}}_{\mathrm{leak}} = \frac{p^{\mathrm{I}}_{\mathrm{pb}}}{R_{\mathrm{leak}}}. \qquad (4.24)$$

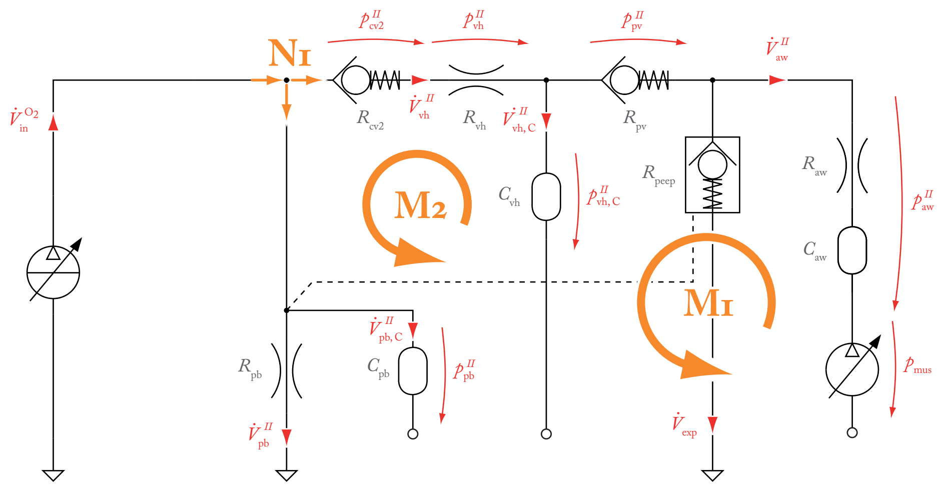

Figure 4.19: Pneumatic Subnetwork 2 for the Oxygen Pneumatic Power Source during Inspiration

Subnetwork 2 — Oxygen Source Figure 4.19 displays the pneumatic subnetwork for the oxygen pneumatic power source during the inspiratory phase. Again, mesh and node equations yield

$$p^{\mathrm{II}}_{\mathrm{vh,C}} - p^{\mathrm{II}}_{\mathrm{aw}} - p^{\mathrm{II}}_{\mathrm{pv}} - p_{\mathrm{mus}} = 0 \tag{M1$^{\mathrm{II}}_{\mathrm{insp}}$}$$

$$p^{\mathrm{II}}_{\mathrm{pb}} - p^{\mathrm{II}}_{\mathrm{vh,C}} - p^{\mathrm{II}}_{\mathrm{vh}} - p^{\mathrm{II}}_{\mathrm{cv,2}} = 0 \tag{M2$^{\mathrm{II}}_{\mathrm{insp}}$}$$

$$\dot{V}^{\mathrm{O_2}}_{\mathrm{in}} - \dot{V}^{\mathrm{II}}_{\mathrm{vh,C}} - \dot{V}^{\mathrm{II}}_{\mathrm{aw}} - \dot{V}^{\mathrm{II}}_{\mathrm{pb}} - \dot{V}^{\mathrm{II}}_{\mathrm{pb,C}} = 0. \tag{N1$^{\mathrm{II}}_{\mathrm{insp}}$}$$

4.10.2 Expiration

The system's topology enters the expiratory phase, if the expiratory valve opens. Check valve 2 is then assumed to close, preventing flow from entering the ventilation hose.

Subnetwork 1 — Blower Figure 4.20 displays the pneumatic subnetwork for the blower pneumatic power source during the expiratory phase. Selected mesh and node equations yield

$$p^{\mathrm{I}}_{\mathrm{peep}} - p^{\mathrm{I}}_{\mathrm{aw}} - p_{\mathrm{mus}} = 0 \tag{M1$^{\mathrm{I}}_{\mathrm{exp}}$}$$

$$\dot{V}^{\mathrm{amb}}_{\mathrm{lbv}} - \dot{V}^{\mathrm{amb}}_{\mathrm{leak}} - \dot{V}^{\mathrm{I}}_{\mathrm{pb,C}} - \dot{V}^{\mathrm{I}}_{\mathrm{pb}} = 0. \tag{N1$^{\mathrm{I}}_{\mathrm{exp}}$}$$

Equation 4.23 applies here as well to introduce the blower and large bore valve as the actuating elements. An additional switch of the system's topology may occur, if check valve 1 closes. This is assumed to only take place during expiration. Furthermore,

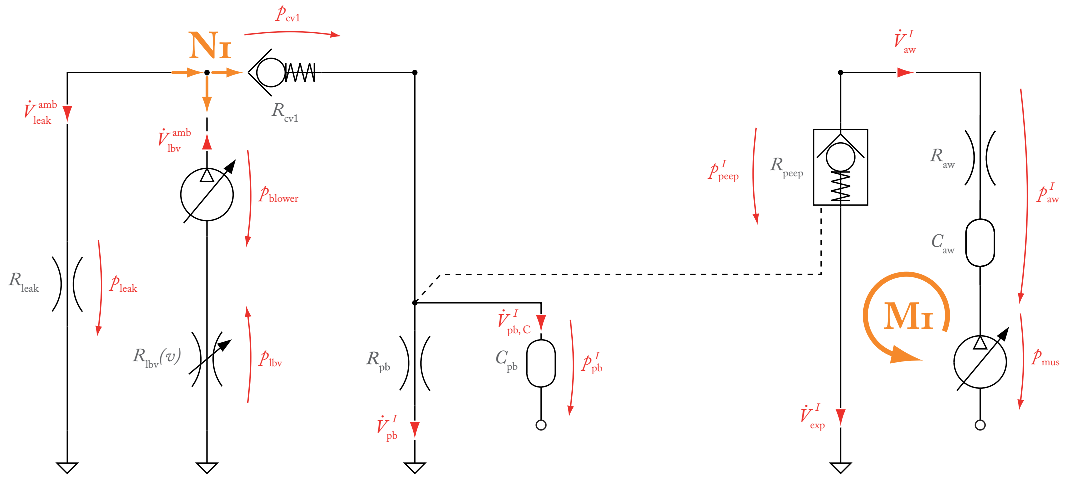

Figure 4.20: Pneumatic Subnetwork 1 for the Blower Pneumatic Power Source during Expiration

the pressure drop over this check valve may have been neglected for simplicity, but its influence on the topology is taken into account (cf. figure 4.21). In this state, the blower is prevented from providing flow through the PEEP blind, which discharges directly against atmosphere.

Subnetwork 2 — Oxygen Source Figure 4.22 displays the pneumatic subnetwork for the oxygen pneumatic power source during the expiratory phase. The right hand side of figure 4.22 remains unchanged compared to the blower power source subnetwork. Still it is part of subnetwork 2 as the state for oxygen volume stored in the patient's lungs is calculated separately from the ambient air.

Mesh and node equations yield

$$p_{\mathrm{peep}}^{\mathrm{II}} - p_{\mathrm{aw}}^{\mathrm{II}} - p_{\mathrm{mus}} = 0 \qquad (\mathrm{M1}_{\mathrm{exp}}^{\mathrm{II}})$$

$$\dot{V}_{\mathrm{in}}^{\mathrm{O_2}} - \dot{V}_{\mathrm{pb}}^{\mathrm{II}} - \dot{V}_{\mathrm{pb,C}}^{\mathrm{II}} = 0. \qquad (\mathrm{N1}_{\mathrm{exp}}^{\mathrm{II}})$$

4.10.3 Subnetwork State Space Formulations

Defining

$$\dot{\mathbf{x}}^{\mathrm{i}} = \begin{bmatrix} \dot{V}_{\mathrm{aw}}^{\mathrm{i}} \\ \dot{V}_{\mathrm{vh,C}}^{\mathrm{i}} \\ \dot{V}_{\mathrm{pb,C}}^{\mathrm{i}} \end{bmatrix}, \qquad \mathbf{x}^{\mathrm{i}} = \begin{bmatrix} V_{\mathrm{aw}}^{\mathrm{i}} \\ V_{\mathrm{vh,C}}^{\mathrm{i}} \\ V_{\mathrm{pb,C}}^{\mathrm{i}} \end{bmatrix}, \qquad (4.25)$$

with $\mathrm{i} \in [\mathrm{I}, \mathrm{II}]$

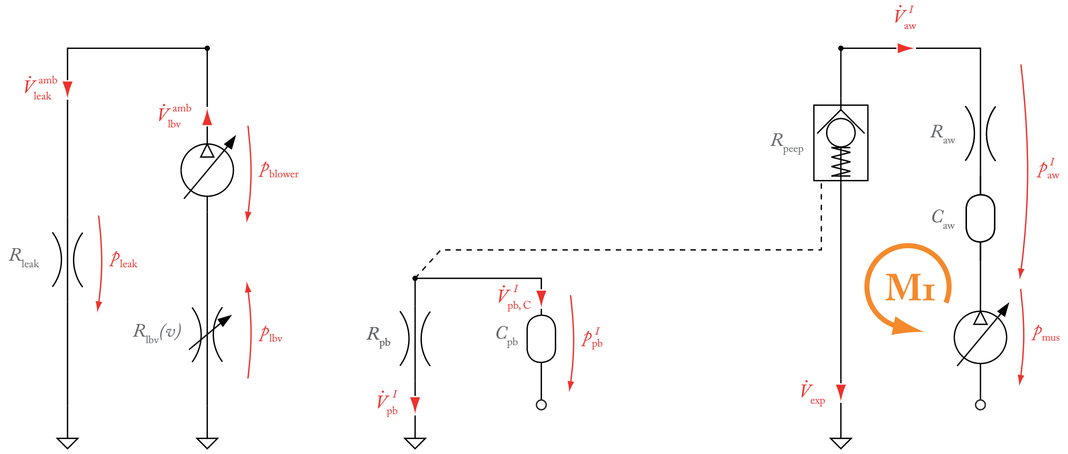

Figure 4.21: Pneumatic Subnetwork 1 for the Blower Pneumatic Power Source during Expiration and Check Valve 1 Shut

as states and state derivatives of subnetworks 1 and 2, respectively, as well as

$$\mathbf{u}^{\mathrm{I}} = \begin{bmatrix} \Delta p_{\mathrm{b}} \\ p_{\mathrm{mus}} \end{bmatrix}, \qquad \mathbf{u}^{\mathrm{II}} = \begin{bmatrix} \dot{V}_{\mathrm{in}}^{\mathrm{O}_2} \\ p_{\mathrm{mus}} \end{bmatrix}, \tag{4.26}$$

as inputs, enables to formulate the subnetwork's dynamics in terms of state space systems with nonlinearly changing gains by calculating the respective Jacobians. The methodical approach employed here is based on standard linearisation, which is well described in [29]. Subscripts $_{\mathrm{insp}}$ and $_{\mathrm{exp}}$ are dropped, since the following derivations apply for both conditions of topology.

Node and mesh equations above are compiled to vector functions

$$\mathbf{f}^{\mathrm{i}}(\dot{\mathbf{x}}^{\mathrm{i}}, \mathbf{x}^{\mathrm{i}}, \mathbf{u}^{\mathrm{i}}) = \mathbf{0} \quad \text{with } \mathbf{f} \in \mathbb{R}^3. \tag{4.27}$$

If a subnetwork's dynamics in a specific condition of topology is sufficiently described by less than 3 equations, a zero equation is added.

The subnetworks' state space formulations in implicit form for $\mathrm{i} \in [\mathrm{I}, \mathrm{II}]$ yield

$$\mathbf{E}^{\mathrm{i}}\dot{\mathbf{x}}^{\mathrm{i}} = \bar{\mathbf{A}}^{\mathrm{i}}\mathbf{x}^{\mathrm{i}} + \bar{\mathbf{B}}^{\mathrm{i}}\mathbf{u}^{\mathrm{i}}$$

where $\mathbf{E}^{\mathrm{i}}$, $\bar{\mathbf{A}}^{\mathrm{i}}$, $\bar{\mathbf{B}}^{\mathrm{i}}$ are derived from

$$\mathbf{E}^{\mathrm{i}} = \frac{\partial}{\partial \dot{\mathbf{x}}^{\mathrm{i}}}\mathbf{f}^{\mathrm{i}}(\cdot), \quad \bar{\mathbf{A}}^{\mathrm{i}} = \frac{\partial}{\partial \mathbf{x}^{\mathrm{i}}}\mathbf{f}^{\mathrm{i}}(\cdot), \quad \bar{\mathbf{B}}^{\mathrm{i}} = \frac{\partial}{\partial \mathbf{u}^{\mathrm{i}}}\mathbf{f}^{\mathrm{i}}(\cdot). \tag{4.28}$$

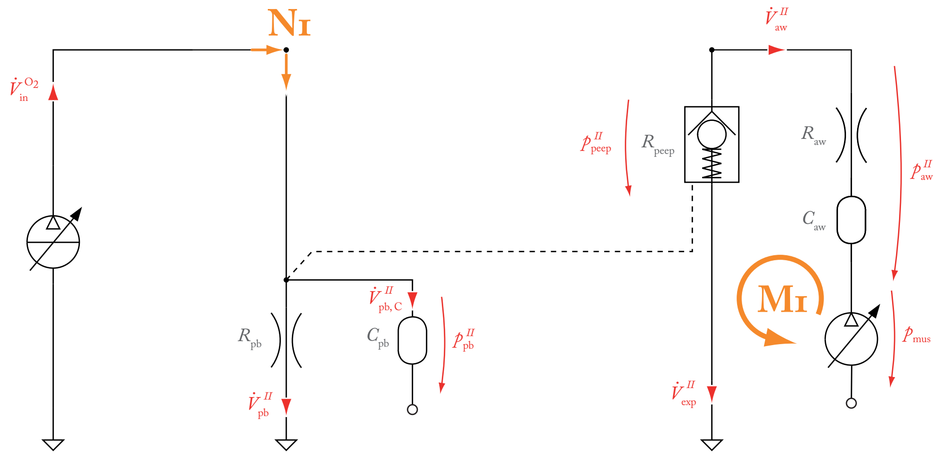

Figure 4.22: Pneumatic Subnetwork 2 for the Oxygen Pneumatic Power Source during Expiration

Since $\mathbf{f}^{\mathrm{i}}(\dot{\mathbf{x}}^{\mathrm{i}}, \mathbf{x}^{\mathrm{i}}, \mathbf{u}^{\mathrm{i}})$ are all differentiable and due to the fact, that all nonlinearities are hidden in the resistance coefficients

$$\underbrace{\mathbf{f}^{\mathrm{i}}(0, \mathbf{x}_0^{\mathrm{i}}, \mathbf{u}_0^{\mathrm{i}})}_{=0} + \begin{bmatrix} -\mathbf{E}^{\mathrm{i}} & \mathbf{A}^{\mathrm{i}} & \mathbf{B}^{\mathrm{i}} \end{bmatrix} \cdot \begin{bmatrix} \dot{\mathbf{x}}^{\mathrm{i}} \\ \mathbf{x}^{\mathrm{i}} \\ \mathbf{u}^{\mathrm{i}} \end{bmatrix} = 0 \tag{4.29}$$

holds. Explicit formulation is obtained by inversion of $\mathbf{E}^{\mathrm{i}}$:

$$\dot{\mathbf{x}}^{\mathrm{i}} = \underbrace{\mathbf{A}^{\mathrm{i}}}_{(\mathbf{E}^{\mathrm{i}})^{-1}\bar{\mathbf{A}}^{\mathrm{i}}} \mathbf{x}^{\mathrm{i}} + \underbrace{\mathbf{B}^{\mathrm{i}}}_{(\mathbf{E}^{\mathrm{i}})^{-1}\bar{\mathbf{B}}^{\mathrm{i}}} \mathbf{u}^{\mathrm{i}} \tag{4.30}$$

The output equations

$$\mathbf{y}^{\mathrm{i}} = \mathbf{C}^{\mathrm{i}} \cdot \begin{bmatrix} \dot{\mathbf{x}}^{\mathrm{i}} \\ \mathbf{x}^{\mathrm{i}} \\ \mathbf{u}^{\mathrm{i}} \end{bmatrix} \tag{4.31}$$

are extended to also depend on state derivatives $\dot{\mathbf{x}}^{\mathrm{i}}$ and inputs $\mathbf{u}^{\mathrm{i}}$. They are obtained in a similar way, by setting up the respective terms that formulate several quantities used in the model. Details are omitted here for brevity.

4.10.4 Topology Switching Conditions

The above derivations have omitted dependency of the system gain matrices on states $\mathbf{x}^{\mathrm{i}}$, state derivatives $\dot{\mathbf{x}}^{\mathrm{i}}$ and system inputs $\mathbf{u}^{\mathrm{i}}$. These directly influence the resistance and conductance values of the pneumatic network compiled in the vector

$$\theta(\dot{\mathbf{x}}, \mathbf{x}, \mathbf{u}) = \begin{bmatrix} G_{\mathrm{cv},1} \\ G_{\mathrm{cv},2} \\ R_{\mathrm{vh}} \\ R_{\mathrm{pb}} \\ G_{\mathrm{pv}} \\ R_{\mathrm{leak}} \\ G_{\mathrm{lbv}} \\ G_{\mathrm{peep}} \end{bmatrix} . \tag{4.32}$$

Superposition is applied to obtain:

$$\begin{aligned} \dot{\mathbf{x}} &= \dot{\mathbf{x}}^{\mathrm{I}} + \dot{\mathbf{x}}^{\mathrm{II}}, \\ \mathbf{x} &= \mathbf{x}^{\mathrm{I}} + \mathbf{x}^{\mathrm{II}}, \\ \mathbf{u}^T &= \begin{bmatrix} \mathbf{u}^{\mathrm{I}T} & \mathbf{u}^{\mathrm{II}T} \end{bmatrix}^T , \end{aligned}$$

Pressure ratios account for discontinuous check valve behaviour. The conditions employed to set check valve conductances to zero are:

$$p_{\mathrm{aw}} > p_{\mathrm{vh,C}} \quad \Leftrightarrow \quad G_{\mathrm{pv}} \equiv 0, \tag{4.33}$$

$$p_{\mathrm{vh,C}} > p_{\mathrm{pb}} \quad \Leftrightarrow \quad G_{\mathrm{cv},2} \equiv 0. \tag{4.34}$$

$$p_{\mathrm{pilot}} \cdot r_{\mathrm{peep}} > p_{\mathrm{aw}} \quad \Leftrightarrow \quad G_{\mathrm{peep}} \equiv 0. \tag{4.35}$$

Condition 4.35 marks the condition for inspiration (cf. section 4.8). In fact, it can be shown, that due to the formulation of the check valve resistances as conductances, the derived state matrices can be separated into topology dependent parts and subsequently added, e.g. :

$$\mathbf{A}^{\mathrm{i}}(\theta) = \underbrace{\mathbf{A}^{\mathrm{i}}_{\mathrm{common}}(\theta)}_{\text{always active}} + \underbrace{\mathbf{A}^{\mathrm{i}}_{\mathrm{insp}}(\theta)}_{\text{active during inspiration}} + \underbrace{\mathbf{A}^{\mathrm{i}}_{\mathrm{exp}}(\theta)}_{\text{active during expiration}} \quad \mathrm{i} \in [\mathrm{I}, \mathrm{II}] \,. \tag{4.36}$$

Figure 4.23 displays a simplified scheme of the nonlinear simulation expressed in terms of a time-varying state space model framework.

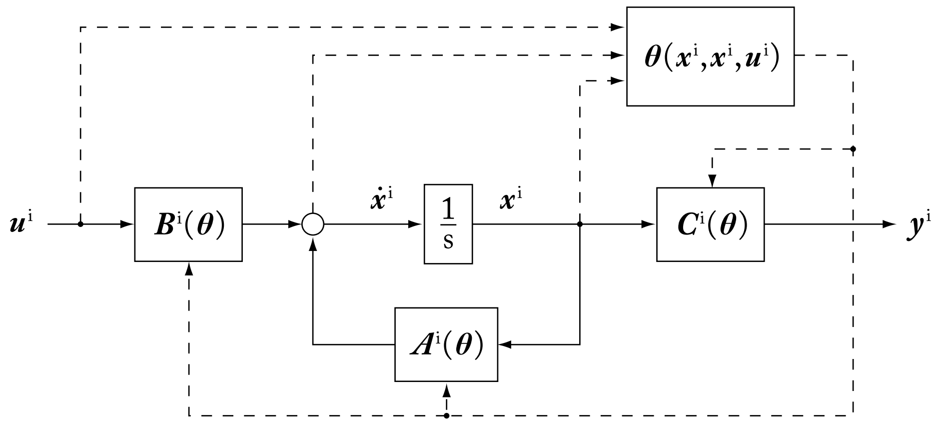

Figure 4.23: Nonlinear Simulation Scheme in Terms of a Time-Varying State Space Model Framework

4.11 Simulation and Validation

Simulation Issues Due to the nonlinear structure of the model (cf. figure 4.23), state space matrix gains can vary strongly. In terms of linear system's theory, dependence of $\mathbf{C}^{\mathrm{i}}(\theta)$ and $\mathbf{A}^{\mathrm{i}}(\theta)$ on state derivatives and inputs introduces implicit direct feedthrough. A solver, which can handle stiff systems is therefore necessary to simulate the nonlinear model. The MATLAB native solver ODE23S provided satisfactory results at resonable computation times. The solver is based on a modified ROSENBROCK formula of order 2 [43].

Validation It has been refrained from doing a thorough validation of the overall system for the following reasons:

- The modelling approach used in this thesis has already been applied to the WEINMANN MEDUMAT Transport and some components are taken from this device. The individual components' dynamic behaviour is thus validated and has already been presented in the respective sections.
- Ambient effects have been introduced for the very reason to extend the potential to analyse the ventilation device's behaviour under circumstances, which can not be reproduced with the facilities available at WEINMANN. For this reason, though the mathematical modelling of the ambient parameters is plausible, Mainly qualitative conclusions can thus be drawn from the simulation model, which predominantly cover the aspect of robustness.

Despite this reasoning, a few measurements have been made, of which figure 4.24 provides an example of the system's response to a step input $v_{\mathrm{mot}}\sigma(t) = \sigma(t - t_{\mathrm{step}})$ with patient airway parameters $R_{\mathrm{aw}} = 50\,\mathrm{mbar\,s/\,L}$ and $C_{\mathrm{aw}} = 0.03\,\mathrm{L/\,mbar}$. An IMTMEDICAL SMART LUNG is attached to the functional model with corresponding parameters.

While the pressure curves match very well, comparing the flow reveals a shortcoming of the model. The simulation model only employs a linear model of the patient airways and neglects nonlinearities. As indicated in figure 2.14, the lung compliance behaves nonlinearly above (and below) a certain volume. This is not accounted for in the simulation model. Since the IMTMEDICAL SMART LUNG is also only a mechanical model of a human lung, it is also not completely capturing the dynamic behaviour of a real lung. Despite this fact, it can saturate, for its construction is based on a frame, in which an inflatable bag is placed.

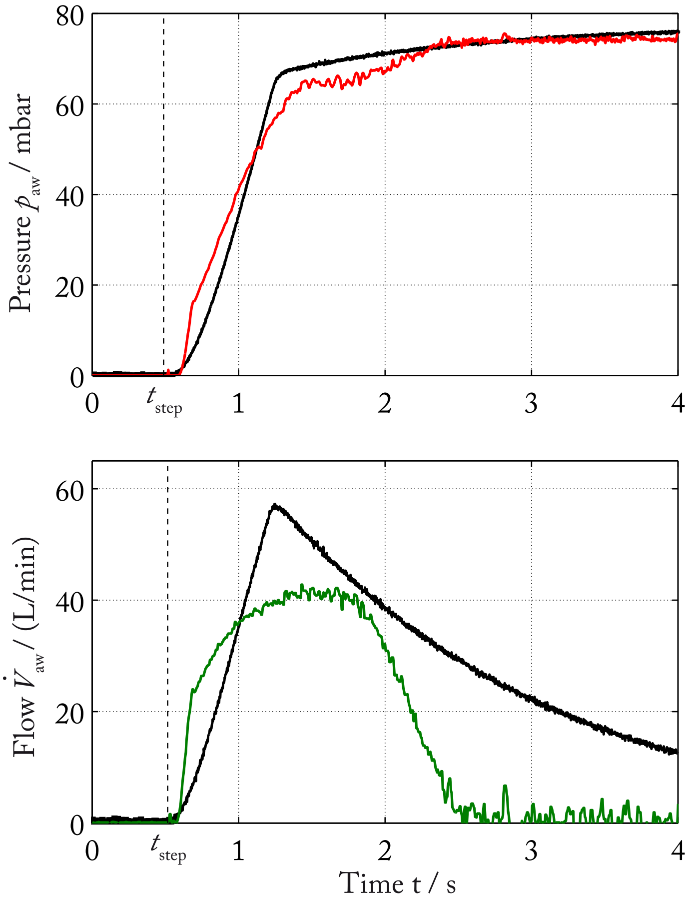

Figure 4.24: Step Response of both Functional Model and Simulation to a Step Input to the Blower, —— Functional Model Airway Pressure, —— Functional Model Airway Flow, —— Corresponding Simulated Quantities

5 Functional Model

This chapter will briefly explain, how the primary concept — which has been modelled in the last chapter — is implemented in hardware. First, the most important components are described. They are mainly taken from already available WEINMANN products or previous research, making use of the company's experience to the largest possible extent. Their interfaces to the existing MEDUMAT Transport hardware, which hosts an INFINEON XC161 16-bit microcontroller for control and an embedded PC for patient monitoring and user interaction, are designed and configured to make a single functional model. These interfaces are briefly explained at the end of this chapter, which gives a concluding overview of the hardware layout.

5.1 Components

Blower The radial blower by MICRONEL (cf. figure 5.1) is powered by a one quadrant, three-phase brushless direct current motor with hall sensors. A Maxon DEC 50/5 motor controller takes over the commutation to power the three phases consecutively, in order to let the motor exert torque. An analog reference signal of up to 5 V can be fed to the controller, which is set to control the motor voltage in open–loop. The closed–loop speed controller is disabled by intention, as the higher-level controller on the XC161 will be designed to enforce zero steady state error with respect to reference pressure. Having the motor controller also enforce reference tracking with regard to the speed results in double integral action and the closed-loop performance deteriorates. The blower voltage control signal is generated by low pass filtering a digital 1 kHz PWM signal output by the microcontroller.

Large Bore Valve The large bore valve is constructed from plastic and has a rotating inner component, whose position is varied by a small stepper motor. Two tear drop shaped orifices are placed onto a conical wall inside the flow channel. The rotating part has gaps to match the orifices and can be turned 90° to either open or close the valve in 400 steps. A schematic illustration of the valve is given in figure 5.2.

The stepper motor's data is listed in table 5.1.

A NANOTEC SMC-11 stepper motor driver processes a clock and direction bit signal output by the microcontroller to rotate the motor. It also provides means to limit the stepper motor current. For every negative flank of the clock signal, the stepper motor performs a single step. Pulse widths have been experimentally identified to be required

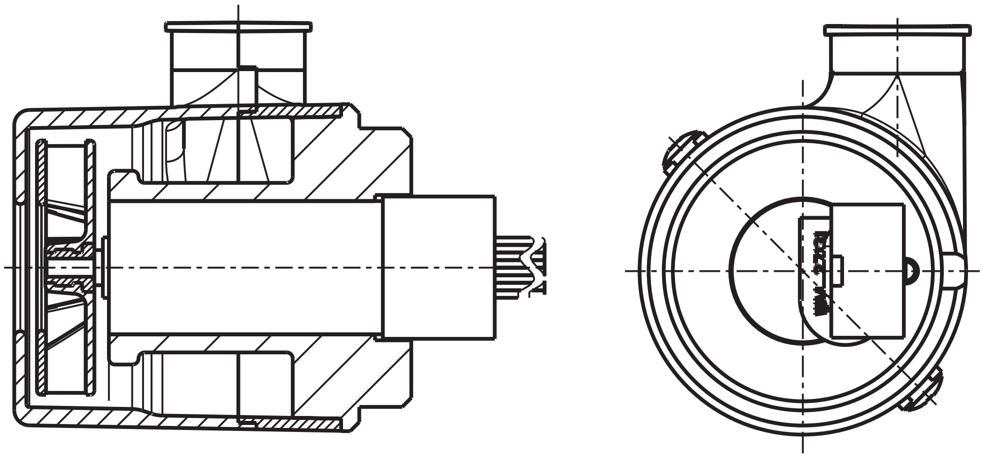

Figure 5.1: Technical Drawing of the MICRONEL Blower Used in WEINMANN Homecare Ventilation Devices [48]

at least 100 µs in duration for robust stepping. Consequently the valve takes 40 ms to completely close or open from the respective opposite starting position. For directional changes almost 2 ms are necessary. A stopping pin can be used to home the stepper motor.

Oxygen Inlet Valve [20] The oxygen inlet valve has been used from the original MEDUMAT Transport hardware. It is a proportional magnetic coil valve driven by currents ranging from 0 . . . 417 mA. The proportional span between opening current and saturation current ranges from 130 . . . 380 mA.

	Characteristic Value	
	Symbol	Value
Number of Gears	N_{gears}	100
Microstep Factor	z	4
Stepper Poles	p	4
Steps	$N_{\text{steps}} = N_{\text{gears}} \cdot z \cdot p$	1600
Step Resolution	$360°/N_{\text{steps}}$	0.25°

Table 5.1: Stepper Motor Characteristic Values [13]

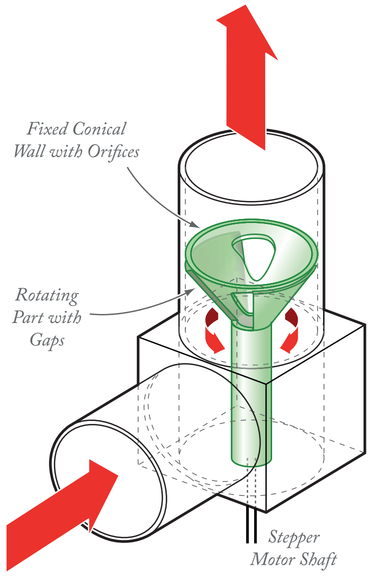

Figure 5.2: Schematic Illustration of the Large Bore Valve

Flow Measurement The functional model hosts two different flow sensors. An ultrasonic sensor uses the pulse transit–time method to infer the volume flow rate of the oxygen. It is part of the original MEDUMAT Transport design. An additional flow sensor is based on differential pressure measurement. A specially designed flow channel (cf. figure 5.3) borrowed from the VentiLogic homecare ventilation device marks a resistance introduced into the flow path. The characteristic curve of both the resistance and a Sensirion SDP1108–W7 differential pressure sensor has been identified at Weinmann during previous work and is implemented on the microcontroller to deduce the total flow. The pressure sensor signal is filtered by a hardware low–pass filter with bandwidth 25 Hz ($\approx 157.1\,\mathrm{rad/s}$).

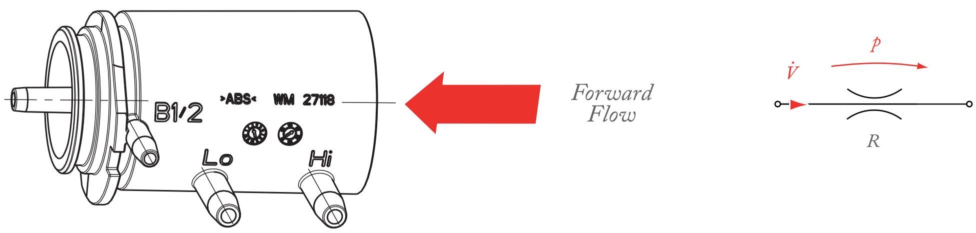

Figure 5.3: Differential Pressure Flow Measurement Channel [48]

Leakage The dimensioning of the intentional leakage behind the blower is subject to the constraint of the lowest possible PEEP, which can be attained. Based on a simplified pneumatic network in steady state (cf. figure 5.4) equation 5.1 can be derived, to investigate this matter.

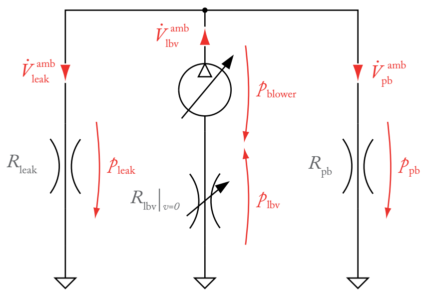

Figure 5.4: Steady State Network Topology for Minimum PEEP

$$p_{\text{peep,min}}(R_{\text{leak}}) = \frac{\sqrt{R_{\text{leak}} R_{\text{pb}}}}{R_{\text{lbv}}|_{v=0}\left(\sqrt{R_{\text{leak}}} + \sqrt{R_{\text{pb}}}\right) + \sqrt{R_{\text{leak}} R_{\text{pb}}}} \cdot p_{\text{blower}} \cdot r_{\text{peep}} \tag{5.1}$$

Figure 5.5 depicts an evaluation of the lowest attainable PEEP versus the leakage resistance for different blower pressures. The dashed line indicates the resistance chosen. A minimum PEEP of 7.2 mbar can be applied, while the blower is still running at full speed and the large bore valve is completely closed. A trade–off between low PEEP and limited leakage flow has to be made.

From figure 5.6 it becomes obvious, that a sufficient amount of cooling flow cannot be guaranteed with the current pneumatic structure. To amend this, the blower needs to reduce speed during expiration. Equation 5.2 is used to calculate the cooling flow during expiration.

$$\dot{V}^{\text{amb}}_{\text{lbv}} = \sqrt{\frac{p_{\text{blower}}}{R_{\text{lbv}}|_{v=0} + \frac{\sqrt{R_{\text{pb}} R_{\text{leak}}}}{\sqrt{R_{\text{pb}}} + \sqrt{R_{\text{leak}}}}}} \approx \dot{V}^{\text{amb}}_{\text{leak}} \tag{5.2}$$

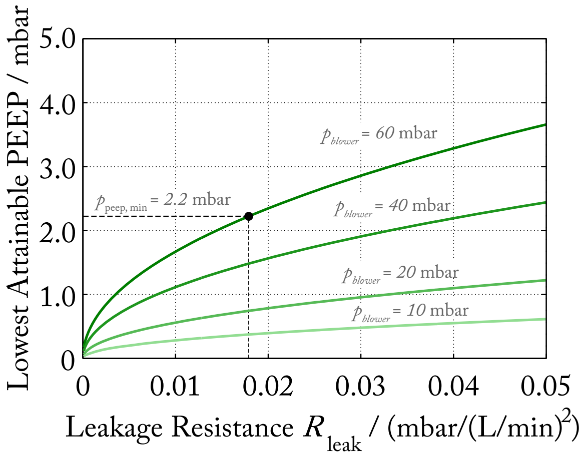

Figure 5.5: Lowest Attainable PEEP versus Leakage Resistance for Different Blower Pressures

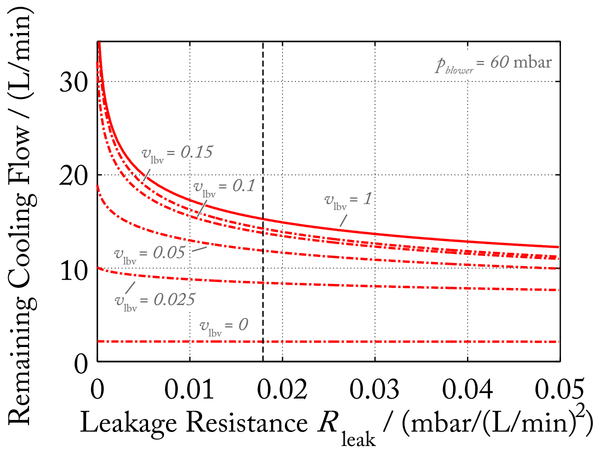

Figure 5.6: Remaining Cooling Flow versus Leakage Resistance for Differen Large Bore Valve Opening Ratios

5.2 Hardware Layout

Figure 5.7 depicts signal flows to and from the microcontroller. Pneumatic elements and networking have been set up according to the concepts described in the previous chapter.

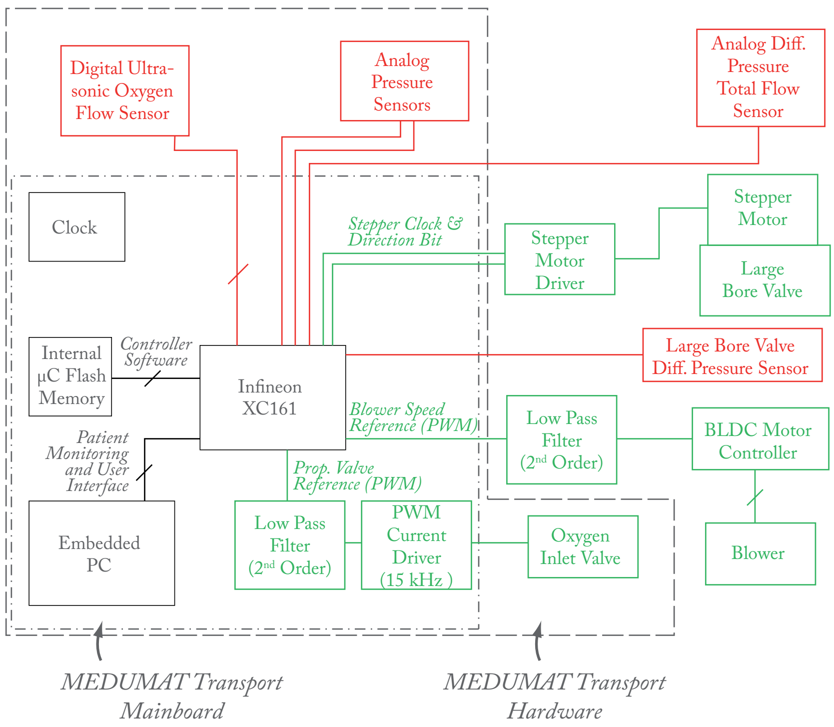

Figure 5.7: Hardware Layout and Signal Flow Diagram of the Functional Model

6 Controller Design

In this chapter, model–based controller synthesis for simulation and implementation in the functional model is covered. The introductory preliminary remarks cover all aspects common to the synthesis of the individual controllers, including a delineation of the controllers synthesised, the common design objectives and relevant parametric uncertainties, as well as the general synthesis procedure employed. After that, controller synthesis is covered in detail in the next three consecutive sections, 6.3, to 6.5. Section 6.6 will briefly explore degrees of freedom with regard to energy optimisation induced by the controller structures chosen and discusses their advantages and limitations. A simple first approach is documented, which has been implemented for the functional model. Section 6.7 provides a short survey about bumpless transfer schemes for controllers of arbitrary structure. Its necessity with respect to the safety of VCV based modes is pointed out, an initial solution is proposed and its effectiveness demonstrated by simulations. The final section 7.2 shows results of both the simulated controlled plant and the controlled functional model.

6.1 Preliminary Remarks

Synthesised Controllers Table 6.1 provides a rough delineation of the relevant controllers to prove the feasibility of the ventilation device concept. Check Marks Indicate Controller Configurations Designed and Tested, Crosses Indicate Combinations Irrelevant in the Context of this Thesis. Since efficient control for oxygen levels of $\mathrm{F_{iO_2}} = 100\,\mathrm{vol.\,\%}$ has already been implemented in the existing MEDUMAT Transport product and the functional model essentially uses the same actuators for that matter, proof of concept in that range is deemed unnecessary.

Common Design Objectives Controllers are synthesised on the basis of linear models of the plant in its respective operating condition. The $\mathcal{H}_\infty$ norm based approach is chosen, in order to conveniently define the desired closed-loop behaviour and demand robustness against parametric uncertainties. Robustness against model inherent nonlinearities due to turbulent flow are neglected and the initial assumption is made, that integral action can cope with them. This is validated by simulation and implementation.

Design objectives common to all controllers exist in the following items:

1. **Robustness** against uncertainty with respect to the patient's airways' parameters, as well as robustness against uncertainty of ambient parameters.

	Mode/Phase of Ventilation		
F_{iO_2}/ vol. %	PCV	VCV	PEEP
21	✓	✓	✓
21...100	✓	×	✓
100	×	×	×

Table 6.1: Matrix of Controllers Designed and Tested, Check Marks Indicate Controller Configurations Designed and Tested, Crosses Indicate Combinations Irrelevant in the Context of this Thesis

2. **Fast Tracking** of reference step inputs with minimum steady state error and no (VCV) to minimum overshoot (PCV and PEEP)[1].
3. **Rejection** of measurement noise and output disturbances.

Parametric Uncertainties The relevant parametric uncertainties are illustrated in figures 6.1 and 6.2. The latter indicates how the ambient parameters pressure p_{amb} and temperature ϑ_{amb} are combined to the single parameter of ambient pressure ϱ_{amb} by means of the ideal gas law.

The choice of values to generate the family of plants with is based on the parameter space method [2]: If uncertain plant parameters are constant or vary only slowly compared to the system dynamics, a controller is guaranteed to perform well in all points of the parameter space enclosed by its physically relevant extrema. Consequently, let $\mathsf{P} := \{(R_{\text{aw}}, C_{\text{aw}})|R_{\text{aw}} = R_{\text{aw},i}, C_{\text{aw}} = C_{\text{aw},i}, i = 0, 1, 2 \ldots, 8\}$ denote the set of vertices representing extremal combinations of patient airways' parameters and let $\mathsf{D} := \{\varrho_{\text{amb}}|\varrho_{\text{amb}} = \varrho_{\text{amb},i}, i = 0, 1, 2\}$ denote the set of extremal ambient densities, where each set also includes the nominal condition for $i = 0$. Furthermore let $\Omega := \mathsf{P} \times \mathsf{D}$ denote the set of parameter combinations used for synthesis. Not displayed here for brevity, ambient parameters also influence the oxygen valve's output flow, which adds further vertices $\mathsf{O} := \{\kappa_{\text{ov}}|\kappa_{\text{ov}} = \kappa_{\text{ov},i}, i = 0, 1, 2\}$ to the parameter space: $\Pi := \Omega \times \mathsf{O}$.

Synthesis Procedure The general synthesis procedure follows the steps described below.

1. **Continuous Time Controller Synthesis** Shaping filters are designed and applied to full order continuous time $\mathcal{H}_\infty$ controller synthesis for the nominal plant.

[1] Though no widely accepted research indicates, that overshoots in both flow or pressure controlled ventilation are particularly harmful to the patient, this is how current ventilation control objectives are expressed.

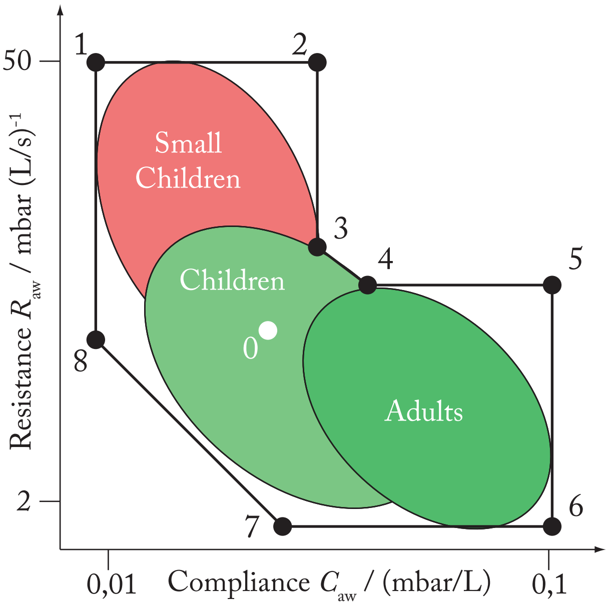

Figure 6.1: Visualisation of the Range of Required Robustness with Respect to the Pulmonary Parameters

2. **Discretisation of Nominal Controller** The found controller is then discretised and reduced in order using balanced reduction. Control has to be sufficiently satisfying at least for the nominal plant.
3. **Direct Synthesis of Robust Low Order Controller** A low order controller is directly synthesised in discrete time, taking into account time delays and parametric uncertainties. The previously discretised reduced order controller is serving as a starting point for the HIFOOD algorithm.
4. **Synthesis of Explicit Static Anti-Windup Controller Augmentation** The controller is eventually augmented by static anti-windup gains by applying theorem 6.1 for robust anti-windup compensator synthesis, an extension to theorem 2.2 found in [41] developed in this thesis.

The design procedure is iterative in nature and also requires some intuition for filter design. However, the following section will only present the final design and reasoning behind it.

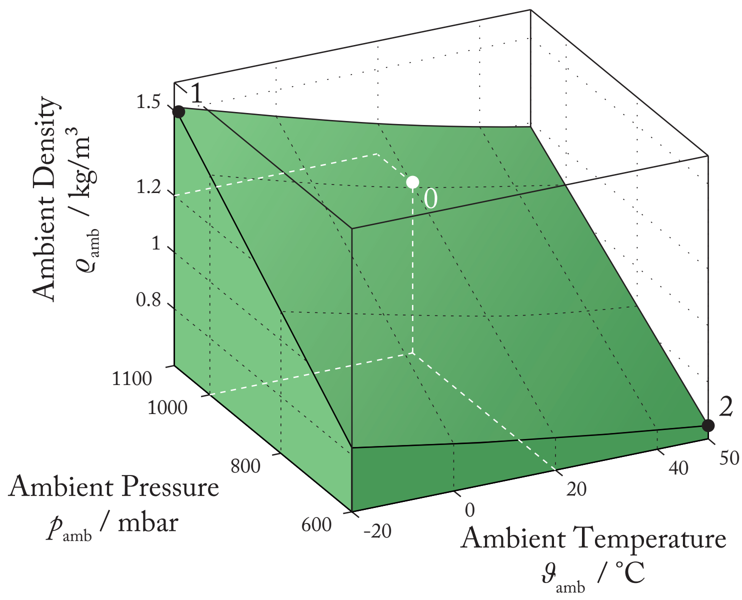

Figure 6.2: Visualisation of the Range of Required Robustness with Respect to the Pulmonary Parameters

6.2 Robust Explicit Static Anti–Windup Compensation

To achieve the best performance, the ventilation controllers are designed to make use of the actuators within the full range constrained by their saturation boundaries. This requires anti–windup compensation as explained in section 2.5.5.

An extension to theorem 2.2 has been developed in this thesis, to also allow for anti–windup controllers, that work for a family of plants, enforcing robust anti–windup performance.

Theorem 6.1. *(Extension of Explicit Static Anti-Windup Synthesis for Uncertain Discrete Time Systems) Define the family of N strictly proper plants*

$$\mathcal{G}_i(z) = \left[\begin{array}{c|c} \mathbf{A}_{g,i} & \mathbf{B}_{g,i} \\ \hline \mathbf{C}_{g,i} & \mathbf{0} \end{array}\right], \quad i = 1, \ldots, N, \tag{6.1}$$

and further definitions are as in theorem 2.2, except that the interconnection 2.59 is accordingly extended to form the family of N interconnections $\mathcal{P}_i(z)$, then any $\mathcal{P}_i(z)$ is globally stable for all $\mathbf{\Psi}$ and has a maximum induced l_2 gain performance of γ, if there exists a matrix $\mathbf{Q} = \mathbf{Q}^T > 0, \mathbf{Q} \in \mathbb{R}^{(n_g+n_k+n_u)\times(n_g+n_k+n_u)}$, a diagonal matrix $\mathbf{M} > 0, \mathbf{M} \in \mathbb{R}^{n_u \times n_u}$, an arbitrary matrix $\mathbf{X} := \begin{bmatrix} \mathbf{\Lambda}_1^T & \mathbf{\Lambda}_2^T \end{bmatrix}^T \mathbf{M} \in \mathbb{R}^{(n_k+n_u)\times n_u}$ and *scalars* $\gamma > 0$, $d > 0$, *such that the following set of* N *LMIs with objective to minimize* γ *are satisfied:*

$$\begin{bmatrix} -\mathbf{Q} & * & * & * & * & * \\ \mathbf{0} & -\gamma\mathbf{I} & * & * & * & * \\ \mathbf{C}_{u,i}\mathbf{Q} & \mathbf{D}_{ur} & -2\mathbf{M} & * & * & * \\ \mathbf{C}_{z,i}\mathbf{Q} & \mathbf{D}_{zr} & \mathbf{0} & -\gamma\mathbf{I} & * & * \\ \mathbf{A}_{,i}\mathbf{Q} & \mathbf{B}_{r,i} & \mathbf{B}_{\delta,i}\mathbf{M} - \mathbf{B}_e\mathbf{X} & \mathbf{0} & -\mathbf{Q} & * \\ \mathbf{0} & \mathbf{0} & \mathbf{M} & \mathbf{0} & \mathbf{0} & -d\mathbf{I} \end{bmatrix} < 0, \quad i = 1, \ldots, N. \tag{6.2}$$

A solution is not guaranteed to exist. However, experience has shown, that redesigning controllers to be more conservative with respect to their performance, increases the likelyness, that a feasible solution with acceptable l_2 gain performance can be found. Therefore, constraints imposed by the shaping filters have been slightly reduced, whenever anti–windup compensation synthesis has been found infeasible. This has always solved the issue in this thesis.

6.3 Volume Controlled Ventilation

Control Problem and Approach Volume controlled ventilation is approached as a SISO control problem. A reference flow $\dot{V}_{\mathrm{aw,ref}}$ and reference fraction of inspired oxygen $\mathrm{F}_{\mathrm{iO_2,ref}}$ is provided by the higher control level, from which two distinct reference flows $\dot{V}^{\mathrm{amb}}_{\mathrm{aw,ref}}$ and $\dot{V}^{\mathrm{O_2}}_{\mathrm{aw,ref}}$ are calculated by making use of the set of equations:

$$\begin{aligned}\mathrm{F}_{\mathrm{iO_2,ref}} \cdot \dot{V}_{\mathrm{aw,ref}} &= 0.21\dot{V}^{\mathrm{amb}}_{\mathrm{aw,ref}} + \dot{V}^{\mathrm{O_2}}_{\mathrm{aw,ref}}, \\ \dot{V}_{\mathrm{aw,ref}} &= \dot{V}^{\mathrm{amb}}_{\mathrm{aw,ref}} + \dot{V}^{\mathrm{O_2}}_{\mathrm{aw,ref}}. \end{aligned} \tag{6.3}$$

Figure 6.3 depicts the defining control loop.

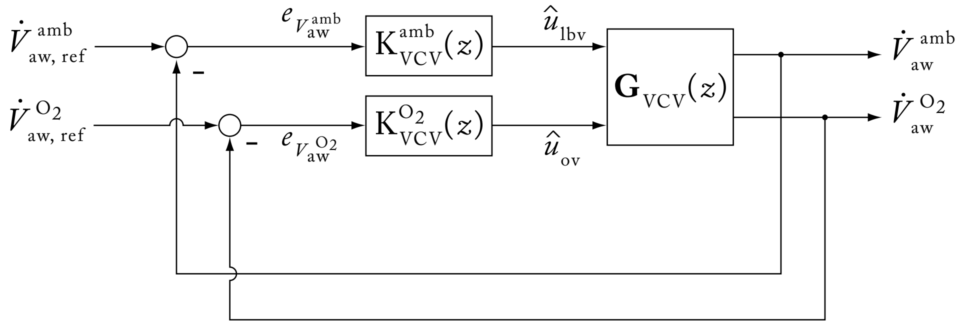

Figure 6.3: Problem Defining Control Loop for Volume Controlled Ventilation

For brevity, only the ambient air flow controller synthesis is explained in this thesis. However, an oxygen valve controller, which is used to track $\dot{V}^{\mathrm{O_2}}_{\mathrm{aw,ref}}$ in both volume controlled and pressure controlled ventilation modes (cf. next section) has been synthesised using the same techniques.

The large bore valve is chosen as the controlled actuator, because, considered as a controllable resistance, it effectively converts the pressure source to a flow controllable flow source and therefore is a natural choice for flow control. The decoupling of the blower setpoint from valve control also gives rise to energy saving feedforward control. Section 6.6 will expand on this.

Linear Plant Model Figure 6.4 displays a simplified pneumatic network used to derive a linear plant model. The differential equation

$$(R_{\mathrm{aw}} + R_{\mathrm{leak}}) \cdot \dot{V}^{\mathrm{amb}}_{\mathrm{aw}} + \frac{1}{C_{\mathrm{aw}}} \cdot V^{\mathrm{amb}}_{\mathrm{aw}} = R_{\mathrm{leak}} \frac{2\alpha a_{\mathrm{lbv}}}{\varrho_{\mathrm{lbv,out}}} \cdot \sqrt{p_{\mathrm{lbv}}} \cdot v_{\mathrm{lbv}} \tag{6.4}$$

defines the system's dynamic behaviour, where $\varrho_{\mathrm{lbv,out}} \approx \varrho_{\mathrm{amb}}$ is simplified and $R_{\mathrm{leak}} = R^0_{\mathrm{leak}} = R_{\mathrm{leak,turb}} \cdot \dot{V}^0_{\mathrm{leak}}$, $p_{\mathrm{lbv}} = p^0_{\mathrm{lbv}}$ are assumed to be at a nominal value. Due to the

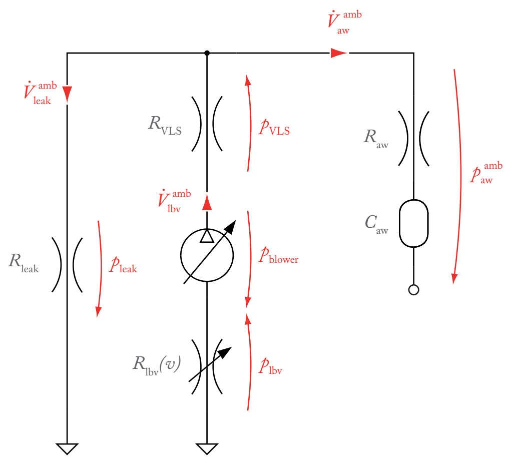

Figure 6.4: Simplified Pneumatic Network for Volume Controlled Ventilation

integral behaviour of the plant, no steady state exists. Considering typical conditions $\dot{V}_{\mathrm{leak}}^{0} = 20\,\mathrm{L/\,min}$ and $p_{\mathrm{lbv}}^{0} = 2.5\,\mathrm{mbar}$ are assumed feasible choices.

Note, that the dependence on the blower pressure p_{blower} is only implicitly contained in the equation by the pressure drop over the large bore valve p_{lbv}. The exact relation is irrelevant, as this fact is exploited to decouple blower speed setpoint from volume controlled ventilation: Since only the large bore valve's opening ratio v_{lbv} is controlled, the controller output $u_{\mathrm{lbv}}(t)$ will be corrected by a factor $\sqrt{p_{\mathrm{lbv}}^{0}/p_{\mathrm{lbv,meas}}}$, for which it is necessary to measure the pressure drop over the large bore valve.

Figure 6.5 details the ambient air flow control problem, by taking into account the aforementioned feedback linearisation and anti-windup feedback.

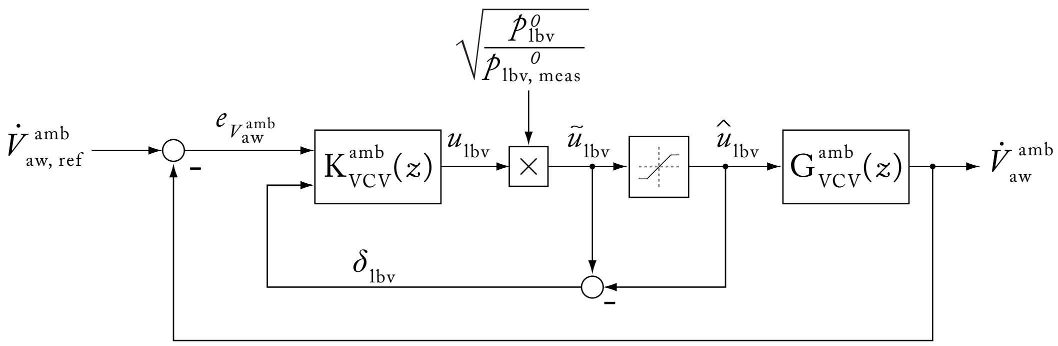

Figure 6.5: Problem Defining Control Loop for Volume Controlled Ventilation (Only Ambient Flow Control is Shown)

The large bore valve's behaviour is modelled to be of first order with time constant τ_{lbv}. A set of plants $G_{\mathrm{VCV},l}(s)$, $l = 0, 1, 2, \ldots, \#\Omega$ can then be represented by normalised state space models of the form (the superscript $^{\mathrm{amb}}$ for system descriptions has been dropped for brevity for the remainder of the section):

$$G_{\mathrm{VCV},l}(s) := \begin{cases} \underbrace{\begin{bmatrix} \dot{V}_{\mathrm{aw}}^{\mathrm{amb}} \\ \dot{x}_{\mathrm{lbv}} \end{bmatrix}}_{\dot{\mathbf{x}}_{\mathrm{VCV}}(t)} = \underbrace{\begin{bmatrix} -\frac{1}{C_{\mathrm{aw}}(R_{\mathrm{aw}}+R_{\mathrm{leak}}^0)} & \frac{2\alpha a_{\mathrm{lbv}} R_{\mathrm{leak}}^0 \sqrt{p_{\mathrm{lbv}}^0}}{(R_{\mathrm{aw}}+R_{\mathrm{leak}}^0)\varrho_{\mathrm{amb}}} \\ 0 & -\frac{1}{\tau_{\mathrm{lbv}}} \end{bmatrix}}_{\mathbf{A}_{\mathrm{VCV,l}}} \cdot \underbrace{\begin{bmatrix} V_{\mathrm{aw}}^{\mathrm{amb}} \\ x_{\mathrm{lbv}} \end{bmatrix}}_{\mathbf{x}_{\mathrm{VCV}}(t)} + \underbrace{\begin{bmatrix} 0 \\ \frac{1}{\tau_{\mathrm{lbv}}} \end{bmatrix}}_{\mathbf{B}_{\mathrm{VCV}}} \cdot \underbrace{v_{\mathrm{lbv}}}_{u_{\mathrm{lbv}}(t)} \\ \underbrace{\dot{V}_{\mathrm{aw}}^{\mathrm{amb},*}}_{y_{\mathrm{VCV}}(t)} = \underbrace{\frac{1}{\dot{V}_{\mathrm{aw}}^0} \cdot \begin{bmatrix} -\frac{1}{C_{\mathrm{aw}}(R_{\mathrm{aw}}+R_{\mathrm{leak}}^0)} & \frac{2\alpha a_{\mathrm{lbv}} R_{\mathrm{leak}}^0 \sqrt{p_{\mathrm{lbv}}^0}}{(R_{\mathrm{aw}}+R_{\mathrm{leak}}^0)\varrho_{\mathrm{amb}}} \end{bmatrix}}_{\mathbf{C}_{\mathrm{VCV,l}}} \cdot \mathbf{x}_{\mathrm{VCV}}(t) \end{cases} \tag{6.5}$$

Shaping Filters and Synthesis Figure 6.6 shows a plot of the singular values of the discretised open-loop system. The positive slope of +20 dB at low frequencies indicates a zero at $z = 1$. Therefore, in order to achieve good reference tracking a near double integral behaviour of the controller is necessary, requiring the controller to be at least of order 2. Weighting filter constraints for the sensitivity and control sensitivity have been

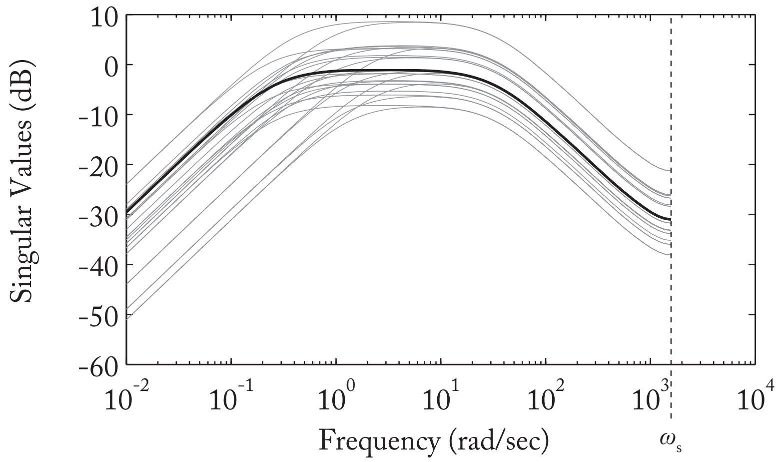

Figure 6.6: Singular Values over Frequency for the Open–Loop Plants, — Nominal Plant $G_{\mathrm{VCV},0}(s)$, — Plants $G_{\mathrm{VCV},l}(s), l > 0$

employed:

$$W_S(s) = \frac{(s+9)(s+5\cdot 10^{-6})}{(s+9\cdot 10^{-2})(s+5\cdot 10^{-4})}, \qquad W_{KS}(s) = \frac{7}{3}\frac{s+1\cdot 10^{-4}}{s+700}.$$

The weight W_S respects the fact, that the synthesis algorithm does not exactly converge to a controller with a perfect integrator cancelling out the zero, and allows the sensitivity

$S(s)$ to approach 1 for very low frequencies. Furthermore, pole–zero cancellation does not occur for numerical inaccuracies.

Figure 6.7 shows frequency responses of the sensitivity functions, which clearly show, that the zero $z = 1$ is still present in the closed-loop.

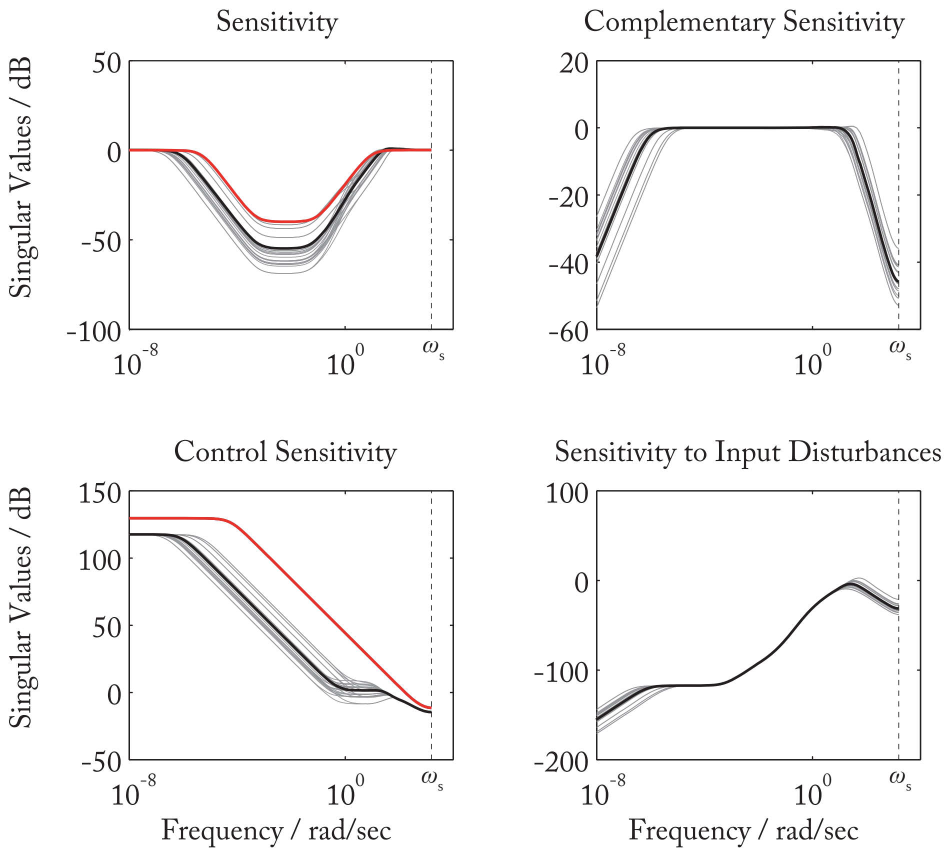

Figure 6.7: Singular Values over Frequency for the Sensitivities of the Controlled Plant, — Nominal Plant $G_{\mathrm{VCV},0}(s)$, — Plants $G_{\mathrm{VCV},l}(s), l > 0$, — Shaping Filters

However, considering the controller transfer function

$$K_{\mathrm{VCV}}(z) = 0.24544 \frac{(z-0.3062)(z-0.9019)(z-0.998)}{(z-0.6694)(z-(1+\varepsilon))(z-(1+\varepsilon))}, \quad 0 < \varepsilon \ll 1,$$

it becomes obvious, that the controller actually exhibits double integral behaviour. Figure 6.8 shows frequency responses with enforced pole–zero cancellation, which then more accurately describe the closed-loop performance perceived in simulation.

The closed-loop bandwidth ranges between $\omega_{\mathrm{cl}} = 10 \ldots 75 \frac{\mathrm{rad}}{\mathrm{s}}$ depending on system parameters. Any attempt to further increase the bandwidth for faster response resulted in adverse effects and, e.g. introduced resonant peaks in the (complementary) sensitivity function.

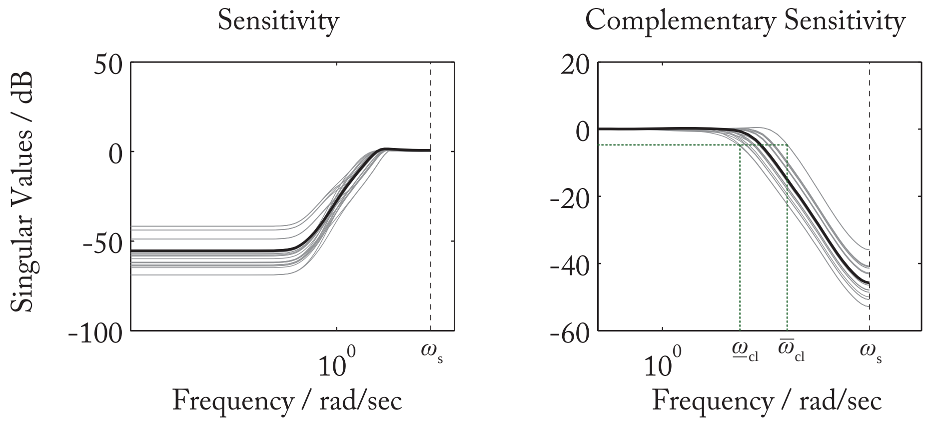

Figure 6.8: Singular Values over Frequency for the Sensitivities of the Controlled Plant after Enforcing Pole–Zero Cancellation, — Nominal Plant $G_{\mathrm{VCV},0}(s)$, — Plants $G_{\mathrm{VCV},l}(s), l > 0$

It has been a further approach, to both manually cancel out the zero of the plant and adding an integrator to the synthesised controller later on. However, the best controller has been found by the procedure described before and is of order 3, achieving an $\mathcal{H}_\infty$ performance of $\gamma = 1.23$, which shows that the constraints are nearly met.

Anti-Windup Synthesis Synthesising robust static anti-windup gains by applying theorem 6.1 has yielded a l_2 performance of $\gamma = 2.92$.

6.4 Pressure Controlled Ventilation

Control Problem and Approach Pressure controlled ventilation is approached as a SISO control problem by actuating the blower to achieve and maintain the desired airways pressure $p_{\text{aw,ref}}$, while a further independet controller tracks an oxygen flow pattern determined by

$$\dot{V}^{\text{O}_2}_{\text{aw,ref}}(t) = \text{F}_{\text{iO}_2,\text{ref}} \cdot \dot{V}_{\text{aw,meas}}(t) - 0.21\dot{V}^{\text{amb}}_{\text{aw,meas}}(t). \tag{6.6}$$

To achieve the best efficiency the large bore valve is usually completely opened. Figure 6.9 depicts the defining control loop.

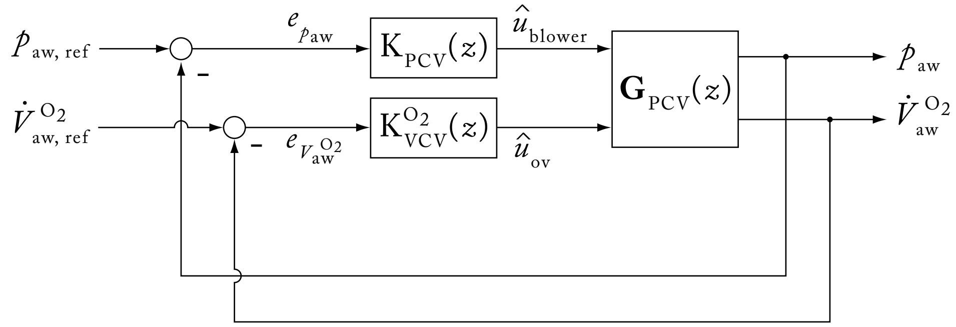

Figure 6.9: Problem Defining Control Loop for Pressure Controlled Ventilation

Linear Plant Model Figure 6.10 displays a simplified pneumatic network used to derive a linear plant model. It is assumed, that the networks for both power sources can be ideally superimposed. Despite that, the pressure induced by the oxygen flow is considered an output disturbance with respect to the pressure controller $K_{\text{PCV}}(z)$. Consequently, only the right hand side of figure 6.10 is deemed relevant for the derivation of the linear plant model.

By formulation of the equation of the right hand side mesh and taking into account equation 4.9 from section 4.1

$$R_{\text{aw}} \cdot \dot{V}^{\text{amb}}_{\text{aw}} + \frac{1}{C_{\text{aw}}} \cdot V^{\text{amb}}_{\text{aw}} + \underbrace{\left(\frac{1}{2}\varrho_{\text{b,out}} R_{\text{blower}} + R_{\text{lbv}}\right)}_{R_{\text{b}}} \cdot \dot{V}^{\text{amb}}_{\text{lbv}} = \frac{1}{2}\varrho_{\text{b,out}} r_{\text{blower}} \cdot n^2 \tag{6.7}$$

and expressing $\dot{V}^{\text{amb}}_{\text{lbv}}$ via the mesh $p_{\text{leak}} = p^{\text{amb}}_{\text{aw}}$ as

$$\dot{V}^{\text{amb}}_{\text{lbv}} = \underbrace{\left(1 + \frac{R_{\text{aw}}}{R_{\text{leak}}}\right)}_{r_{\text{b}}} \cdot \dot{V}^{\text{amb}}_{\text{aw}} + \frac{1}{R_{\text{leak}} C_{\text{aw}}} V^{\text{amb}}_{\text{aw}} \tag{6.8}$$

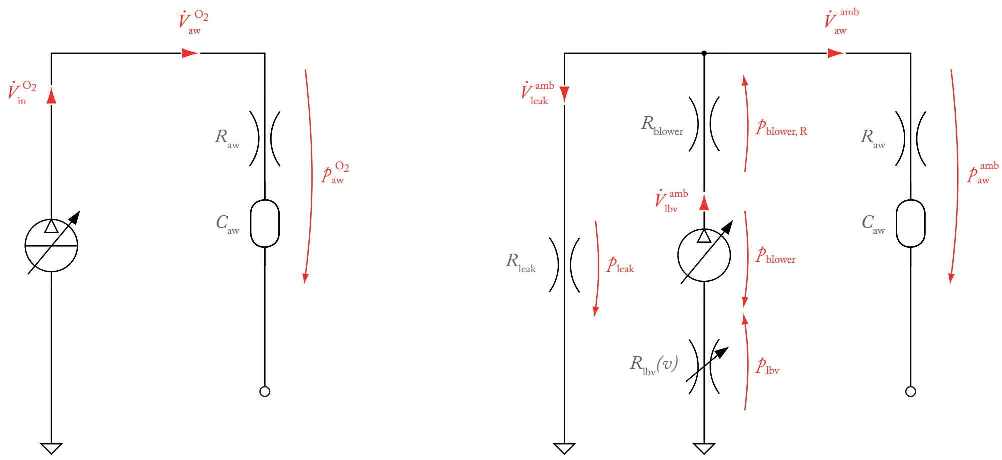

Figure 6.10: Simplified Pneumatic Network for Pressure Controlled Ventilation, (l.) Oxygen Flow Source, (r.) Blower Pressure Source

the differential equation to define the system's dynamic behaviour in terms of the state V^{amb}_{aw} can be found:

$$(R_{aw} r_b + R_b) \cdot \dot{V}^{amb}_{aw} + \frac{1 + r_b}{C_{aw}} \cdot V^{amb}_{aw} = \frac{1}{2} \varrho_{b,out} r_{blower} \cdot n^2, \tag{6.9}$$

$$\text{where } R_b = \left(\frac{1}{2} \varrho_{b,out} R_{blower} + R_{lbv} \right),$$

$$r_b = 1 + \frac{R_b}{R_{leak}},$$

Again, $\varrho_{b,out} \approx \varrho_{amb}$ is simplified and $R^0_{leak} = R_{leak,turb} \cdot \dot{V}^0_{leak}$, $R^0_{lbv} = R_{lbv,turb} \cdot \dot{V}^{0,amb}_{lbv}$ are assumed to be at a nominal value. Also $R^0_{blower} = R_{blower,turb} \cdot \dot{V}^{amb,0}_{lbv}$ is set to a nominal value, which is chosen, such that it approximates the blower's characteristic curve best in the regime from $\dot{V}^{amb}_{lbv} = 0 \ldots 200\,\mathrm{L/\,min}$. Figure 6.11 illustrates this linear approximation.

Inserting equation 6.8 into

$$p^{amb}_{aw} + R_b \cdot \dot{V}^{amb}_{lbv} = \frac{1}{2} \varrho_{b,out} r_{blower} \cdot n^2 \tag{6.10}$$

yields the output equation:

$$p^{amb}_{aw} = \frac{R_b r_{aw}}{C_{aw}(R_{aw} + R_b r_{aw})} \cdot V^{amb}_{aw} + \frac{R_{aw}}{R_{aw} + R_b r_{aw}} \frac{1}{2} \varrho_{b,out} r_{blower} \cdot n^2, \tag{6.11}$$

$$\text{where } r_{aw} = 1 + \frac{R_{aw}}{R_{leak}},$$

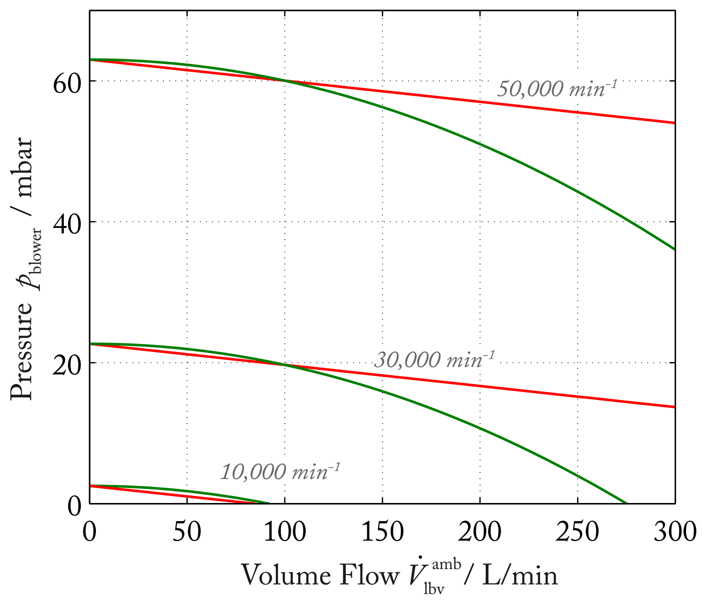

Figure 6.11: Linear Approximation of the Blower's Characteristic Curve for Use in the Linear Plant Model, —— Linear Approximation, —— Quadratic Model

The blower's behaviour is assumed to be of first order with time constant τ_n.

A set of plants $G_{\text{PCV},l}(s)$, $l = 0, 1, 2, \ldots, \#\Pi$ can then be represented by normalised state space models of the form:

$$G_{\text{PCV},l}(s) := \begin{cases} \underbrace{\begin{bmatrix} \dot{V}^{\text{amb}}_{\text{aw}} \\ \dot{x}_n \end{bmatrix}}_{\dot{\mathbf{x}}_{\text{PCV}}(t)} = \underbrace{\begin{bmatrix} -\frac{1+r_{\text{b}}}{C_{\text{aw}}(R_{\text{aw}}r_{\text{b}}+R_{\text{b}})} & \frac{1}{2}\frac{\varrho_{\text{amb}}r_{\text{blower}}}{R_{\text{aw}}r_{\text{b}}+R_{\text{b}}}n^2_{\text{max}} \\ 0 & -\frac{1}{\tau_n} \end{bmatrix}}_{\mathbf{A}_{\text{PCV,l}}} \cdot \underbrace{\begin{bmatrix} V^{\text{amb}}_{\text{aw}} \\ x_n \end{bmatrix}}_{\mathbf{x}_{\text{PCV}}(t)} + \underbrace{\begin{bmatrix} 0 \\ \frac{1}{\tau_n} \end{bmatrix}}_{\mathbf{B}_{\text{PCV,l}}} \cdot u_{\text{blower}}(t) \\ \underbrace{p^*_{\text{aw}}}_{y_{\text{PCV}}(t)} = \underbrace{\frac{1}{p^0_{\text{aw}}}\begin{bmatrix} \frac{R_{\text{b}}r_{\text{aw}}}{C_{\text{aw}}(R_{\text{aw}}+R_{\text{b}}r_{\text{aw}})} & \frac{1}{2}\frac{\varrho_{\text{amb}}r_{\text{blower}}R_{\text{aw}}}{R_{\text{aw}}+R_{\text{b}}r_{\text{aw}}}n^2_{\text{max}} \end{bmatrix}}_{\mathbf{C}_{\text{PCV,l}}} \cdot \mathbf{x}_{\text{PCV}}(t) \end{cases} \tag{6.12}$$

A time delay of 9 sampling instants with regard to the measured pressure, to account for the pressure signal both being transfered to the expiration valve and being transmitted back to the sensor has been added after discretisation of the plant. Thus, the plant is of order 11.

	Controller Order		
γ	Order 1	Order 2	Order 3
$\mathcal{H}_\infty$ Performance	3.44	3.44	3.45
l_2 Anti–Windup Performance	3.55	5.08	4.05

Table 6.2: Best $\mathcal{H}_\infty$ Performance Versus Controller Order for Pressure Controlled Ventilation Controller Synthesis with HIFOOD

Shaping Filters and Synthesis The initial continous time $\mathcal{H}_\infty$ controller is designed with the shaping filters

$$W_S(s) = 8 \cdot 10^{-1} \frac{s+20}{s+0.02}, \quad W_{KS}(s) = \frac{1}{3}. \tag{6.13}$$

The sensitivity shaping filter allows for a slight overshoot to improve rise time. For a first design, the control sensitivity is only shaped by the constant filter, which already resulted in feasible outcomes. Continuous time synthesis results in a third order controller, since only the undelayed plant can be used with the native tools of the MATLAB robust control toolbox. Any robust discrete time controller using the discretised controller as an initial starting point for optimisation by HIFOOD is thus limited to this maximum order of three. Table 6.2 lists achieved $\mathcal{H}_\infty$ performances versus the controller order.

As it turns out, first order (PI) control is sufficiently capable of achieving robust stability and performance. In fact, anti–windup compensation synthesis for this controller yielded the lowest l_2 gain. Therefore the controller of lowest order is selected.

Figure 6.12 shows singular value plots of the controlled plant including time delay. The closed-loop bandwidth for pressure control ranges between $\omega_{\mathrm{cl}} = 7.75 \ldots 18.5 \frac{\mathrm{rad}}{\mathrm{s}}$ depending on system parameters.

Anti-Windup Synthesis Synthesising robust static anti-windup gains by applying theorem 6.1 has yielded a l_2 performances as given in table 6.2.

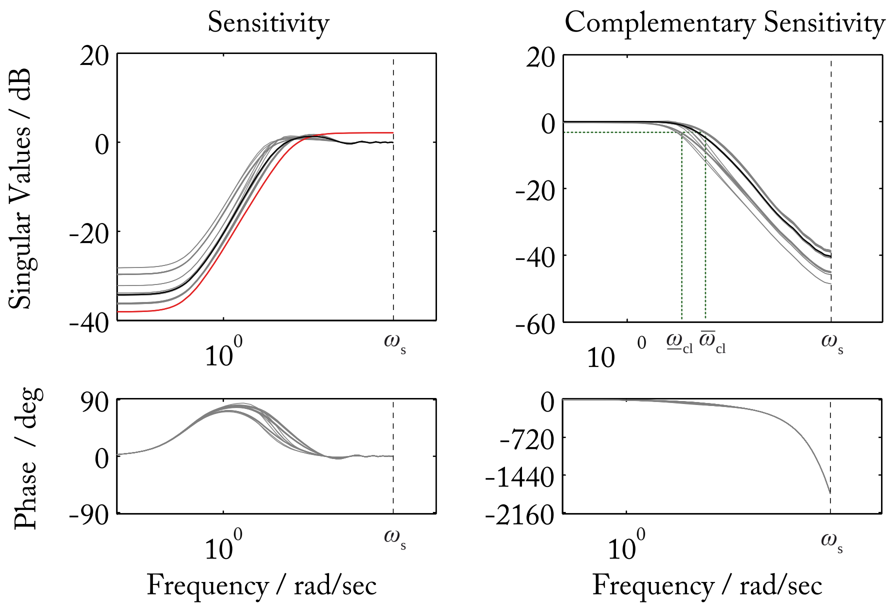

Figure 6.12: Singular Values over Frequency for the Sensitivities of the Controlled Plant for Pressure Control, — Nominal Plant $G_{\mathrm{PCV},0}(s)$, — Plants $G_{\mathrm{PCV},l}(s), l > 0$, — Shaping Filters

6.5 Expiratory Pressure Control

Control Problem and Approach Expiration is a passive process. By means of ventilation device control, it cannot be accelerated beyond the rate of discharge governed by the time constant $\tau_{\mathrm{aw}} = R_{\mathrm{aw}} C_{\mathrm{aw}}$. The only means to control the expiratory pressure is by applying a positive pilot pressure $p_{\mathrm{pilot}} = p_{\mathrm{pb}}$ to the expiration valve membrane.

If the initial pressure drop due to the airway's resistance has already happened and the patient's airway pressure is still above the desired PEEP level, the control error

$$e_{p_{\mathrm{aw}}} = p_{\mathrm{aw,ref}} - p_{\mathrm{aw}}$$

is negative, while the expiration valve is in saturation, i.e. $p_{\mathrm{pb}} = 0$. A patient with restrictive disease — having a low compliance — could bear an example, where this effect is prominent. This demands for an anti–windup compensator.

Furthermore, at the beginning of the expiration a pressure drop of

$$\Delta p_{\mathrm{aw}} = R_{\mathrm{aw}} \left. \dot{V}_{\mathrm{exp}} \right|_{t = T_{\mathrm{insp}} + \varepsilon}$$

occurs. For certain patients with obstructive diseases, this can lead to a drop below the desired PEEP level at the very instant. Considering, that it takes up to 10 ms for the pilot pressure to reach the expiration valve and another 10 ms for the airways pressure sensor to register, control relying on the feedback signal p_{aw} alone, will always lack without some sort of predictive algorithm.

Figure 6.13 illustrates both effects described above schematically for volume controlled ventilation.

To amend the issue of strong undershoots with regard to PEEP control, two approaches have already been examined in previous works:

Using p_{pb} for Feedback Relying on the PEEP blind pressure drop as a feedback signal eliminates the time delay, but demands for gain scheduling to obtain satisfactory control performance in case of a saturating expiration valve. This approach is implemented in the Weinmann MEDUMAT Transport and provides feasible results.

Cascaded Control [20] A cascaded control approach has employed an inner control loop, with aggressive control of the pilot pressure, whose reference value is provided by an outer control loop, which tries to track the airways pressure. This strategy has not been developed up to a feasible implementation, but has yielded robust results in simulation.

A new approach is proposed in this thesis, which uses both the pilot and the airway pressures for feedback, where the reference values are chosen, such that the airway

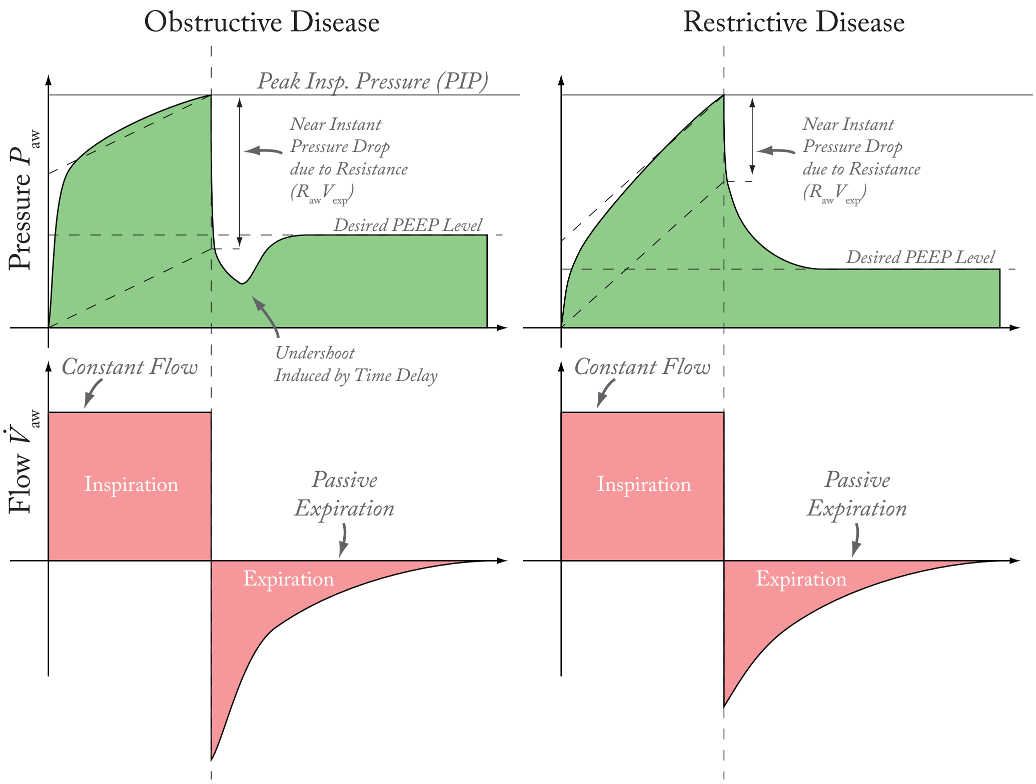

Figure 6.13: Schematic Illustration of Strong Undershoots (Obstructive Patient) and Low Compliance (Restrictive Patient) Effects on PEEP Control

pressure marks the desired PEEP level and the pilot pressure is chosen according to the membrane area ratio of the expiration valve:

$$p_{\text{aw,ref}} = p_{\text{peep,ref}},$$
$$p_{\text{pb,ref}} = \frac{1}{r_{\text{peep}}} \cdot p_{\text{peep,ref}}.$$

Figure 6.14 depicts the defining control loop.

Linear Plant Model Figure 6.15 displays a simplified pneumatic network used to derive a linear plant model.

The differential equations

$$R_{\text{leak}} \cdot \dot{V}_{\text{pb,C}} + \frac{1}{C_{\text{pb}}}(1 + \frac{R_{\text{leak}}}{R_{\text{pb}}}) \cdot V_{\text{pb,C}} = R_{\text{leak}} \frac{2\alpha a_{\text{lbv}}}{\varrho_{\text{lbv,out}}} \cdot \sqrt{p_{\text{lbv}}} \cdot v_{\text{lbv}} \tag{6.14}$$

$$(R_{\text{aw}} + R_{\text{peep}}) \cdot \dot{V}_{\text{aw}} + \frac{1}{C_{\text{aw}}} \cdot V_{\text{aw}} - \frac{r_{\text{peep}}}{C_{\text{pb}}} \cdot V_{\text{pb,C}} = 0 \tag{6.15}$$

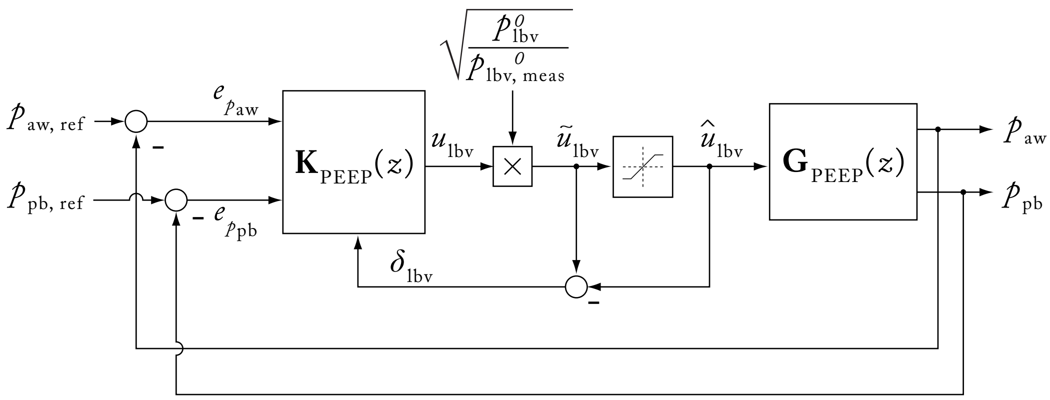

Figure 6.14: Problem Defining Control Loop for Positive Expiratory Pressure Control

define the system's dynamic behaviour. As before, $\varrho_{\text{b,out}} \approx \varrho_{\text{amb}}$ is simplified and $R_{\text{leak}} = R^0_{\text{leak}} = R_{\text{leak,turb}} \cdot \dot{V}^0_{\text{leak}}$, $p_{\text{lbv}} = p^0_{\text{lbv}}$ are assumed to be at a nominal value. The feedback linearisation with respect to the pressure drop over the large bore valve p_{lbv} is employed as with the volume controlled ventilation.

The output equations yield:

$$p_{\text{aw}} = \frac{R_{\text{peep}}}{C_{\text{aw}}(R_{\text{aw}} + R_{\text{peep}})} \cdot V_{\text{aw}} + \frac{1}{C_{\text{pb}}} \left(1 - \frac{R_{\text{peep}} r_{\text{peep}}}{(R_{\text{aw}} + R_{\text{peep}})}\right) \cdot V_{\text{pb,C}} \tag{6.16}$$

$$p_{\text{pb}} = \frac{1}{C_{\text{pb}}} \cdot V_{\text{pb,C}} \tag{6.17}$$

Consequently, a set of plants $G_{\text{PEEP},l}(s)$, $l = 0, 1, 2, \ldots, \#\Pi$ represented by normalised state space models of the form:

$$G_{\text{PEEP},l}(s) := \begin{cases} \dot{\mathbf{x}}_{\text{PEEP}}(t) & = \mathbf{A}_{\text{PEEP,l}} \cdot \mathbf{x}_{\text{PEEP}}(t) + \mathbf{B}_{\text{PEEP,l}} \cdot u_{\text{lbv}}(t) \\ y_{\text{PEEP}}(t) & = \mathbf{C}_{\text{PEEP,l}} \cdot \mathbf{x}_{\text{PEEP}}(t) \end{cases}, \tag{6.18}$$

$$\text{with } \mathbf{x}_{\text{PEEP}}(t) = \begin{bmatrix} V_{\text{aw}} \\ V_{\text{pb,C}} \\ x_{\text{lbv}} \end{bmatrix}, \quad \mathbf{y}_{\text{PEEP}}(t) = \begin{bmatrix} p^*_{\text{aw}} \\ p^*_{\text{pb}} \end{bmatrix}, \quad \mathbf{B}_{\text{PEEP,l}} = \begin{bmatrix} 0 \\ 0 \\ \frac{1}{\tau_{\text{v}}} \end{bmatrix},$$

$$\mathbf{A}_{\text{PEEP,l}} = \begin{bmatrix} -\frac{1}{C_{\text{aw}}(R_{\text{aw}}+R_{\text{peep}})} & \frac{r_{\text{peep}}}{C_{\text{pb}}(R_{\text{aw}}+R_{\text{peep}})} & 0 \\ 0 & -\frac{R_{\text{leak}}+R_{\text{pb}}}{C_{\text{pb}}(R_{\text{leak}}+R_{\text{pb}})} & \frac{2\alpha a_{\text{lbv}}\sqrt{p^0_{\text{lbv}}}}{\varrho_{\text{amb}}} \\ 0 & 0 & -\frac{1}{\tau_{\text{v}}} \end{bmatrix},$$

$$\mathbf{C}_{\text{PEEP,l}} = \begin{bmatrix} \frac{1}{p^0_{\text{aw}}} \frac{R_{\text{peep}}}{C_{\text{aw}}(R_{\text{aw}}+R_{\text{peep}})} & \frac{1}{p^0_{\text{aw}}}(1 - \frac{R_{\text{peep}}}{R_{\text{aw}}+R_{\text{peep}}}) \frac{r_{\text{peep}}}{C_{\text{pb}}} & 0 \\ 0 & \frac{1}{p^0_{\text{pb}}} \frac{1}{C_{\text{pb}}} & 0 \end{bmatrix}$$

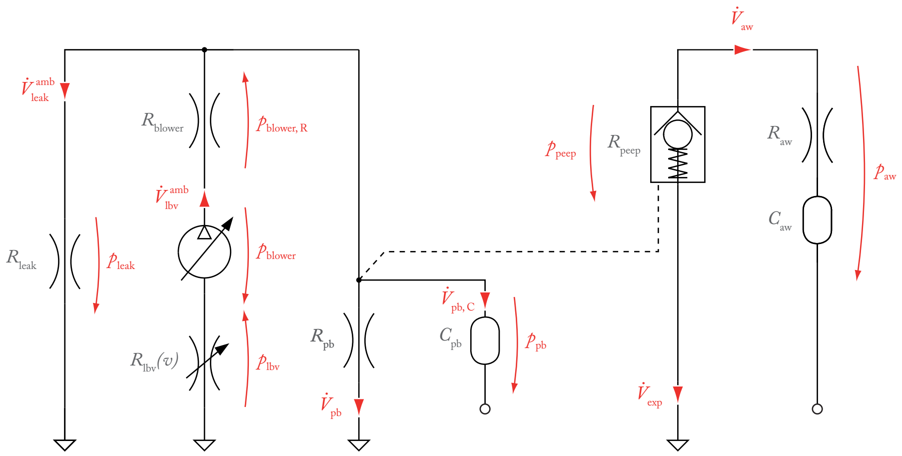

Figure 6.15: Simplified Pneumatic Network for Positive Expiratory Pressure Control

A time delay of 9 sampling instants with regard to the measured pressure p_{aw}, to account for the pressure signal both being transfered to the expiration valve and being transmitted back to the sensor has been added after discretisation of the plant. The PEEP blind pressure p_{pb} is not subject to time delay.

Figure 6.16 displays the open–loop singular values.

Shaping Filters and Synthesis In order to achieve a fast response, the shaping filters have been designed to allow overshoots, while pushing the closed–loop bandwidth high. Both tracking performances are inherently coupled by the nature of the control problem, thus enforcing fast response and good reference tracking in one channel will also affect the other channel. Furthermore, it has been observed, that the plant is sensitive to input disturbances at frequencies between 1 rad/ s and the sampling frequency ω_s. Attempts to explicitly shape the sensitivity function $\mathbf{SG}(s)$ to amend this, have not resulted in feasible solutions. Filters on $\mathbf{S}(s)$ influence $\mathbf{SG}(s)$ as well. Consequently, is has been tried to find a compromise between both reference tracking and sensitivity to input disturbances by employing the standard sensitivity shaping approach described in section 2.5.4. Additionally, apart from quantisation errors introduced by the stepper motor, no severe input disturbances are expected, since the motor has been configured to robustly attain the desired angle without loosing a step.

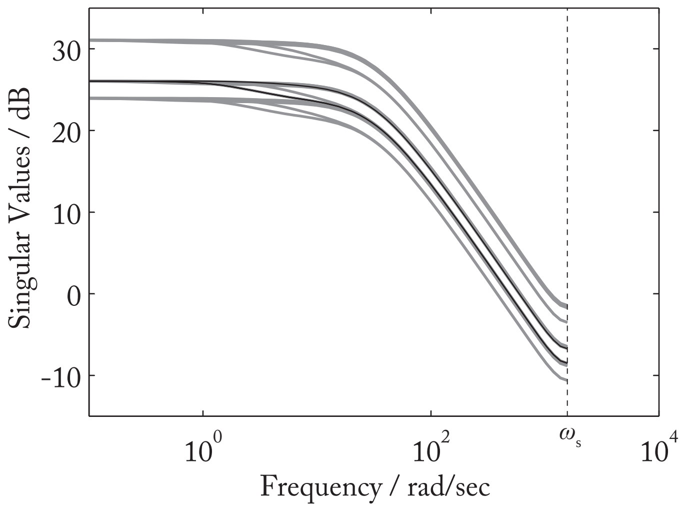

Figure 6.16: Singular Values over Frequency for the Open–Loop Plants, —— Nominal Plant $G_{\text{PEEP},0}(s)$ (p_{aw} Channel), ---- Nominal Plant $G_{\text{PEEP},0}(s)$ (p_{pb} Channel), —— Plants $G_{\text{PEEP},l}(s), l > 0$

This has resulted in filters, that are non–optimal with respect to the achievable $\mathcal{H}_\infty$ performance.

$$\mathbf{W}_S(s) = \begin{bmatrix} W_{S,\text{peep}}(s) & 0 \\ 0 & W_{S,\text{pb}}(s) \end{bmatrix}, \quad W_{KS}(s) = \frac{s+15}{s+785} \tag{6.19}$$

$$\text{with } W_{S,\text{peep}}(s) = \frac{s+200}{s+0.36}, \quad W_{S,\text{pb}}(s) = \frac{s+12}{s+0.0012}. \tag{6.20}$$

Rescaling and reshaping to obtain a better performance measure is deemed unnecessary, because the resulting controller provides satisfactory results in terms of the closed–loop sensitivities (cf. figures 6.17 and 6.18).

The complementary sensitivities with the highest bandwidth correspond to the largest resonant peaks visible in the sensitivity and input disturbance sensitivity plots. These peaks occur at low ambient pressure as is deduced by the family of $G_{\text{PEEP},l}(s)$. Further optimisations are therefore postponed to future work.

The resulting closed–loop bandwidth for PEEP control ranges between $\underline{\omega}_{\text{cl}} = 5\,\text{rad/s}$ and $\bar{\omega}_{\text{cl}} = 50\,\text{rad/s}$.

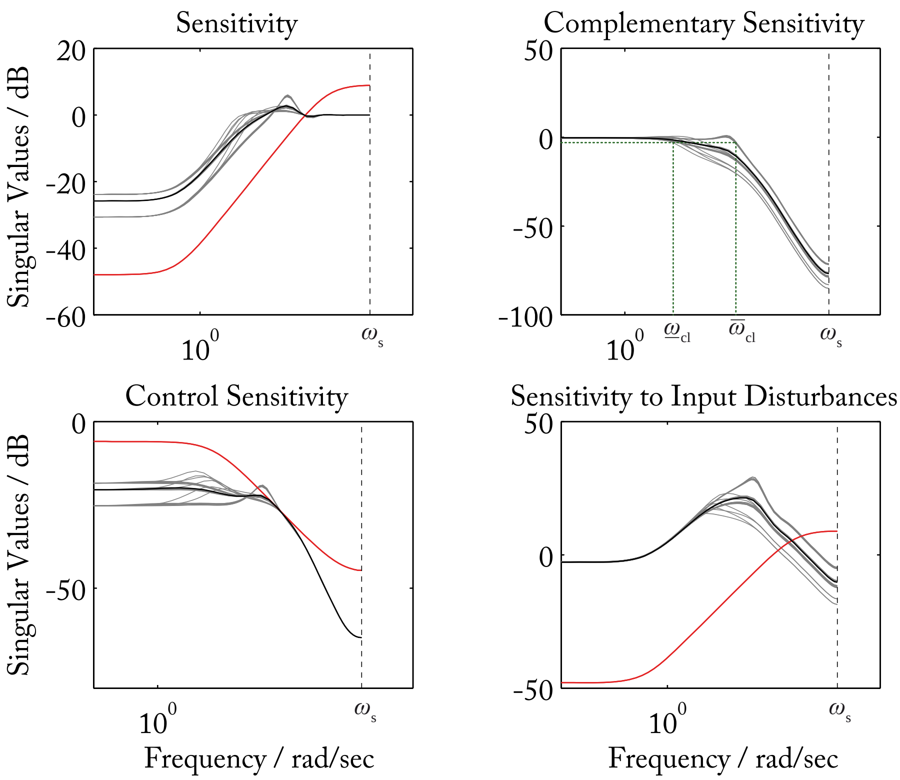

Figure 6.17: Singular Values over Frequency for the Sensitivities of the Controlled Plant from $p_{\text{aw,ref}}$ to p_{aw}, —— Nominal Plant $G_{\text{PEEP},0}(s)$, —— Plants $G_{\text{PEEP},l}(s), l > 0$, —— Shaping Filters

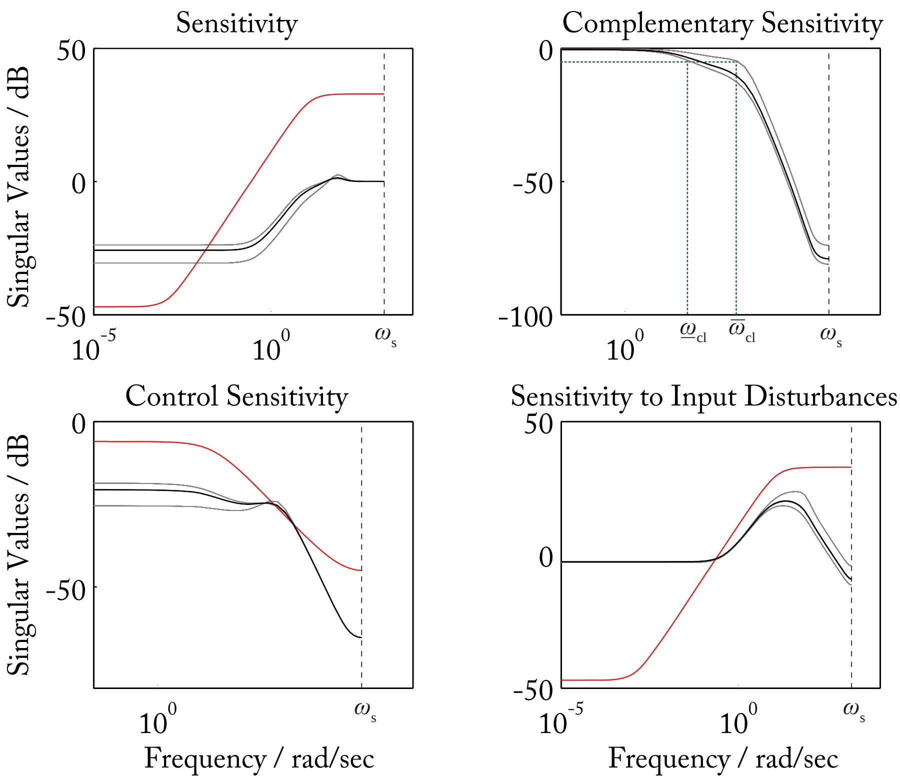

Figure 6.18: Singular Values over Frequency for the Sensitivities of the Controlled Plant from $p_{\mathrm{pb,ref}}$ to p_{pb}, — Nominal Plant $G_{\mathrm{PEEP},0}(s)$, — Plants $G_{\mathrm{PEEP},l}(s), l > 0$, — Shaping Filters

6.6 Energy Efficient Ventilation Control

The previous sections have provided a scheme for synthesising VCV and PEEP controllers, that are largely independent from the blower pressure. The only limitation resides in the fact, that the blower should be able to deliver the desired amount of flow and pressure during inspiration. This not only bears the potential, but also the necessity, to develop a blower pressure feedforward control scheme for increasing energy efficiency. It has been shown, that frequent changes in blower speed can be disadvantageous for energy consumption. Given an approximation for the power consumption of the blower during ventilation [13]

$$P_{\mathrm{el,blower}} = \frac{1}{\eta_{\mathrm{blower}}} \Big(t^*_{\mathrm{insp}} P_{\mathrm{insp}} + t^*_{\mathrm{exp}} P_{\mathrm{exp}} + f_{\mathrm{vc}} W(\Delta n) \Big) , \tag{6.21}$$

$$\text{where } t^*_{\mathrm{insp}} = \frac{T_{\mathrm{insp}}}{T_{\mathrm{insp}} + T_{\mathrm{exp}}}, \quad t^*_{\mathrm{exp}} = \frac{T_{\mathrm{exp}}}{T_{\mathrm{insp}} + T_{\mathrm{exp}}},$$

P_{insp} marks the power consumption during inspiration,

P_{exp} marks the power consumption during expiration,

$W(\Delta n) = \frac{1}{2} J(n^2_{\mathrm{insp}} - n^2_{\mathrm{exp}})$ denotes the work needed for accelerating the blower,

it can be observed, that the degrees of freedom in the above equation are P_{insp} and P_{exp} for VCV modes and P_{exp} for PCV modes. Δn depends on both inspiratory and expiratory power. Thus, pressure and volume controlled ventilation have to be distinguished.

Limitations, Delineation Inspiratory and expiratory durations during intermittent mandatory ventilation are defined in terms of ventilation frequency and I:E ratio. Patient parameters are unknown, therefore no statement with regard to the slope of the airway pressure during volume controlled ventilation can be made. Furthermore, if spontaneous breathing is allowed, there is also no telling as to when inspiration is triggered or ended. These uncertainties generally limit the potential for optimisation. Safety margins are therefore suggested for the feedforward blower pressure control, to prevent deterioration of PEEP or flow control.

Volume Controlled Ventilation $P_{\mathrm{insp,max}}$ is implicitly defined by the desired ventilation parameters $p_{\mathrm{aw,max}}$ and $\dot{V}_{\mathrm{aw,ref}}$. It is therefore reasonable, to employ a lookup table or functional approximation to compute the corresponding necessary blower speed at the end of the inspiration:

$$n(t) = g \cdot \sqrt{\frac{2}{r_{\mathrm{blower}} \cdot \varrho_{\mathrm{out}}} \cdot p_{\mathrm{aw,max}} + \frac{R_{\mathrm{blower}}}{r_{\mathrm{blower}}} \cdot \dot{V}^2_{\mathrm{aw,ref}}}. \tag{6.22}$$

Values for r_{blower} and R_{blower} have been obtained by multiple linear regression from blower characteristic data measured at nominal ambient air density $\varrho_{\mathrm{amb,0}} \approx 1.2\,\mathrm{kg/\,m^3}$, such that equation 6.22 is consistent with equation 4.9. As with the expression of the blower's static characteristics in the nonlinear model, equation 6.22 will have to be corrected at different ambient pressures, simplifying $\varrho_{\text{out}} = \varrho_{\text{amb,meas}}$.

For $g = 1$, setting the blower speed computed by equation 6.22 will result in the full use of the large bore valve's span of opening ratios during inspiration, consequently reducing pneumatic losses and increasing flow control accuracy. A gain factor $g > 1$, however, is introduced to provide a safety margin.

During expiration, the blower should be kept at a level, which is sufficiently high, such that it is able to deliver the sudden pressure increase $\Delta p_{\text{aw}} = R_{\text{aw}} \dot{V}_{\text{aw,ref}}$ at the beginning of the inspiration. This incorporates knowledge of the patient airway resistance, which is not available, and is suggested to be subject to intra–breath optimisation algorithms not subject to this thesis.

Figure 6.19 pictures a diagram of a first blower feedforward control scheme implemented in this thesis.

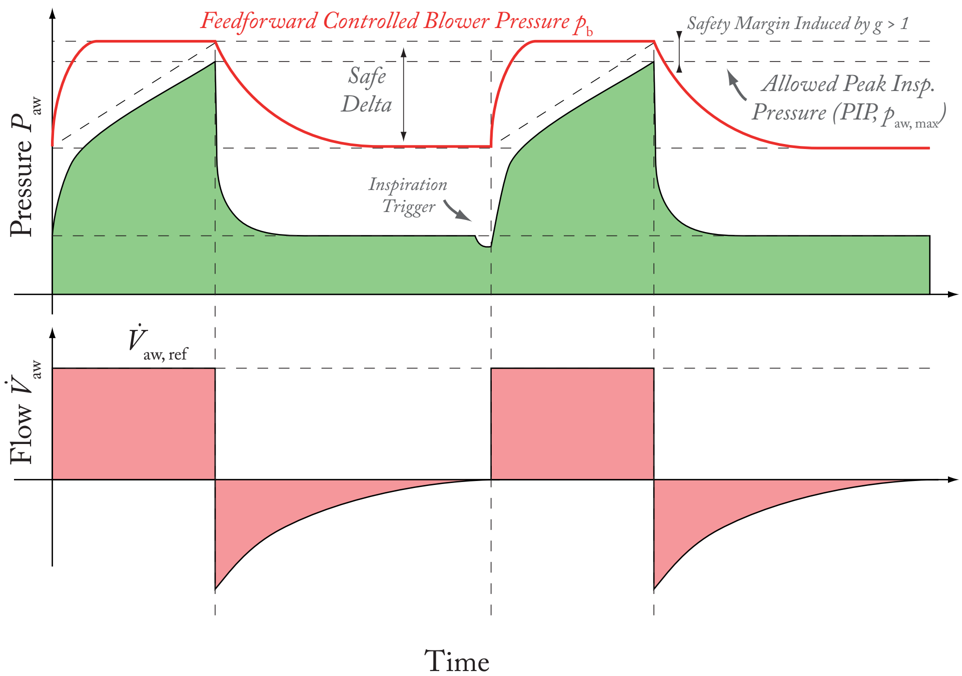

Figure 6.19: Simple First Scheme for Blower Feedforward Control

Additionally, the blower speed can also be computed dynamically using the current measured airway pressure. It is expected, that this reduces the need for sudden accelerations of the blower, thus eliminating peaks in blower currents. The energy consumption of both approaches will be compared in section 7.2.

Pressure Controlled Ventilation During inspiration, blower power is determined by $p_{\mathrm{aw,ref}}$. In order to obtain high quality of control, the blower could be kept at a speed level using equation 6.22 for no flow during expiration. The speed can be lowered, but in theory the inspiratory pressure would then take longer to attain the reference value.

In practice, though, it can be observed, that opening the large bore valve at the beginning of the inspiration leads to a pressure pulse induced by the blower's inertia, which is not accounted for by the simulation model. More accurate simulations may give rise to exploiting this fact for improving both energy efficiency and quality of control.

6.7 Bumpless Transfer

For safety reasons, ventilation devices have to incorporate controlled means of limiting the pressure applied to the patient during volume controlled ventilation. This requires transfering controller authority to the PCV controller at the instant — or slighlty before — the airway pressure reaches a safety margin set by the physician. If the controller the authority is transfered to is not initialised appropriately, a *bump* will become apparent in the controlled variable — the pressure p_{aw}.

An advantage of employing a pressure source in conjunction with a large bore valve to deliver a reference volume flow consists in the fact, that the pressure can be limited implicitly by the amount, the blower is capable to deliver at a certain rotational speed. This eliminates the need for controller authority transfer, but requires suitable feedforward control of the blower as discussed in the previous section. However, this advantage is void, if $\mathrm{F_{iO_2}}$ levels above 21 vol. % are strived for, because the injection of oxygen in conjunction with the check valves employed in the pneumatic structure will result in increased pressures.

Bumpless transfer remains an active field of research, in spite of it being a goal, which has been documented since the early stages of applied control theory. Solutions for conventional PI/PID controller structures are well known [34]. Two philosophies are distinguished: Bumpless transfer is defined as achieving

$$\mathbf{u}_{\mathbf{K}1}(t = t_{\mathrm{t}}) \approx \mathbf{u}_{\mathbf{K}2}(t = t_{\mathrm{t}}),$$

i.e. trying to have equal controller outputs when switching from controller $\mathbf{K}_1$ to $\mathbf{K}_2$ at switching instant $t = t_{\mathrm{t}}$. The conditioning technique, on the other hand, is defined as adjusting $\mathbf{u}_{\mathbf{K}2}$, such that the tracking response is optimised. In [50] a solution based on a filter is proposed, which poses an LMI condition minimising the $\mathcal{L}_2$ or l_2 gain, respectively. The filter, however, explicitly contains the plant's system matrix, thus enforcing robustness with respect to a set of plants remains non–trivial. [49] relates the bump phenomenon to the controller states, which have to be initialised accordingly. References are made to schemes, which enforce idle controllers to track the plant output, while waiting to be activated. This raises performance issues, since this essentially means, that the controllers are always active, consuming processing power. Controllers, that are unstable in open–loop require at least a *virtual* connection to the plant. This, however, does not guarantee stability.

In terms of the ventilation controller structure proposed in this thesis, both the controlled and the actuating variable switch. The oxygen flow controller can be neglected, for only its reference value will change according to the respective ventilation control mode. Figure 6.20 depicts the control loop at the point of switching from VCV to PCV controller authority.

Often bumpless transfer and anti–windup compensation are presented in a unified framework. Though, authors frequently caution not to confuse both terms, anti–windup designs may sometimes be efficiently adapted to the needs of bumpless transfer. Applying

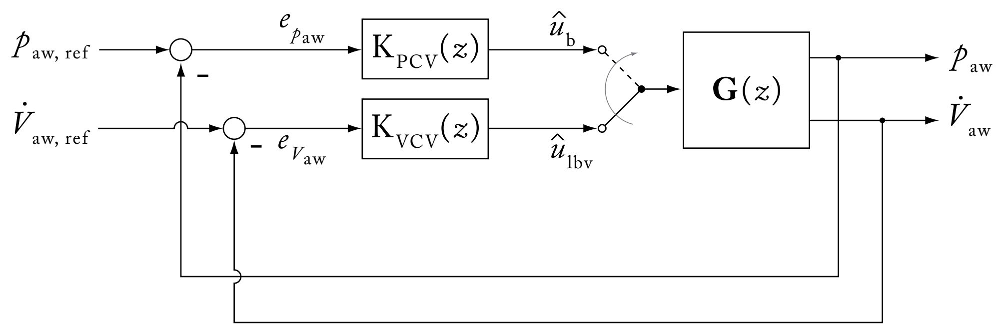

Figure 6.20: Controller Authority Transfer from VCV to PCV

this notion to ventilation control, a suggestion for appropriately conditioning the PCV controller resides in imposing a fictitious upper saturation bound calculated from the blower characteristics. As described in the previous section, the blower's speed can be drawn from a function

$$n(t) = g \cdot \sqrt{\frac{2}{r_{\text{blower}} \cdot \varrho_{\text{out}}} \cdot p_{\text{aw,desired}} + \frac{R_{\text{blower}}}{r_{\text{blower}}} \cdot \dot{V}^2_{\text{aw,desired}}}, \tag{6.23}$$

where $p_{\text{b,desired}}(t) = p_{\text{aw,max}}$ is chosen as the maximum airway pressure
$\dot{V}_{\text{b,desired}}(t) = \dot{V}_{\text{aw}}(t)$ is chosen as the current airway flow

A gain factor $g > 1$ is necessary to account for pressure losses. The anti–windup compensator (theorem 6.1) already in place stabilises the PCV controller and limits its output. At the switching instant $t = t_{\mathrm{t}}$ the PCV controller is therefore conditioned to approximately apply the pressure $p_{\text{aw,max}}$, while being able to maintain the flow $\dot{V}_{\text{aw}}(t = t_{\mathrm{t}})$. The bump induced by the switch of the actuating variable is attenuated by employing the blower feedforward control described in the previous chapter. Consequently, the large bore valve will be in almost opened position, when the airway pressure reaches $p_{\text{aw}}(t) = p_{\text{aw,max}}$. A drawback of this approach consists in the need for computing the PCV controller, while it is effectively idle.

Figure 6.21 shows a successful simulation run employing the principle described above for a reference oxygen concentration of $\mathrm{F_{iO_2}} = 21\,\text{vol.}\,\%$. A steady state error of approximately 1 mbar can be observed, which might be improved by further tuning.

The ventilation is assumed to remain in PCV mode during the remainder of the inspiration phase, eliminating the need for retransfering authority to the VCV controller. A more elaborate scheme, including a parameterisation of controllers to share the same state variables, is given in [49]. The execution of this is deemed beyond the scope of this thesis, though.

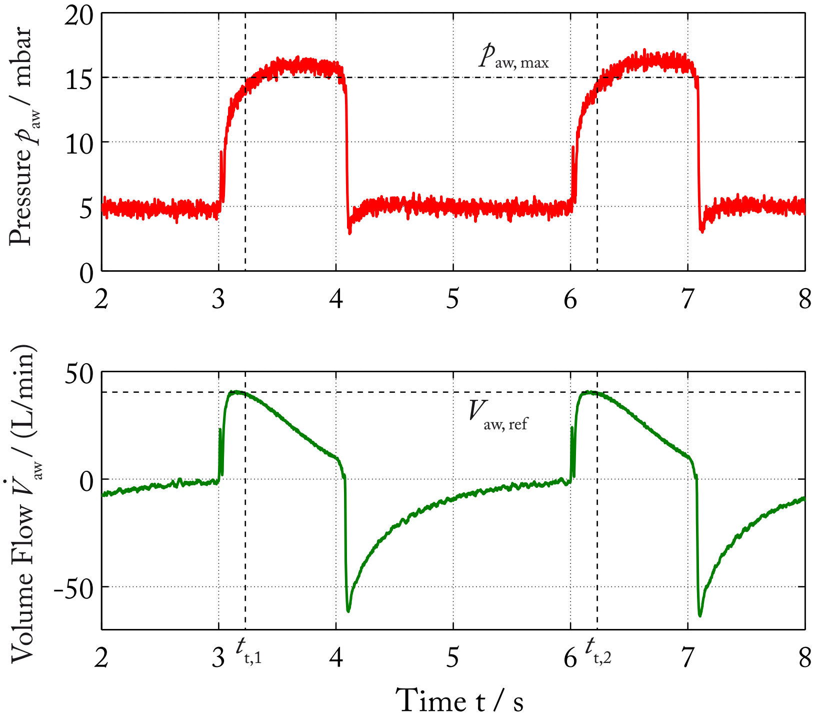

Figure 6.21: Simulation of a Volume Controlled Ventilation with Upper Bound on the Airway Pressure Employing a Simple Bumpless Transfer Scheme, Time Instants $t_{t,i}$, $i = 1, 2$, Indicate Controller Authority Transfer to PCV, $\dot{V}_{aw,ref}$ Marks the Reference Flow during the Initial Inspiration Phase, $p_{aw,max}$ Marks the Maximum Airway Pressure, Whose Overstepping Triggers Transfer to PCV

7 Results

This chapter presents results of the controlled plant obtained by nonlinear simulation in section 7.1 and by experiments conducted on the functional model in section 7.2.

7.1 Simulation Results

Before controllers have been implemented, they have been tested in simulation for various patient and ambient parameter extremes. Below, exemplary plots for PCV and VCV of a patient with parameters $R_{\mathrm{aw}} = 50\,\frac{\mathrm{mbar}}{\mathrm{L/\,s}}$ and $C_{\mathrm{aw}} = 30\,\frac{\mathrm{mL}}{\mathrm{mbar}}$ are shown. The reference oxygen concentration has been set to $\mathrm{F_{iO_2}} = 50\,\mathrm{vol.\,\%}$, $p_{\mathrm{peep,ref}} = 3\,\mathrm{mbar}$ and reference inspiratory flow and pressure are $\dot{V}_{\mathrm{aw,ref}} = 20\,\mathrm{L/\,min}$ and $p_{\mathrm{aw,ref}} = 30\,\mathrm{mbar}$, respectively. The I:E ratio has been set to 1:1.7 at a ventilation frequency of $f_{\mathrm{vc}} = 12\,\mathrm{min}^{-1}$.

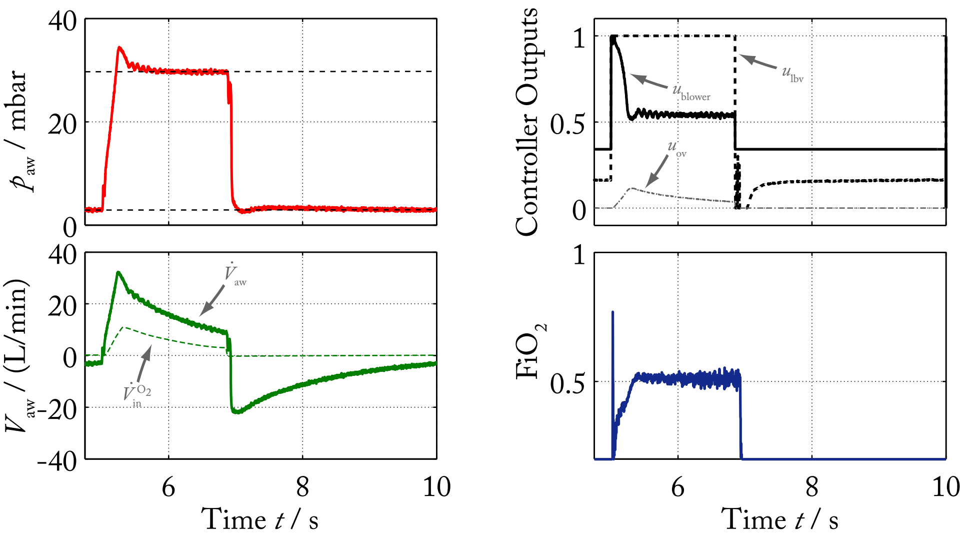

Figure 7.1: Simulated Pressure Controlled Ventilation with Reference Values $\mathrm{F_{iO_2}} = 50\,\mathrm{vol.\,\%}$, $p_{\mathrm{peep,ref}} = 3\,\mathrm{mbar}$, $p_{\mathrm{aw,ref}} = 30\,\mathrm{mbar}$ with Patient Parameters $R_{\mathrm{aw}} = 50\,\frac{\mathrm{mbar}}{\mathrm{L/\,s}}$ and $C_{\mathrm{aw}} = 30\,\frac{\mathrm{mL}}{\mathrm{mbar}}$ at Normal Ambient Pressure Level $p_{\mathrm{amb}} = 1013\,\mathrm{mbar}$

Figure 7.1 depicts pressure and flow curves of PCV at normal ambient pressure level $p_{\text{amb}} = 1013\,\text{mbar}$, as well as the corresponding controller outputs and resulting F_{iO_2}. A slight overshoot is visible, which is acceptable during PCV and in accordance to the shaping filter design and synthesis results shown in section 6.4 for the linear plant. PEEP control is excellent, while the controller output u_{lbv} clearly indicates, that anti–windup compensation works effectively in preventing the actuator from remaining in saturation for too long. Oxygen concentration is attained well within the inspiratory phase.

Figure 7.2 depicts PCV at a reduced ambient pressure level $p_{\text{amb}} = 600\,\text{mbar}$. As expected, the blower actuation u_{blower} is increased compared to normal ambient pressure, indicating higher rotational speed. Still the ventilatory curves show only a slightly lower slope of the pressure. The other curves are nearly unchanged.

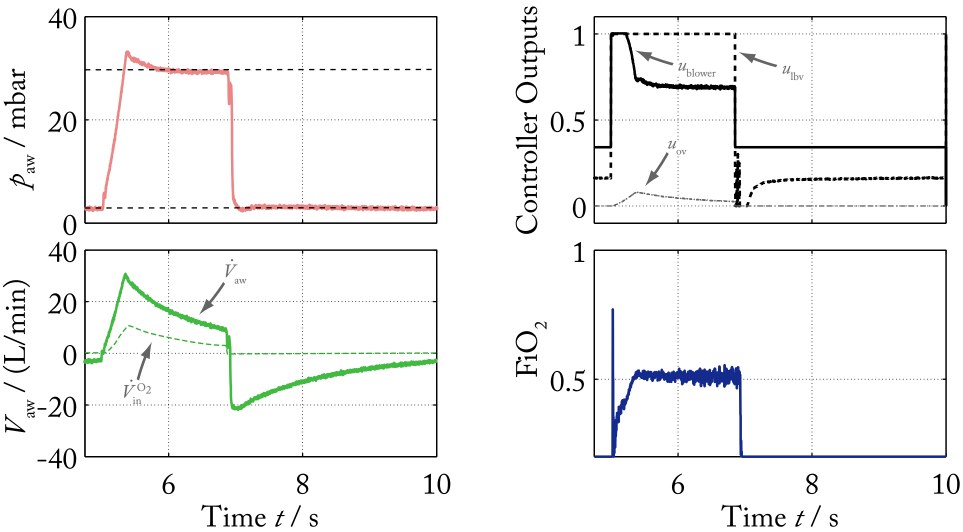

Figure 7.2: Simulated Pressure Controlled Ventilation with Reference Values $F_{iO_2} = 50\,\text{vol.}\,\%$, $p_{\text{peep,ref}} = 3\,\text{mbar}$, $p_{\text{aw,ref}} = 30\,\text{mbar}$ with Patient Parameters $R_{\text{aw}} = 50\,\frac{\text{mbar}}{\text{L/s}}$ and $C_{\text{aw}} = 30\,\frac{\text{mL}}{\text{mbar}}$ at Reduced Ambient Pressure Level $p_{\text{amb}} = 600\,\text{mbar}$

Figure 7.3 show ventilation curves for VCV. The same observations can be made with respect to anti–windup compensation with regard to PEEP control. In comparison with PCV, the oxygen concentration is maintained even quicker, which is expected, as the oxygen reference flow is independent from any measurement. The ambient air flow controller's reference tracking is slightly impaired and tracks the reference flow with an error of $+0.5\,\text{L/min}$.

Tracking of all reference values is nevertheless deemed satisfactory. An additional plot of VCV at reduced ambient pressure is omitted, as no additional information can be infered. Instead, the resulting curve for u_{lbv} has been added in figure 7.3, which indicates an increased opening ratio of the valve.

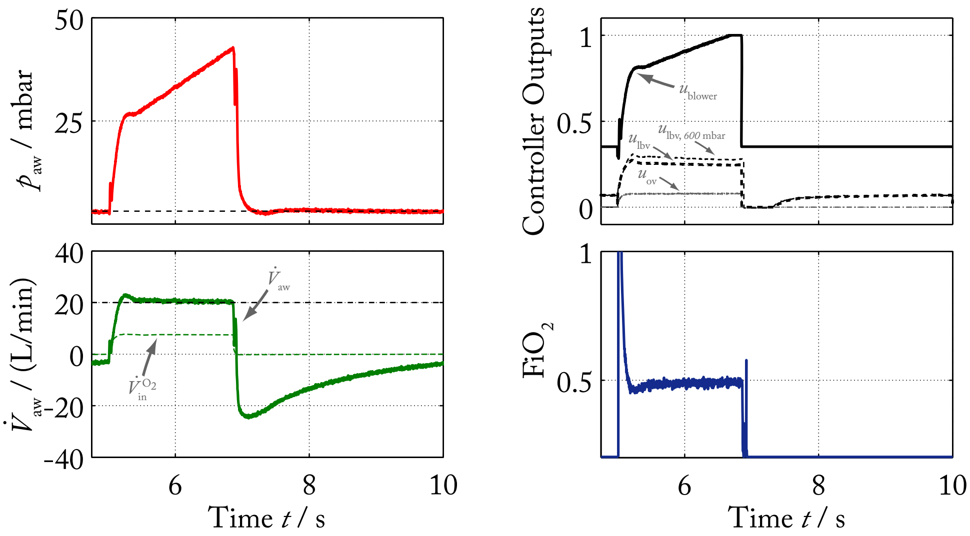

Figure 7.3: Simulated Pressure Controlled Ventilation with Reference Values $F_{\mathrm{iO_2}} = 50\,\mathrm{vol.\,\%}$, $p_{\mathrm{peep,ref}} = 3\,\mathrm{mbar}$, $\dot{V}_{\mathrm{aw,ref}} = 20\,\mathrm{L/\,min}$ with Patient Parameters $R_{\mathrm{aw}} = 50\frac{\mathrm{mbar}}{\mathrm{L/\,s}}$ and $C_{\mathrm{aw}} = 30\frac{\mathrm{mL}}{\mathrm{mbar}}$ at Normal Ambient Pressure Level $p_{\mathrm{amb}} = 1013\,\mathrm{mbar}$

7.2 Experimental Results

Ventilation Patterns The ventilation patterns listed in table 7.1 reflect relevant patients, though no claim is made for this list to be exhaustive. The patterns range from patients suffering from COPD[1], neuromuscular diseases, OHS[2] and ARDS[3] and contain a healthy adult, as well as a neonate. Their ventilation parameters and dynamic behaviour is simulated by the Active Servo Lung 5000 by IngMar Medical Inc., which is also used to measure patient pressure and flow. An additional imtMedical PF300 has been employed to measure the oxygen flow. The specific settings have been adapted from [13] and are only slightly changed: The user interface of the MEDUMAT Transport only allows to select integer PEEP reference values, therefore instead of 0.5 mbar, 0 mbar has been selected to let the controller try to attain the lowest possible PEEP value. Furthermore, a ventilation frequency of 12 min^{-1} with the *adult* pattern more accurately reflects a human being in a healthy state. No details were available with regard to the simulated functional residual capacity of the Active Servo Lung in [13]. This has been set to 0.5 L for the experiments.

		Airways		Device Settings			
Mode	Pattern	$R_{\mathrm{aw}}/\frac{\mathrm{mbar}}{\mathrm{L/s}}$	$C_{\mathrm{aw}}/\frac{\mathrm{L}}{\mathrm{mbar}}$	$p_{\mathrm{aw,ref}}/\,\mathrm{mbar}$ $\dot{V}_{\mathrm{aw,ref}}/(\mathrm{L/min})$	$p_{\mathrm{peep,ref}}/\,\mathrm{mbar}$	$f_{\mathrm{vc}}/\,\mathrm{min}^{-1}$	I : E
PCV	COPD	20	0.075	25.0	6.0	15	1 : 4
	Neurom.	8	0.075	15.0	0.0 / (0.5)	35	1 : 2.5
	Neonate	100	0.010	15.0	0.0 / (0.5)	60	1 : 2.5
	OHS	25	0.035	45.0	6.0	17	1 : 4
VCV	Adult	3.5	0.090	45.0	3.0	12 / (18)	1 : 3
	ARDS	8	0.040	25.0	0.0 / (0.5)	17	1 : 2.5

Table 7.1: Ventilation Patterns, Airway Parameters and Ventilation Device Settings, Values in Parentheses are Used in [13] and are Slightly Altered in this Thesis

Ventilation Pattern: PCV–*COPD* Figures 7.4 to 7.7 show experimental results of a COPD patient subject to pressure controlled ventilation. Curves show, that in the cases of $F_{iO_2} = 21, 50$ and 80 vol. % the reference pressure of $p_{\mathrm{aw}} = 25$ mbar is met and the set oxygen concentration is obtained at the end of the inspiration. The oxygen flow controller does not succeed to actually track the ambient air flow's shape as during simulation. The differential pressure flow sensor's bandwidth is high enough and therefore should not impair the tracking. It is therefore assumed, that the hose between oxygen inlet valve and mixing chamber, combined with the additional resistances of the PF300 flow measurement device and the check valve introduce a pneumatic low–pass, which would be eliminated in a final product.

[1]COPD — Chronic Obstructive Pulmonary Disease
[2]OHS — Obesity Hypoventilation Syndrome
[3]ARDS — Acute Respiratory Distress Syndrome

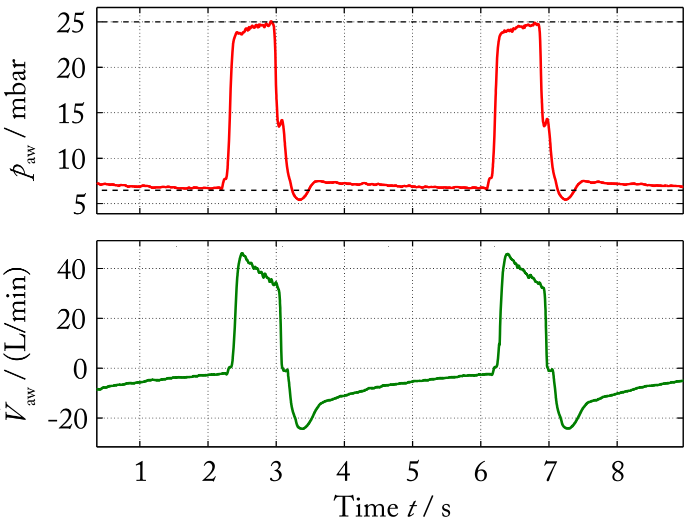

Figure 7.4: Pressure and Flow Curves of Experimental Results: Pressure Controlled Ventilation with Ventilation Pattern *COPD* at $F_{iO_2} = 21\,\mathrm{vol.\,\%}$

At a desired oxygen concentration of $100\,\mathrm{vol.\,\%}$ pressure control performance deteriorates, as the oxygen flow approaches its reference signal. This is expected, as the open–loop nature of the F_{iO_2} control concept during PCV basically relies on a measurable flow induced by the blower pressure to generate the oxygen flow reference with. The pneumatic design, however, allows for ventilation at $F_{iO_2} = 100\,\mathrm{vol.\,\%}$ solely by the oxygen valve. Furthermore, the check valves prevent the blower from actively lowering pressure applied to the patient.

PEEP is maintained within a control error of $1\,\mathrm{mbar}$. A small undershoot $p_{\mathrm{peep,ref}} - p_{\mathrm{peep}} < 1.5$ can be observed and PEEP is slowly dropping afterwards. This is explained with the relatively slow integral behaviour apparent in the sensitivity plots in figure 6.17. Before dropping to PEEP level, patient pressure remains at a plateau level of approximately $15\,\mathrm{mbar}$ after the end of the inspiration. The higher the desired oxygen concentration, the longer the plateau is enduring. The existence of the plateau is explained by the PEEP blind's discharge time constant. This time constant is enlarged for higher oxygen concentrations due to a shortcoming in the construction of the functional model: The hose through which oxygen is fed into a mixing chamber can only discharge the built up pressure via the check valve and the PEEP blind. The volume of the hose thus effectively enlarges the mixing chamber's compliance.

Figure 7.8 shows the measured blower current for ventilation at $F_{iO_2} = 21\,\mathrm{vol.\,\%}$. Current measurements have not differed significantly at higher levels and additional plots are thus omitted. During the acceleration phase, the plot indicates a rather high peak current of $i_{\mathrm{max}} = 1.91$.

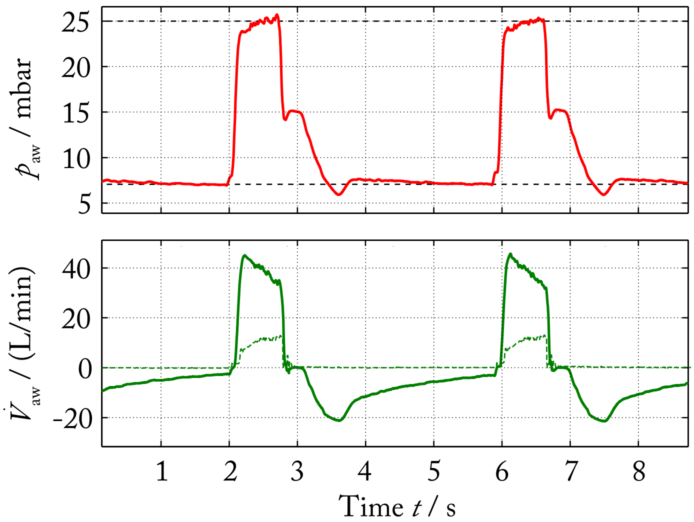

Figure 7.5: Pressure and Flow Curves of Experimental Results: Pressure Controlled Ventilation with Ventilation Pattern *COPD* at $F_{iO_2} = 50\,\text{vol.}\,\%$, ----- Oxygen Flow

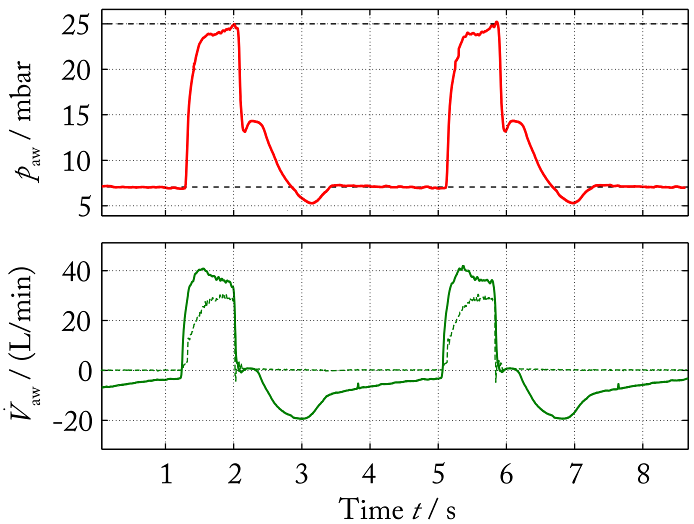

Figure 7.6: Pressure and Flow Curves of Experimental Results: Pressure Controlled Ventilation with Ventilation Pattern *COPD* at $F_{iO_2} = 80\,\text{vol.}\,\%$, ----- Oxygen Flow

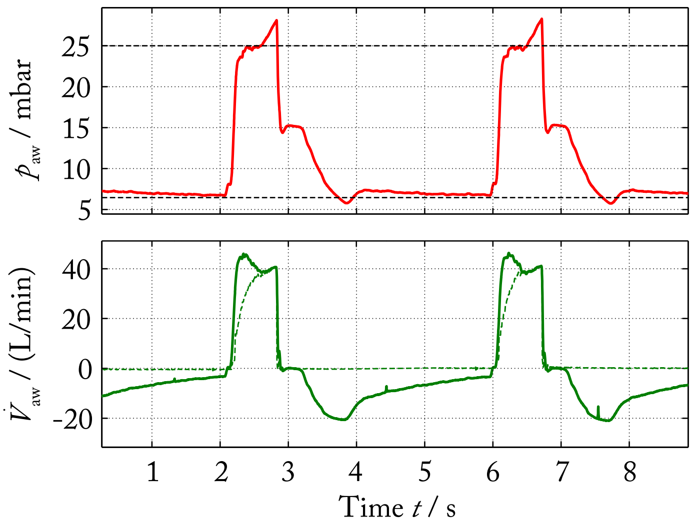

Figure 7.7: Pressure and Flow Curves of Experimental Results: Pressure Controlled Ventilation with Ventilation Pattern *COPD* at $F_{iO_2} = 100$ vol. %, ----- Oxygen Flow

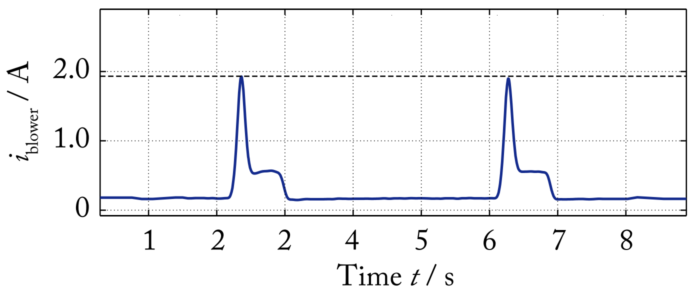

Figure 7.8: Measured Blower Current Curve of Experimental Results: Pressure Controlled Ventilation with Ventilation Pattern *COPD*

Ventilation Patterns: PCV–*Neuromuscular Disease* and PCV–*Neonatal Ventilation* The results of the neuromuscular disease pattern reveal a general shortcoming of the PEEP control concept: The control quality is impaired due to blower inertia. For both high PEEP levels or the blower not yet having decelerated to the lower expiratory speed level, rapidly opening the large bore valve results in a sudden rise in patient pressure. Though, this could actually be beneficial to obtain perfect square shaped reference tracking, the PCV controller is currently not initialised correctly, such that tracking is consequently delayed.

The patient pressure tracking error during expiration — actually never attaining the desired PEEP level — can be explained by the minimum leakage of the large bore valve. As shown in section 5.1 in figure 5.5, the lowest attainable PEEP is influenced by the blower pressure. The applied pressure would, however, only account for approximately 0.5 mbar. Further 0.4 mbar are caused by the expiratory flow of $\dot{V}_{exp} \approx 10\,\mathrm{L/\,min}$, which causes a pressure drop over the expiration valve according to

$$p_{\mathrm{peep}} = R_{\mathrm{peep}} \cdot \dot{V}_{exp}. \tag{7.1}$$

Still, both effects do not explain the slow tracking. A look at the sensitivity plots in figure 6.17 reveals, that the patient parameter combination at hand marks the low end of the achieved controller bandwidth spectrum with approximately 5.3 rad/ s. Furthermore, the PEEP controller is sensitive to input disturbances, which occur due to oscillations of the expiration valve. Such an oscillation becomes apparent at the beginning of the expiration by a small bump, which is a known effect [13]. Figure 7.9 shows the experimental results.

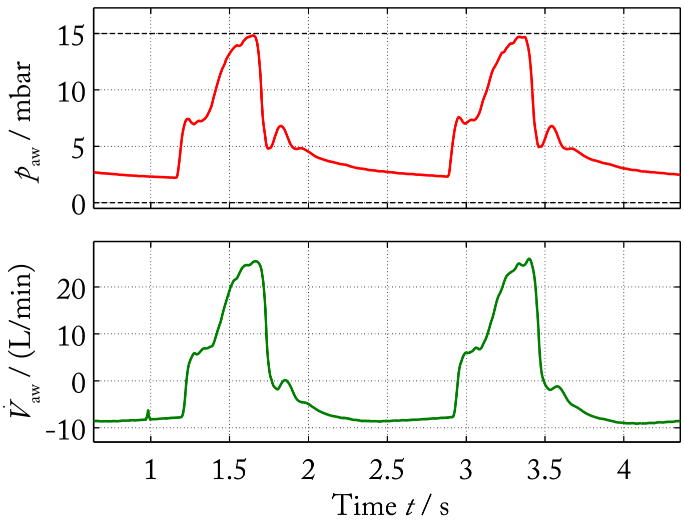

Figure 7.9: Pressure and Flow Curves of Experimental Results: Pressure Controlled Ventilation with Ventilation Pattern *Neuromuscular Disease* at $F_{iO_2} = 21\,\mathrm{vol.\,\%}$

For the neonatal ventilation pattern, the pressure controller proves to be too slow, rendering ventilation infeasible. The same initial plateau as with the latter pattern is observable and explained by the opening of the large bore valve. Maximum current and mean power consumption therefore provide little information of interest. Figure 7.10 shows the experimental results.

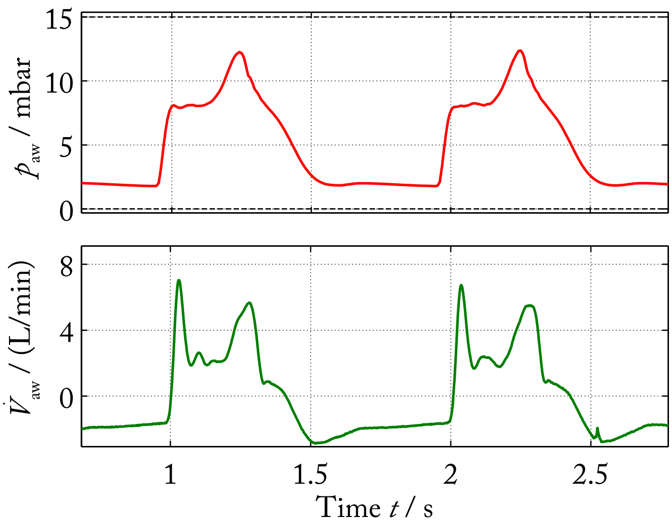

Figure 7.10: Pressure and Flow Curves of Experimental Results: Pressure Controlled Ventilation with Ventilation Pattern *Neonate* at $F_{iO_2} = 21\,\text{vol.}\,\%$

The frequency of ventilation for both neonate ventilation and the neuromuscular disease pattern happened to be too high for the oxygen flow controller to inject oxygen for any concentration.

Ventilation Pattern: PCV−*OHS* Figure 7.11 and 7.12 show results of pressure ventilation with the obesity hypoventilation syndrome pattern for $F_{iO_2} = 21\,\mathrm{vol.\,\%}$ and $80\,\mathrm{vol.\,\%}$. Relatively high inspiratory flows and pressures combined pose high demands on the blower's pneumatic performance. Consequently, the power consumption is high (cf. figure 7.13).

Apart from again observing the prolonged plateau at the end of inspiration for higher oxygen concentrations, quality of control is deemed satisfactory.

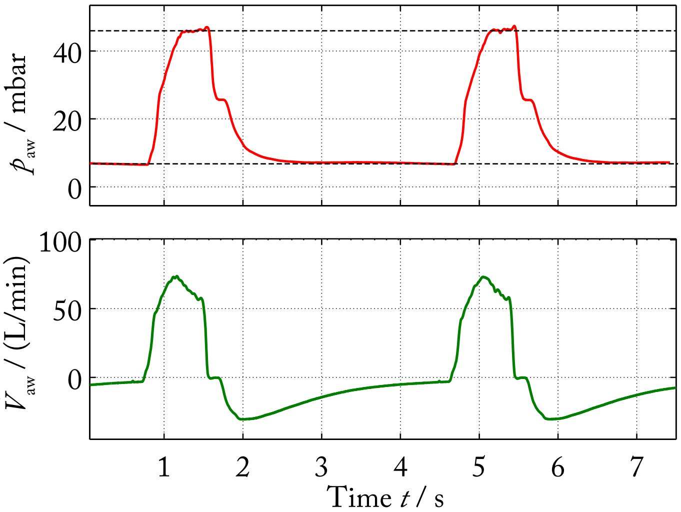

Figure 7.11: Pressure and Flow Curves of Experimental Results: Pressure Controlled Ventilation with Ventilation Pattern *OHS* at $F_{iO_2} = 21\,\mathrm{vol.\,\%}$

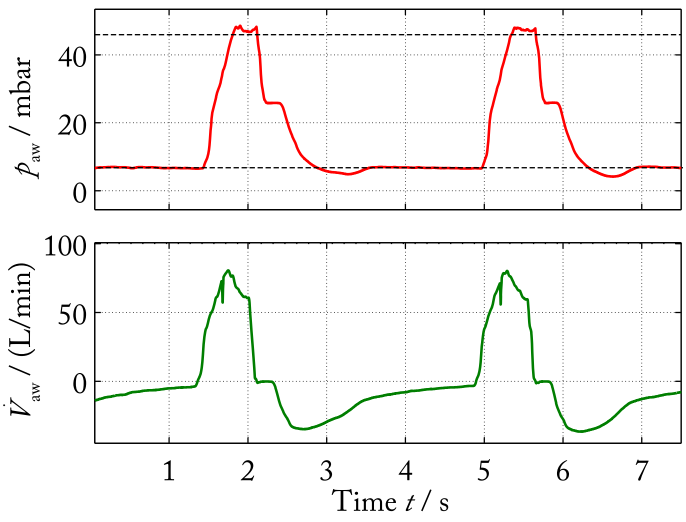

Figure 7.12: Pressure and Flow Curves of Experimental Results: Pressure Controlled Ventilation with Ventilation Pattern *OHS* at $F_{iO_2} = 80\,\text{vol.}\,\%$

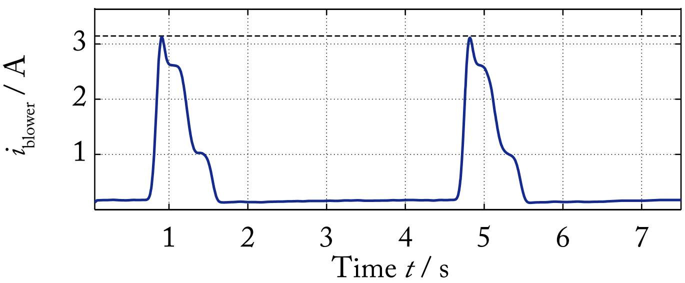

Figure 7.13: Measured Blower Current Curve of Experimental Results: Pressure Controlled Ventilation with Ventilation Pattern *OHS* — Independent from F_{iO_2}

Ventilation Pattern: VCV–*Adult* The ACTIVE SERVO LUNG is known to oscillate for low airway resistance values. These oscillations are clearly visible in figure 7.14, though quality of flow control is not impaired by this, for the reference flow is quickly attained. However, control of the expiratory pressure deteriorates, because it is sensitive to input disturbances as explained above. In fact, the oscillations have a frequency of approximately 70 rad/ s, which is well within the frequency region, the PEEP controller amplifies.

Oxygen concentration control works well and the respective plots have been added in figure 7.14. The main inspiratory flow profile is virtually independent of the desired F_{iO_2}, which is why the figure's curve is valid also for ventilation with pure oxygen.

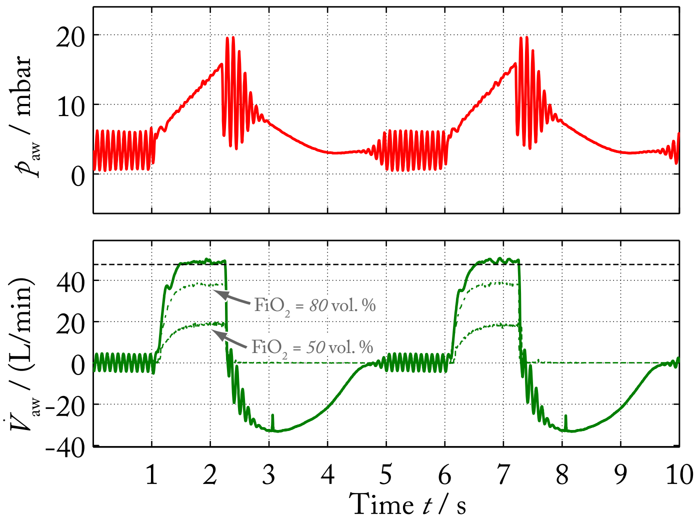

Figure 7.14: Pressure and Flow Curves of Experimental Results: Volume Controlled Ventilation with Ventilation Pattern *Adult* at $F_{iO_2} = 21, 50, 80, 100$ vol. %, ----- Oxygen Flow at Levels as Indicated

Expectedly, as a result of the blower feedforward scheme proposed in section 6.6 the blower's power consumption drops with increasing oxygen concentration. The lower bound appears, if the limit $F_{iO_2} \to 100$ vol. % is taken. In this special case, however, the blower can be disabled. Figure 7.15 compares blower currents for different oxygen concentrations. The blower feedforward scheme employed has been set to maintain a pressure $p_{\text{blower}} = 1.35 \cdot p_{\text{aw}}$ at the inspiratory reference flow, saturating at the preset maximum airway pressure with 10 % safety margin (cf. figure 7.16 (l.)). The safety factor 1.35 has been chosen conservatively as to not impair flow control quality and can be subject to optimisation. Figure 7.18 compares the above–mentioned feedforward scheme with maintaining a steady blower speed determined by peak pressure as illustrated in figure 7.16. The accelerating scheme gets rid of the initial high current peak at the cost of

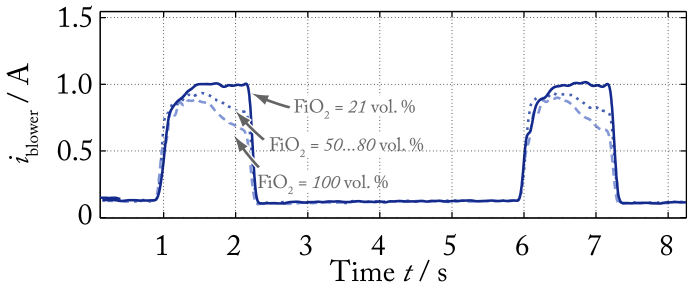

Figure 7.15: Measured Blower Current Curve of Experimental Results: Volume Controlled Ventilation with Ventilation Pattern *Adult*

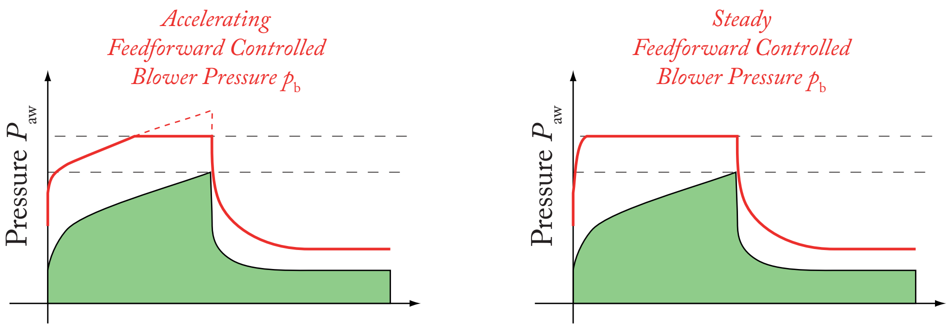

Figure 7.16: Illustration of Blower Feedforward Schemes with Accelerating or Steady Blower Speed Pattern

an increased end-inspiratory current, caused by near constant acceleration. As indicated in figure 7.18, the mean current during inspiration for the steady feedforward scheme is $\bar{i}_{\text{steady}} = 0.91\,\text{A}$ and therefore slightly higher than $\bar{i}_{\text{accel}} = 0.78\,\text{A}$. Since flow control performance has remained unchanged — since virtually the same tidal volumes are applied (cf. figure 7.17) —, this shows the potential of the blower pressure independent volume flow controller with respect to energy optimisation. Mean power consumption during inspiration then compares $\bar{P}_{\text{steady}} = 36.4\,\text{W}$ versus $\bar{P}_{\text{accel}} = 31.2\,\text{W}$, lowering by 15 %. Further reductions are subject to optimisation.

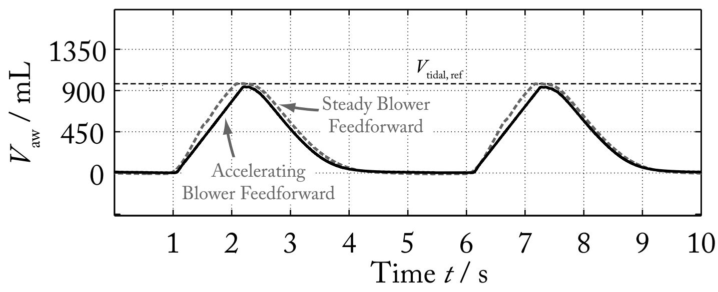

Figure 7.17: Comparison of Applied Tidal Volumes for Accelerating or Steady Blower Speed Pattern, —— Volume for Accelerating Blower Speed Pattern, ----- Volume for Steady Blower Speed Pattern

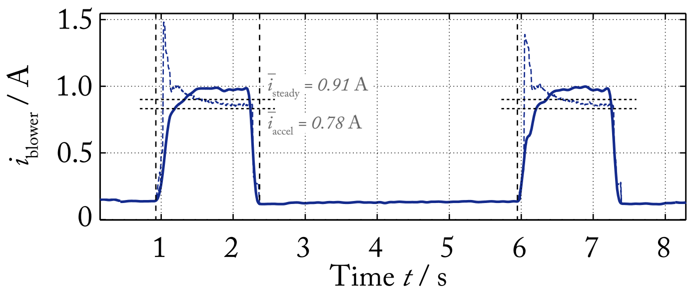

Figure 7.18: Comparison of Blower Currents for Accelerating or Steady Blower Speed Pattern Using VCV and Ventilation Pattern *Adult* at $F_{iO_2} = 21\,\text{vol.}\,\%$ as an Example, —— Current for Accelerating Blower Speed Pattern, ----- Current for Steady Blower Speed Pattern

Ventilation Pattern: VCV–*ARDS* The Active Servo Lung again oscillates with this ventilation pattern, such that the quality of PEEP control can not be judged. Inspiratory flow control shows good results, except for a small overshoot. With regard

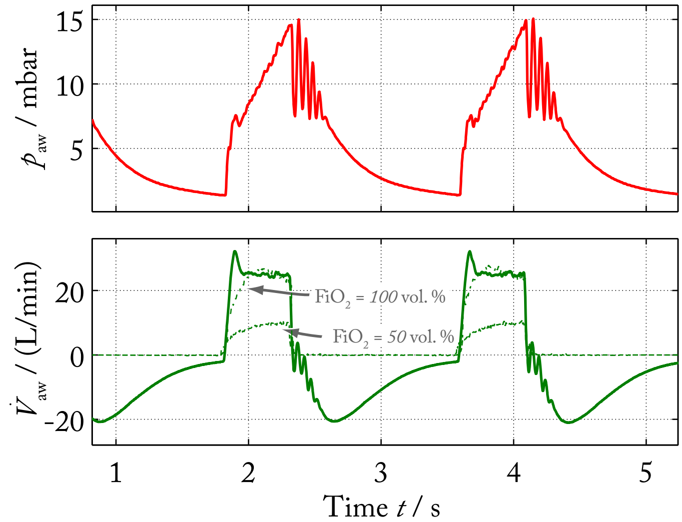

Figure 7.19: Pressure and Flow Curves of Experimental Results: Volume Controlled Ventilation with Ventilation Pattern *ARDS* at $F_{iO_2} = 21, 50, 100$ vol. %, ----- Oxygen Flow at Levels as Indicated

to the power consumption, the low flow (compared to VCV—*Adult*) applied renders the differences with respect to different F_{iO_2} levels insignificant (cf. figure 7.20).

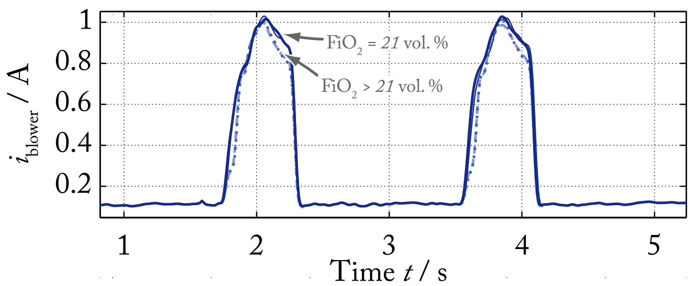

Figure 7.20: Measured Blower Current Curve of Experimental Results: Volume Controlled Ventilation with Ventilation Pattern *ARDS*

Additional Ventilation Pattern: VCV/PCV For the purpose of displaying an unimpaired experimental result of controlled ventilation, a further passive test lung has been employed. The ventilation pattern is set to an airway resistance of $R_{\text{aw}} = 50\,\frac{\text{mbar}}{\text{L/s}}$ and $C_{\text{aw}} = 30\,\frac{\text{mL}}{\text{mbar}}$, indicating both resistive and obstructive symptoms. PEEP is set to 3 mbar and the respective reference values for PCV and VCV are indicated in figures 7.21 and 7.22.

The plots indicate unimpaired PEEP control performance and confirm the controllers' good tracking capabilities. Figure 7.22 again reveals the initial pressure pulse. The blower speed has been kept at a slightly increased level, i.e. higher than necessary to attain PEEP level with opened large bore valve, during expiration for the purpose of displaying this effect.

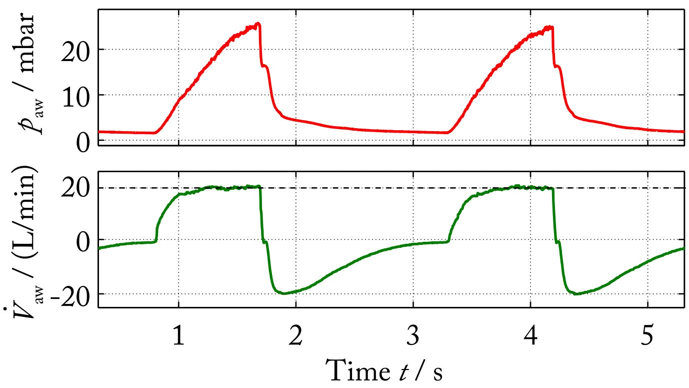

Figure 7.21: Pressure and Flow Curves of Experimental Results: Volume Controlled Ventilation with Additional Ventilation Pattern at $F_{iO_2} = 21$ vol. %

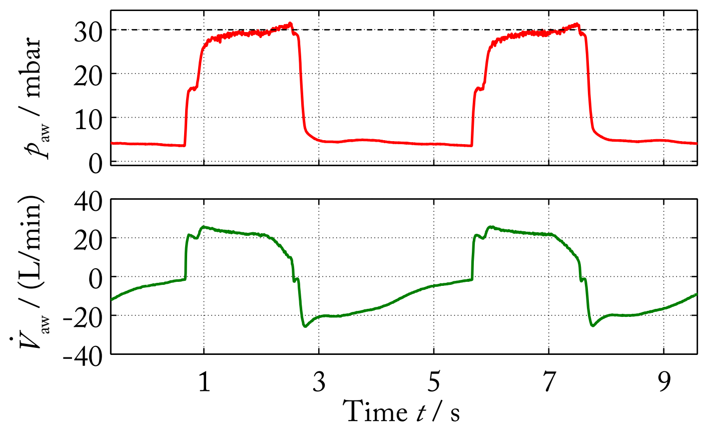

Figure 7.22: Pressure and Flow Curves of Experimental Results: Volume Controlled Ventilation with Additional Ventilation Pattern at $F_{iO_2} = 21$ vol. %

Comparison with Previous Work Table 7.2 summarises results with regard to the energy consumption and also provides the results from [13].

		Energy Consumption		Energy Consumption [13]	
Mode	Pattern	$i_{\mathrm{max}}/\,\mathrm{A}$	$P_{\mathrm{el,mean}}/\,\mathrm{W}$	$i_{\mathrm{max}}/\,\mathrm{A}$	$P_{\mathrm{el,mean}}/\,\mathrm{W}$
PCV	COPD	1.91	9.4	1.80	7.4
	Neurom.	1.22	11.1	2.10	6.9
	Neonate	0.98	8.8	1.60	7.2
	OHS	3.12	19.6	1.80	11.2
VCV	Adult	0.89 . . . 1.0	10.6 . . . 12.2	1.40	5.4
	ARDS	1.0	12.3	1.20	6.4

Table 7.2: Ventilation Patterns, Energy Consumption

However, comparability is limited due to the following reasons:

Ventilation Setting Leakage ventilation is considered in [13], instead of fully invasive ventilation considered in this thesis. The pneumatic structure differs in various aspects and the systems' total resistances are unknown.

Blower This thesis' motor controller is fed 40 V supply voltage instead of 35 V, causing an increase in power consumption, which is potentially unnecessary to obtain an increase in control quality. The blower model is identical, but the motor controllers differ. In [13] a motor control hardware has been used, with which the microcontroller could directly control the blower via three different PWM signals, which also allowed for efficient braking. This architecture is potentially more energy efficient.

The VCV control scheme chosen in [13] used the blower to control for a constant pressure drop over a large bore valve of a different type to allow for linear behaviour of the large bore valve. Furthermore, the PEEP has been controlled directly by the blower and a constant pressure divider.

The following conclusions can be drawn from the comparison:

Relatively High Energy Consumption of PEEP Control Controlling the PEEP by the large bore valve effectively wastes pneumatic energy of the blower. Its advantage resides in the potential to keep the blower speed level for ventilation at high frequencies. This, however, raises the problem of bumplessly entering pressure controlled inspiration phase. This fact and a possibly higher total resistance of the pneumatic structure, e.g. due to check valves, accounts for an increased power consumption during PCV.

Elimination of Peak Currents by Blower Feedforward Scheme The feedforward scheme proposed in this thesis effectively reduces the required degree of dynamic blower motor actuation during volume controlled ventilation. Figure 7.23 compares blower currents for the ventilation pattern VCV–*Adult* at $\mathrm{F_{iO_2}} = 21\,\mathrm{vol.\,\%}$.

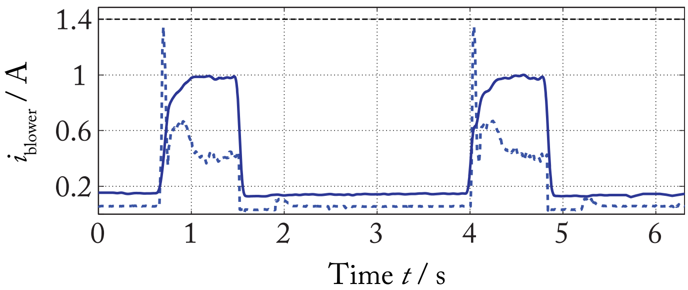

Figure 7.23: Comparison of Blower Currents for the Ventilation Pattern VCV–*Adult* at $F_{iO_2} = 21\,\text{vol.}\,\%$ between this Thesis' Implementation (——) and the Implementation in [13] (-----)

Summary The experimental results validate the controllers' robustness and to a certain degree their performance, which has been observed during multiple simulation runs. However, unmodelled phenomena have been revealed, including expiration valve oscillations, non–ideal pneumatic topology and bumpy behaviour at the beginning of pressure controlled inspiration. These effects consequently result in reduced controller performance, which is mainly due to the PEEP controller's sensitivity to input disturbances. Stability, however, is robustly maintained. The energy consumption is still subject to optimisation, but the potential has clearly become visible.

8 Conclusion and Outlook

In the course of this thesis, an electro–pneumatic topology for a novel mechanical ventilator has been designed, motivated by application scenarios, in which prepressurised oxygen supplies are lacking or administering oxygen concentrations below 40 vol. % — the lower limit of current market leading products, the MEDUMAT Transport and the DRÄGER OXYLOG 3000 — are desired. It has been this thesis' task to further explore the combination of the existing WEINMANN MEDUMAT Transport emergency ventilator platform with blower and valve technology to obtain a device capable of functioning this extended field of application. The derived concept has been nonlinearly modelled and constructed as a functional model. The main concept is based on the combination of pressurised oxygen and a blower to enable application of oxygen concentrations ranging from 21 vol. % to 100 vol. %. Ambient air flow control has been achieved by introducing a large bore valve as a further actuator.

Control of the device has been considered by deriving individual low–order, discrete time, $\mathcal{H}_\infty$ norm based, robust stability/robust performance controllers for pressure and volume controlled ventilation and the control of PEEP. These controllers have been augmented with anti–windup compensation, synthesised by LMI conditions, which impose l_2 gain optimality. These LMI conditions have been extended to guarantee robust performance. An ambient air flow control scheme has been proposed and implemented, which decouples blower control from valve control. This enabled the application of linear control theory techniques and has also given rise to the development of blower feedforward control schemes, which — though still subject to optimisation — effectively reduce the demands on blower dynamic control and provide means for power consumption optimisation. Following this same notion, control of PEEP has been designed to rely on the large bore valve as the main actuator, allowing for trading off power consumption against the ability to maintain good control performance for increasing frequencies of ventilation. The control of the fraction of the inspired oxygen has been considered as an open–loop problem by applying the respective reference flows to a dedicated oxygen flow controller.

Simulation results have shown, that the robust controllers generate satisfactory trajectories for the imposed range on patient parameters and ambient parameters. Experimental results have affirmed robustness with regard to patient parameters. However, sensitivity to input disturbances of the PEEP controller design have been revealed, which became apparent in conjunction with a lung simulator also known to be prone to oscillations for particular patient parameters. Conservativeness introduced by demands for robustness has also rendered control too slow for ventilation frequencies upwards of approximately $35\,\mathrm{min}^{-1}$. During experiments, a further issue has been revealed, which consists in a bumpy transfer from large bore valve actuated expiratory pressure control to inspiratory pressure control taken over by the blower.

Control of different F_{iO_2} levels has been proven to work excellently during volume and pressure controlled ventilation in simulation. During pressure controlled ventilation performed by the functional model in the experiments, the desired concentration has only been attained at the end of every inspiration, though, as the tracking of the reference flow pattern appeared to be too slow for reasons found in the non–optimal pneumatic structure of the function model. For concentrations of $F_{iO_2} > 80\,\text{vol.}\,\%$, pressure control performance has deteriorated, when using the blower to maintain patient pressure both in simulation and in the experiments. This has been expected and tolerated, as in practice, it is most important to have the options to choose from $F_{iO_2} = 100\,\text{vol.}\,\%$, $40 < F_{iO_2} < 70\,\text{vol.}\,\%$ and $F_{iO_2} = 21\,\text{vol.}\,\%$.

8.1 Outlook

With respect to the design and control of a blower–based mechanical ventilator, different approaches have been investigated and tried, both in this thesis and in previous work at Weinmann. Previous work and findings of this thesis can now be synthesised to conclude a definite solution. A structured brief outlook on potential future work on that topic will be given next.

Pneumatic Structure The topology derived in this thesis incorporates a major weakness. As the focus has been laid on improving the blower's energy efficiency by placing the large bore valve at the inlet, this directly results in the intentional leakage being shut off during valve controlled expiration. A sufficient cooling flow cannot be maintained and it is supposed, that for high ventilation frequencies, heat problems may arise. Initial thoughts on solutions include deriving a trade off between increasing the minimum valve leakage at the cost of an increased minimum attainable PEEP. A flow–dependent leakage after the blower with high resistance at high flows and low resistance at low flows would further reduce the pneumatic losses, which caters to the notion, that at high flows the cooling flow is already maintained, rendering an additional leakage unnecessary. A further shortcoming of the proposed pneumatic concept resides in the check valves preventing the blower to balance pressure during forced expiration. This results in a pressure increase, which could be avoided, if back–breathing in direction of the blower would be possible. This is currently accepted, because no other way has been found to combine ambient air and oxygen source without losses of oxygen.

Pressure and Flow Control Though robust controllers have been proven effective for a wide range of operating conditions, including patient, ambient and ventilation parameters, a certain amount of conservativeness is introduced, which becomes particularly apparent at high ventilation frequencies. With the expiratory pressure control and volume flow control in particular, the bandwidth spans for different patient and ambient parameters almost range within an order of magnitude. Dedicated controllers for different classes of patients (e.g. neonates, children, adults) could be synthesised, which would only require the physician to make an initial choice before setting up further parameters of the ventilation. Specialised feedforward schemes for blower control could then be derived to obtain the best quality of control. From the notions of blower or valve actuated PEEP control and keeping the blower speed relatively level or actively braking it, the combination best suited to the control problem could then be selected by the engineer and linked to the presets. Further theoretical insight to the problem of bumplessly transfering controller authority will then become mandatory. Optimisation of the blower speed during inspiration and expiration can also be made subject to interbreath closed–loop control, by introducing a cost function to assess control performance and measuring the electrical power consumed, which is to be minimised. The proposed control of PEEP by the large bore valve — though offering potential to reduce blower dynamics — seems to be prone to a high sensitivity to input disturbances. As attempts at directly shaping the input sensitivity have not resulted in feasible solutions, it is considered a structural problem. At the cost of higher power consumption, a dedicated miniature pressure source could be reconsidered for PEEP control, which would maintain independence from the blower.

Control of F_{iO_2} As an extension to the open–loop F_{iO_2} control scheme proposed in this thesis, interbreath closed–loop control can be considered, to ensure that the desired oxygen concentration is obtained on average in each ventilation cycle. As simulation results showed, that — in principle — tracking the ambient air flow is feasible, it is expected, that the feedforward F_{iO_2} control scheme can be implemented on an optimised pneumatic structure and provide satisfactory results.

List of Figures

Bibliography

[1] *VDI-Wärmeatlas*. VDI Buch. Springer-Verlag Berlin Heidelberg, Berlin, Heidelberg, 10. edition, 2006.

[2] Jürgen Ackermann and Andrew Bartlett. *Robuste Regelung: Analyse und Entwurf von linearen Regelungssystemen mit unsicheren physikalischen Parametern*. Springer, Berlin, 1993.

[3] Airox. LEGENDAIR — Bedienerhandbuch: Druck– und Volumengesteuertes Lungenbeatmungsgerät für den Heimgebrauch. Parc d'Activités Pau-Pyrénées, L'Echangeur – BP 833, 64008 PAU Cedex – FRANCE.

[4] Andreas Kwiatkowski. *LPV Modeling and Application of LPV Controllers to SI Engines*. PhD thesis, Technische Universität Hamburg-Harburg, Hamburg, 2007.

[5] P. Apkarian and D. Noll. Nonsmooth H Infinity Synthesis. *IEEE Transactions on Automatic Control*, 51(1):71–86, 2006.

[6] Peter Beater. *Pneumatic Drives: System Design, Modelling and Control*. Springer-Verlag Berlin Heidelberg, Berlin, Heidelberg, 2007.

[7] Leopold Böswirth. *Technische Strömungslehre: Lehr- und Übungsbuch*. Friedr. Vieweg & Sohn Verlag / GWV Fachverlage GmbH Wiesbaden, Wiesbaden, 7 edition, 2007.

[8] J. X. Brunner. History and principles of closed-loop control applied to mechanical ventilation, August 2002.

[9] J. V. Burke, D. Henrion, A. S. Lewis, and Overton L. M. HIFOO - A MATLAB Package for Fixed-Order Controller Design and H Infinity Optimization. Washington, Seattle, WA.

[10] Robert L. Chatburn. Classification of Ventilator Modes: Update and Proposal for Implementation. *Respiratory Care*, 52(3):301–323, 2007.

[11] Daniel W. Chipman, Maria P. Caramez, Eriko Miyoshi, Joseph P. Kratohvil, and Robert M. Kacmarek. Performance Comparison of 15 Transport Ventilators. *Respiratory Care*, (52, No. 6):740–751, June 2007.

[12] Deutsches Institut für Normung e.V. DIN EN 794-3: Lungenbeatmungsgeräte – Teil 3: Besondere Anforderungen an Notfall- und Transportbeatmungsgeräte, 1998.

[13] Marcus Diehl. Entwicklung einer energieoptimierten Beatmungsregelung als Kombination aus Gebläsen und Proportionalventilen: Diplomarbeit. Hamburg, April 2009.

[14] Florian Dietz. *Flowregelung für die nicht-invasive Beatmung unter Berücksichtigung von Maskenleckage und Spontanatmung.* PhD thesis, RWTH Aachen, Aachen, 2003.

[15] Dräger Medical GmbH. Gebrauchsanweisung Carina: Sub-Acute Care Ventilator Software 3.n, December 2008.

[16] Drägerwerk AG & Co. KGaA. Carina Product Brochure: Ein flexibles und kompaktes NIV-Beatmungsgerät — Mit Carina auf dem richtigen Weg.

[17] EN ISO. 5167-2(2003): Measurement of fluid flow by means of pressure differential devices inserted in circular cross-section conduits running full, Part 2: Orifice plates, 2008-09-30.

[18] S Fludger and A Klein. Portable ventilators. *Continuing Education in Anaesthesia, Critical Care & Pain*, 8(6):199–203, 2008.

[19] Michael Green and David J. N. Limebeer. *Linear robust control.* Prentice Hall, Englewood Cliffs, NJ, 1995.

[20] Benjamin Günther. Modellierung und Regelung eines Notfall-Beatmungsgeräts: Diplomarbeit. Hamburg, Januar 2006.

[21] Christoph Haberthür. *Beatmungskurven: Kursbuch und Atlas.* Springer, Berlin, 2001.

[22] Gerhard Univ.-Prof. Dr.-Ing. Dr. h.c. Henneberger. *Electrical Machines I: Basics, Design, Function, Operation: Lecture Notes.* Aachen.

[23] Herbert Werner. *Optimal and Robust Control: Lecture Notes.* Technische Universität Hamburg-Harburg, 2009.

[24] Heinz Herwig. *Technische Thermodynamik A-Z: Systematische und ausführliche Erläuterung wichtiger Größen und Konzepte.* TuTech Innovation GmbH, Hamburg, 2008.

[25] S. E. Hill, O. Njie, M. Sanneh, M. Jallow, D. Peel, M. Njie, and M. Weber. Oxygen for treatment of severe pneumonia in The Gambia, West Africa: A situational analysis. *The International Journal of Tuberculosis and Lung Disease*, 13(5):587–593, 2009.

[26] Mayuresh V. Kothare, Peter J. Campo, Manfred Morari, and Carl N. Nett. A Unified Framework for the Study of Anti-Windup Designs: Technical Memorandum. Pasadena, CA, June 1993.

[27] M. Kozarski, K. Zielinski, K. J. Palko, D. Bosewicz, and M. Darowski. The Hybrid Pneumatic-Numerical Model of Lungs: Metrological Aspects of the Design. Lisbon, Portugal, September, 2009.

[28] Reinhard Larsen and Thomas Ziegenfuß. *Beatmung: Grundlagen und Praxis*. Springer Berlin Heidelberg, Berlin, Heidelberg, 4. edition, 2009.

[29] Uwe Mackenroth. *Robust control systems: Theory and case studies*. Springer, Berlin, 2004.

[30] Maxon Motors. Maxon EC 22 50 Watt Brushless DC Motor Datasheet, April 2007.

[31] A. Prof. Dr.-Ing. Mertens. Elektrische Antriebstechnik II: Lecture Notes. Hannover, 2008.

[32] Wolfgang Oczenski and Harald Andel. Atmen - Atemhilfen: Atemphysiologie und Beatmungstechnik ; 53 Tabellen. 2006.

[33] Paragon Space Development Corporation. Solid Oxide Electrolysis.

[34] Youbin Peng, Damir Vrancic, and Raymond Hanus. Anti-windup, bumpless, and conditioned transfer techniques for PID controllers - IEEE Control Systems Magazine. *IEEE Control Systems*, 1996.

[35] Andrey P. Popov, Herbert Werner, and Marc Millstone. Fixed-Structure Discrete-Time H Infinity Controller Synthesis with HIFOO. Hamburg, 2010.

[36] PulmoneticSystems. LTV Series Ventilator: Operator's Manual, August 2005.

[37] Jörg Rathgeber. *Grundlagen der maschinellen Beatmung: Handbuch für Ärzte und Pflegepersonal*. Aktiv Druck & Verlag GmbH, Ebelsbach, 1999.

[38] Richard D. Branson and Bryce R. H. Robinson. Oxygen: when is more the enemy of good? *Intensive Care Med*, 2010.

[39] G. Schneider. Oxygen supply in rural Africa: A personal experience. *The International Journal of Tuberculosis and Lung Disease*, 5(6):524–526, 2001.

[40] D. Sonntag. Important New Values of the Physical Constants of 1986, Vapor Pressure Formulations based on the ITS-90 and Psychrometer Formulae. *Z. Meteorol.*, 70(5):340–344, 1990.

[41] Arief Syaichu-Rohman and Richard H. Middleton. Anti-windup Schemes for Discrete Time Systems: An LMI-based Design. Callaghan, Australia.

[42] Fleur T Tehrani. Automatic Control of Mechanical Ventilation. Part 1: Theory and History of the Technology. *Journal of Clinical Monitoring and Computing*, 22(6):409–415, 2008.

[43] The MathWorks Inc. Simulink 7: User's Guide, 2010.

[44] Tom Ritchey. General Morphological Analysis: A general method for non-quantified modelling. *Swedish Morphological Society*, 2010.

[45] R. M. Towey and S. Ojara. Intensive care in the developing world. *Anaesthesia*, (62):32–37, 2007.

[46] Matthew C. Turner, Guido Herrmann, and Ian Postlethwaite. Discrete-Time Anti-Windup: Part I - Stability and Performance. *Proceedings of the 7th European Control Conference, Cambridge-UK.*

[47] Holger Watter. *Hydraulik und Pneumatik: Grundlagen und Übungen-Anwendungen und Simulation.* Friedr. Vieweg & Sohn Verlag | GWV Fachverlage GmbH, Wiesbaden, 2007.

[48] WEINMANN Geräte für Medizin GmbH + Co. KG. Research & Development Archive.

[49] Joseph J. Yamé and Michel Kinnaert. On Bumps and Reduction of Switching Transients in Multicontroller Systems. *European Control Conference*, 2007:1–18.

[50] Luca Zaccarian and Andrew R. Teel. The L2 (l2) Bumpless Transfer Problem: Its Definition and Solution. *43rd IEEE Conference on Decision and Control December 14-17, 2004*, December, 2004.

[51] Guisheng Zhai, Shinichi Murao, Naoki Koyama, and Masaharu Yoshida. Low order H infinity controller design: An LMI approach. *European Control Conference*, 2003.